NASA Contractor Report 3514

Computation of Transonic Potential Flow About Three-Dimensional Inlets, Ducts, and Bodies

Theodore A. Reyhner

MARCH 1982

NASA

NASA Contractor Report 3514

Computation of Transonic Potential Flow About Three-Dimensional Inlets, Ducts, and Bodies

Theodore A. Reyhner
Boeing Commercial Airplane Company
Seattle, Washington

Prepared under Cooperative Agreement
with NASA Langley Research Center
and Boeing Commercial Airplane Company

NASA
National Aeronautics
and Space Administration

**Scientific and Technical
Information Branch**

1982

TABLE OF CONTENTS

SUMMARY

An analysis has been developed and a computer code, P465 Version A, written for predicting three-dimensional transonic potential flow about inlets, ducts, and bodies. The basic approach is very general and essentially independent of geometry. The analysis, as programmed, uses cylindrical coordinates and admits boundary conditions for the aforementioned configurations. Solutions of the full potential equation are obtained using finite differences and successive line over-relaxation (SLOR). Extrapolation and a sequence of increasingly denser grids are used to accelerate convergence and thus decrease the computer time required to obtain a solution.

The analysis has been programmed in extended FORTRAN IV for the Control Data Corporation CYBER 203 computer. Use of reasonably dense meshes for three-dimensional computations requires either a very large computer, such as the CYBER 203, or a great amount of complex software to use disk memory for backup of core memory. The run time on the CYBER 203 for a typical inlet calculation is about five minutes. Some special features of the CYBER 203 have been used in the computer code to maximize efficiency of the code. Use of the analysis on another super computer, such as the CRAY 1, is practical but would require a certain amount of recoding.

Comparisons between computer results and experimental measurements are presented to verify the capabilities of the code. Agreement between analysis and experiment is excellent for flowfields which are essentially inviscid and irrotational. The greatest disagreements between the analysis and experiment occur for flows where viscous (boundary-layer) effects are significant.

Program input and output formats are described and examples are presented.

This report does not discuss geometry specification. The analysis code requires input of a computational mesh and all intersections of the computational mesh with surfaces, including coordinates and components of the surface normal. This geometry specification can come from any source and the file of intersections can be in any order. The program does extensive checking of the geometrical input.

NOMENCLATURE

a	speed of sound
C_p	coefficient of pressure, $(p/p_\infty - 1)/\frac{1}{2}\gamma M^2$
M	Mach number
$M_{C.F.}$	Mach number at compressor face for uniform flow parallel to axis
$\bar{n}$	unit normal to surface oriented into flowfield
n_x, n_r, n_θ	components of $\bar{n}$
p	static pressure
q	velocity, $(u^2 + u_r^2 + u_\theta 2)$
r	radius
r_{FAN}	radius of engine fan
r_{max}	r at outer edge of computational cylinder
s	arc length
u	axial velocity component, $u = \phi_x$
u_r	radial velocity component, $u_r = \phi_r$
u_s	component of velocity along cut of surface
u_θ	circumferential velocity component, $u_\theta = \frac{1}{r}\phi_\theta$
v	velocity component in y direction, $v = \phi_y$
w	velocity component in z direction, $w = \phi_z$
x	axial coordinate
y	coordinate, $y = r \cos \theta$
z	coordinate, $z = r \sin \theta$
α	angle of attack, v_∞/u_∞
β	angle of yaw, w_∞/u_∞
$\beta, \beta_x, \beta_{1x}, \ldots$	weighting parameters
γ	ratio of specific heats

$\Delta x, \Delta r, \ldots$	step size in x, r etc
$\Delta\phi$	change in ϕ between relaxation sweeps
η	nondimensional coordinate, $0 \leq \eta \leq 1.0$
θ	circumferential coordinate
θ_ξ	value of θ for additional plane of symmetry
ξ	radial coordinate along plane of symmetry, $\theta = \theta_\xi$
λ	extrapolation factor
ϕ	potential function
ϕ_n	velocity normal to surface
ϕ_s	$\partial\phi/\partial s$, velocity in direction of s
$\phi_{s_x}, \phi_{s_r}, \phi_{s_\theta}$	velocity components for constant x, r, and θ cuts of surface respectively
ω_x	local x over-relaxation parameter
$\bar{\omega}_x$	reference x over-relaxation parameters ($\bar{\omega}_x = 1.85$)
ω_θ	local θ under-relaxation parameter
$\bar{\omega}_\theta$	reference θ under-relaxation parameter ($\bar{\omega}_\theta = 0.9$)

Superscript

+	value after updating

Subscripts

i	index for x mesh values
j	index for r mesh values
k	index for θ mesh values
$\ell, \ell\ell, u$	step-size subscripts
A,B,P,P'...	points on grid or surface
S, S_1, S_2	surface points
x,y,z,r,θ,s	partial derivatives
0,1,2	step-size subscripts

∞	freestream

Special

$\phi_{x\|S}$	ϕ_x at point S
$\mathfrak{C}$	centerline (axis)
$\|\|\ \ \|\|$	norm

LIST OF FIGURES

LIST OF TABLES

1.0 INTRODUCTION

This report describes a computer code, P465 Version A, for predicting the inviscid irrotational flowfield about a three-dimensional inlet, duct, or body. The flowfield is generated by a finite-difference, line-relaxation solution of the complete potential flow equation. The predicted results are excellent approximations of actual flowfields where viscous effects are small, i.e., flows with thin attached boundary layers.

During the past decade there has been tremendous progress in the field of transonic potential-flow computation. The work started with Murman and Cole[1] who used upwind differencing in supersonic flow regions to solve mixed elliptic and hyperbolic equations. Their work was based on small disturbance theory where the flow was principally aligned with one coordinate. Jameson[2] extended this approach to the full potential equation with arbitrary flow direction. Several classes of three-dimensional geometries have been solved using the full potential equation[2-5]. Most extensions to three dimensions have been based on some mapping from the physical coordinates to a more convenient computational coordinate system. If such mappings can be found, the computational problem, exclusive of the generation of the mapping, can be greatly simplified. This approach becomes more difficult as the geometry of objects to be considered becomes more complex, because it becomes more difficult to find convenient mappings that will provide reasonable coordinates for the computation. A further disadvantage with a complex mapping is that it can be very difficult to have any physical understanding of the solution process.

The approach used for this analysis separates the coordinate system and the geometry. Thus, this approach does not require the finding of a new transformation for every family of geometries. The method was originally tested for axisymmetric problems[6] and later applied to axisymmetric inlets at angle of attack[3]. This report describes the extension of the method to general three-dimensional geometries. The method also has the advantage that the solution is obtained in a physical coordinate system with physical variables and hence the entire solution process is more understandable. The analysis, as programmed, uses cylindrical coordinates since they are suited to nacelle calculations, but the analysis could easily be changed to use a Cartesian, skewed Cartesian, or any other coordinate system.

The analysis is independent of the coordinate system except that if the coordinate system is a poor choice for the problem, accuracy will suffer as there will be insufficient mesh nodes. The practical limit on the number of mesh nodes is dictated by computational time. The nature of the relaxation process imposes an exponential increase in computational time with increasing mesh density. This severely limits the number of mesh nodes and makes it essential that the coordinate system be such that the mesh nodes are well placed. The cylindrical coordinate system used in the computer code gives reasonable node placement for nacelle, duct, and body geometries where such geometries are approximately bodies of revolution. Cylindrical coordinates can be used for geometries that are not nearly bodies of revolution, but they may not be very efficient.

2.0 ANALYSIS

Solutions to the full partial differential equation for compressible potential flow along with appropriate boundary conditions are desired for three-dimensional flow. Approximate solutions of this equation are obtained by replacing the partial differential equation and boundary conditions with finite-difference equations for the value of the potential function, at discrete points in the flowfield and on the boundary. The finite-difference equations are obtained by replacing partial derivatives in the differential equations with difference quotients. The difference equations are coupled, nonlinear, algebraic equations in the value of the potential function at field and surface mesh points. The nonlinear difference equations are solved by an iterative process to the desired accuracy. The degree of approximation of the difference solution to the true solution of the partial differential equation is a function of the mesh spacing.

The solution technique can use an arbitrary mesh as long as the mesh is dense enough to ensure that there are several mesh nodes between independent surfaces. As programmed, a cylindrical mesh with variable mesh-line spacing is used because it is relatively efficient for inlet and nacelle configurations. A typical constant θ cut showing the mesh and an inlet cowl is displayed in figure 1. The mesh is not required to intersect with the body in any predescribed manner. Nodes used in the calculation are mesh intersects in the flowfield and intersections of mesh lines with surfaces. Difference quotients are written to take into account variable spacing between field and surface nodes.

The difference equations consist of a large number of coupled, nonlinear, algebraic equations. The direct solution of such a set of equations is certainly impractical if not impossible. A multistep process is used to develop a solution procedure for the difference equations. The basic approach uses an iterative technique, starting with an initial guess, computing an approximate solution, and then repeating the cycle or sweep with the approximate solution used to compute a better approximate solution. As a minimum requirement, the iteration technique has to be convergent. In practice, for the three-dimensional transonic potential-flow problem, the iteration technique has to converge rapidly enough that the computation time is practical.

The first step in the iterative solution process is to linearize the difference equations. This is done by dividing terms into coefficients and unknowns, and using the initial guess or solution for the previous iteration to approximate the coefficients. The linear equation system that results is fully coupled, or implicit, and would have to be solved simultaneously. Simultaneous solution of such a large system of linear equations is not practical. As a consequence, the equations have to be at least partly decoupled by substituting old values of the potential function, ϕ, for some of the (unknown) values of ϕ (denoted by ϕ^+). How this substitution is done affects stability, convergence, convergence rate, and the practicality of the solution procedure. The process of mixing old and new values and iterating (sweeping) to obtain a solution is commonly called relaxation and is discussed in many references. (See ref. 7, for example.) Generally, the more thoroughly the equations are decoupled, the less work is required to take one relaxation sweep; however, the more relaxation sweeps are required to reach a given level of convergence or degree of accuracy of the solution. A fully decoupled system, where only one equation needs to be solved at a time, is known as explicit and generally exhibits very slow convergence properties.

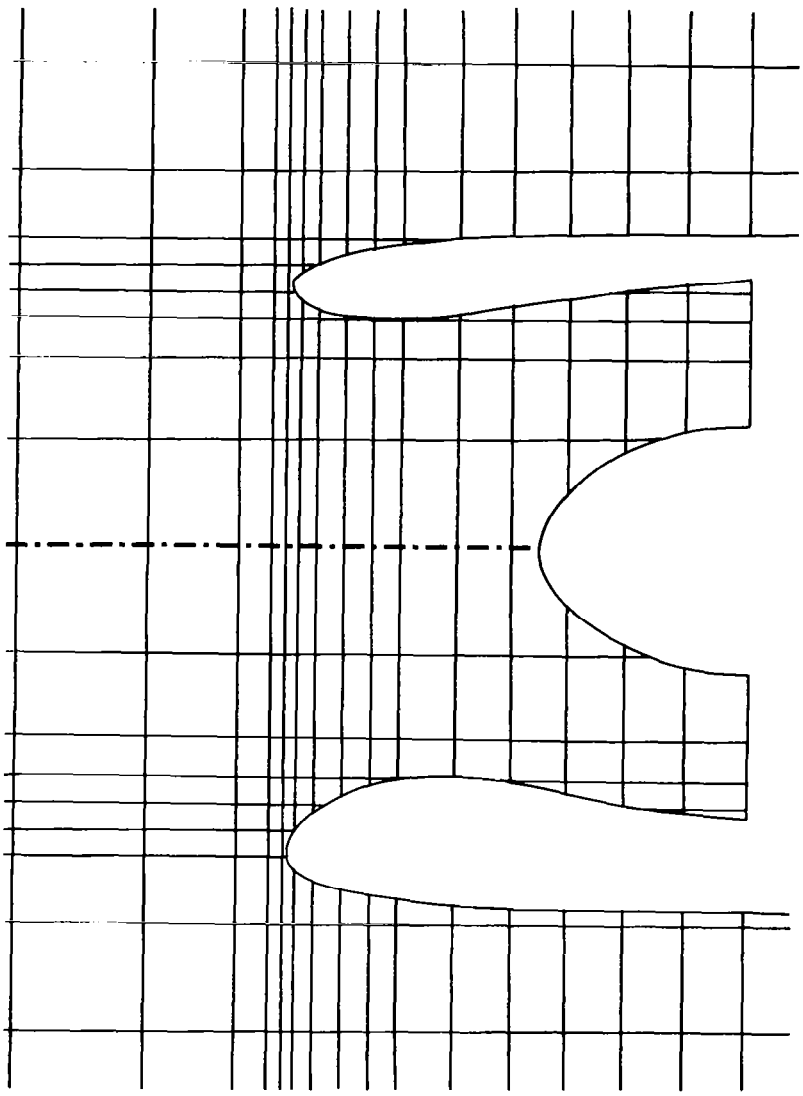

Figure 1. Typical Coarse Computational Mesh for a Constant θ Cut in the Vicinity of the Inlet

A decoupling of the equation system so that all the equations along one mesh line are solved simultaneously is known as line relaxation. It is a popular technique because there exists a very efficient algorithm known as the Thomas or tridiagonal algorithm to obtain the solution for such an equation system. The relaxation process can be accelerated or stabilized, as desired or required, by processes known as over- or under-relaxation, respectively. Over-relaxation consists of taking the difference of the new and previous solutions, multiplying the difference by a factor between one and two, and adding the difference to the previous solution to create an improved new solution. Under-relaxation is similar except the multiplication factor is less than one. In this code over-relaxation is used for one term of the partial differential equation and under-relaxation for another. The combination of line relaxation and over-relaxation is commonly called successive line over-relaxation (SLOR). This is basically the technique used in the analysis discussed herein.

A penalty involved in using a line-relaxation scheme on a vector computer is that the tridiagonal algorithm, used to solve the simultaneous equations for a line, does not vectorize efficiently. However, the ratio of computing time spent solving the equations with the tridiagonal solver, versus the time spent calculating the equation coefficients, is small. Also, the SLOR scheme takes many less relaxation sweeps to reach a given level of convergence than an explicit technique. A sweep is a complete solution in sequential order of all the difference equations for the flowfield.

Each relaxation sweep is computed using SLOR. Additional techniques have also been employed to accelerate convergence. One such technique is extrapolation using intermediate solutions. Extrapolation is based on the theory of linear algebraic equations and the existence of eigenvalues and eigenvectors. When the solution process appears to be developing in a particular manner it can be extrapolated to obtain a much better approximation of the final solution. Another technique is the use of a sequence of meshes of increasing density. The initial field is assumed to be uniform flow and is applied on a very coarse mesh. Relaxation is continued on this mesh until partial convergence is obtained. The initial mesh is too coarse to be used to compute an accurate solution to the flow problem, but the solution from the coarse mesh is a much better starting guess for the next mesh than uniform flow. The advantage of using a sequence of meshes is that computation is cheaper per sweep, and convergence is faster on a coarser mesh.

Along with the consideration of the practicality of making a relaxation sweep, the linearization and decoupling of the difference equations has to be such that the relaxation process converges. One aspect critical to the transonic flow solution is the use of upwind differencing where the flow is supersonic.

The organization of this analysis, as programmed, is biased by the strengths and weaknesses of the computer for which the code was originally written. In particular, the CDC CYBER 200 family of computers has large memory and operates most efficiently with long-vector operations. The large memories make three-dimensional codes possible. The efficiency of long-vector operations makes it desirable to decouple the equations so that many coefficients can be calculated at once.

2.1 EQUATION AND BOUNDARY CONDITIONS

The equation to be solved is the complete equation for inviscid, irrotational flow formulated in terms of a velocity potential, ϕ. This form of the equation has the significant advantage that there is only one unknown that has to be stored at mesh nodes. This is particularly important for a three-dimensional elliptic problem where computer storage is very critical.

2.1.1 POTENTIAL FLOW EQUATION

The equation for the velocity potential in cylindrical coordinates is

$$\left(a^2-\phi_x^2\right)\phi_{xx} + \left(a^2-\phi_r^2\right)\phi_{rr} + \left(a^2-\frac{\phi_\theta^2}{r^2}\right)\frac{\phi_{\theta\theta}}{r^2} - 2\phi_x\phi_r\phi_{xr} - 2\phi_r\phi_\theta\frac{\phi_{r\theta}}{r^2} - 2\phi_\theta\phi_x\frac{\phi_{\theta x}}{r^2} + \left(a^2+\frac{\phi_\theta^2}{r^2}\right)\frac{\phi_r}{r} = 0 \tag{1}$$

where ϕ is the velocity potential and the local speed of sound, a, is given by

$$a^2 = a_\infty^2 - \frac{\gamma-1}{2}\left(\phi_x^2 + \phi_r^2 + \frac{\phi_\theta^2}{r^2} - q_\infty^2\right). \tag{2}$$

The potential equation in Cartesian coordinates is

$$\left(a^2-\phi_x^2\right)\phi_{xx} + \left(a^2-\phi_y^2\right)\phi_{yy} + \left(a^2-\phi_z^2\right)\phi_{zz} - 2\phi_x\phi_y\phi_{xy} - 2\phi_y\phi_z\phi_{yz} - 2\phi_z\phi_x\phi_{zx} = 0. \tag{3}$$

This form of the equation is used in generating difference equations for points on the axis.

The velocity components in the flowfield (u, u_r, u_θ) for the cylindrical coordinate system are obtained from the potential function with the following relationships:

$$\begin{aligned} u &= \phi_x, \\ u_r &= \phi_r, \\ u_\theta &= \frac{\phi_\theta}{r}. \end{aligned} \tag{4}$$

The velocity components for a Cartesian reference frame (u, v, w) are obtained using the equations,

$$v = \phi_y = u_r \cos\theta - u_\theta \sin\theta$$

$$w = \phi_z = u_r \sin\theta + u_\theta \cos\theta \ . \tag{5}$$

2.1.2 BOUNDARY CONDITIONS

The boundary condition at solid surfaces is that the velocity normal to the surface, ϕ_n, equals zero. The boundary condition at the exit of a duct, or at the compressor face of an inlet, is that the axial velocity is fixed at the uniform value that gives a specified mass flow. At the left boundary of the computational field, the potential function, ϕ, is specified. For an inlet flowfield computation (figure 2), at the left boundary,

$$\phi = u_\infty x + v_\infty r \cos\theta + w_\infty r \sin\theta + \text{constant}. \tag{6}$$

This is also the equation for the initial flowfield approximation.

For an isolated inlet in a freestream, the following additional boundary conditions are used. Equation 6 is used to specify ϕ for 90 degrees $\leq \theta \leq$ 270 degrees and $r = r_{max.}$. The outflow velocity, ϕ_n, for the computational cylinder is specified by

$$\phi_n\Big|_{r=r_{max.}} = \phi_r\Big|_{r=r_{max.}} = v_\infty \cos\theta + w_\infty \sin\theta \tag{7}$$

for 0 degrees $\leq \theta <$ 90 degrees and 270 degrees $< \theta \leq$ 360 degrees and $r = r_{max.}$. ϕ_x is specified as equal to u_∞ at the right boundary of the computational field outside of the inlet.

The boundary conditions on the far field for an isolated nacelle or body are only approximate. The correct boundary condition is that the velocities approach the freestream values far from the body. This boundary condition cannot be directly satisfied for a potential-flow solution in a finite computational volume. As written, the boundary conditions specify either the normal or tangential component of velocity at any surface. In most cases the normal component of velocity is specified for outflow surfaces and the tangential component for inflow surfaces. The exceptions are nonzero yaw angle or negative angle of attack. For these cases, the boundary conditions on some of the surfaces could be changed; for example, the analysis is convergent for a negative angle of attack which essentially reverses the boundary conditions on the top and bottom of the computational cylinder. Changes to the far-field boundary conditions would probably affect accuracy and convergence rate of the solution, however, no extensive studies of these effects have been made.

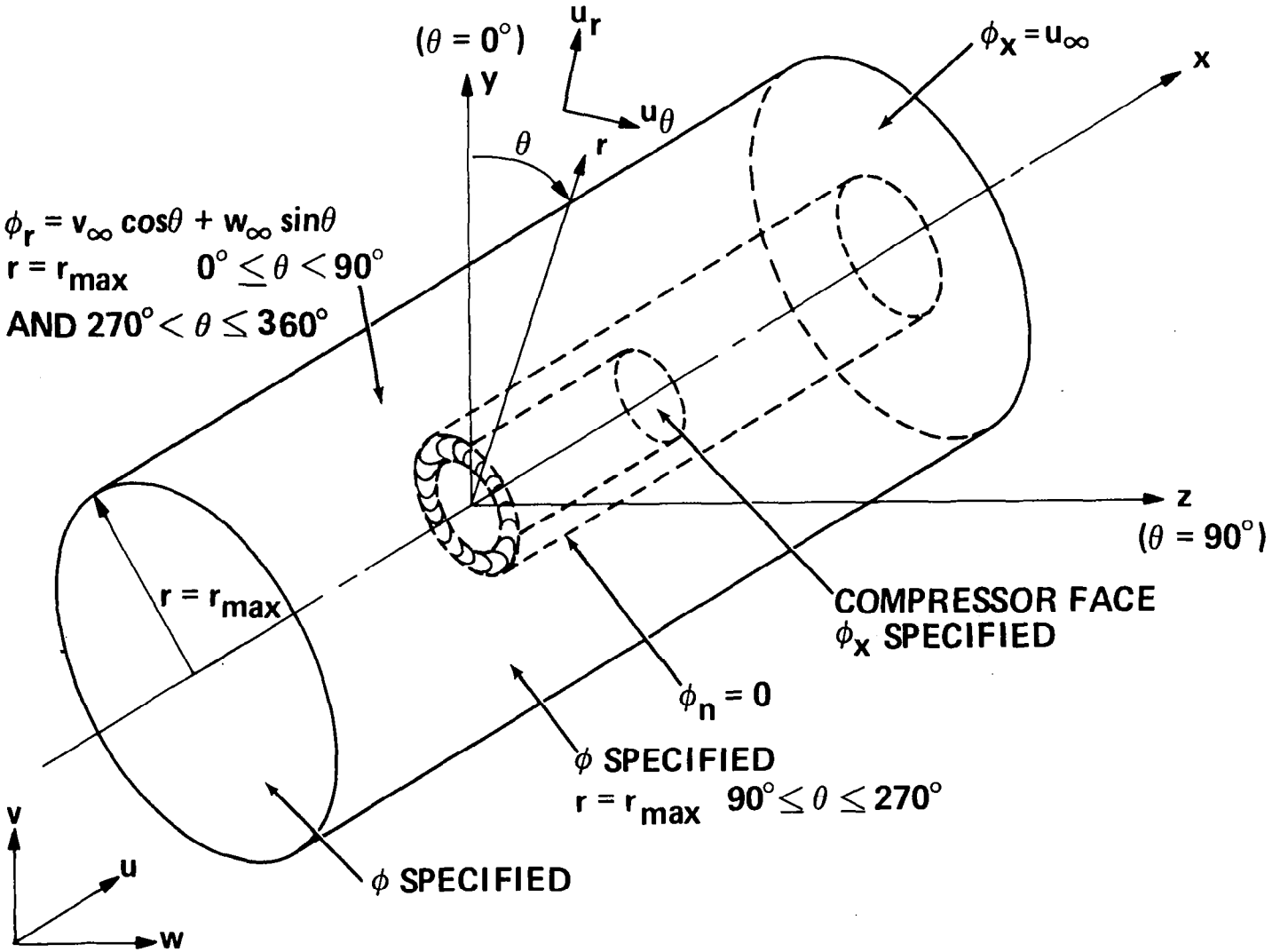

Figure 2. Geometry and Boundary Conditions for Inlet Flowfield Computation

The present far-field boundary conditions are satisfactory provided the boundaries are located far enough from the body. Locating the far-field boundaries five to ten nacelle diameters away from the body is usually sufficient to ensure negligible effects of the boundary conditions on the computed flowfield near the body. If the far-field boundary is so placed, the effects of the boundary conditions are of the order of or smaller than other approximations such as treating a nacelle as an isolated nacelle.

2.2 WEIGHTING AND ALTERNATE FORMULAS

A possible problem with this approach to solving the potential flow equation is that the step size between a surface point and an adjacent field point is uncontrolled and can become arbitrarily small. Derivatives are calculated by dividing by the step size and thus any error in the potential function, ϕ, can be magnified by the reciprocal of the step size, which can become arbitrarily large. This can cause accuracy and stability problems if not considered. To avoid this problem, alternate formulas that do not use the field point ϕ value are used when the step size to a surface point is very small. To obtain a smooth solution process, a weighted combination of the regular and alternate formulas is used if the surface points are closer to the field points than one-half the local field-point spacing. This procedure, which is called weighting in this document, has been used for many difference quotients. Typical formulas are presented in this report.

The ϕ values at field points adjacent to surface points are used in differencing at other field nodes, even when they are very close to surface nodes. It is essential that as a field and surface node become close, the ϕ values at these nodes approach the same value. This behavior is ensured by calculating the ϕ value at the field node by interpolation between the surface value and other field-point values, if the spacing to the surface is very small. A weighted combination of interpolation and the usual field-point difference equation is used when the spacing between the field node and any surface node is less than one-half the local mesh spacing.

2.3 DIFFERENCE QUOTIENTS

Difference equations are generated by replacing partial derivatives in the partial differential equation with difference quotients. The choice of difference quotients is not arbitrary, nor is it unique. The difference quotients chosen are based on several, often conflicting, criteria. First, the difference quotients chosen must lead to a stable convergent solution process. Second, the use of more nodes in a difference quotient can give greater accuracy, but normally at the price of greatly increased complexity. For this analysis, where the body can intersect the mesh arbitrarily, the use of complex, many-point difference quotients would be extremely difficult.

The highest-order derivatives in the partial differential equation are second derivatives, which require at least three points in the difference quotients. As any more than three points in the difference quotients would greatly complicate many aspects of the problem, three-point difference quotients have been used.

There are three general categories of difference quotients: central, forward, and backward differences. Categorization is based on where the additional nodes used in the differencing lie with respect to the node at which the derivative is to be evaluated. Forward or backward differences relate to the use of additional nodes which lie ahead of or behind, in time or space, the node where the derivative is to be evaluated. In general, central differencing is preferred because of smaller truncation errors, however, in some

situations, central-difference quotients may result in unstable difference equations. In particular, for this problem, stability requires the use of one-sided differences for second derivatives where the flow is supersonic. These differences are termed "upwind" as the direction of the differencing is opposite the flow direction.

2.3.1 FORMULAS FOR FIRST DERIVATIVES (VELOCITIES)

The difference quotients for first-degree partial derivatives are central differenced for greater accuracy. Three-point differences are used giving second-order accuracy with truncation errors proportional to the square and/or product of the two step sizes involved. If surface points are used, alternate formulas may be weighted into the calculation to avoid problems due to dividing by the step size to the surface when the step size becomes very small. The first derivatives represent the flow velocities except for ϕ_θ which equals ru_θ. Difference quotients and weighting formulas are given here for x derivatives. The r and θ derivatives are calculated the same way. Typical configurations for differencing are shown in figure 3.

All old ϕ values are used in the first-derivative calculations, except for the calculation of ϕ_r in the last term of equation 1. Old ϕ values are used for the first derivatives because they are used to calculate the coefficients of the terms in the difference equations before the difference equations are solved.

For a regular field point (or a field point that is not adjacent to a surface point in the x coordinate) (fig. 3a)

$$\phi_x\Big|_{i,j,k} = \frac{\Delta x_\ell^{\,2}\phi_{i+1,j,k} + \left(\Delta x_u^{\,2}-\Delta x_\ell^{\,2}\right)\phi_{i,j,k} - \Delta x_u^{\,2}\phi_{i-1,j,k}}{\Delta x_\ell \Delta x_u\left(\Delta x_\ell+\Delta x_u\right)} \tag{8}$$

For a field point that is surface-adjacent in x (fig. 3b)

$$\phi_x^{(1)}\Big|_A = \frac{\Delta x_2^{\,2}\phi_S + \left(\Delta x_1^{\,2}-\Delta x_2^{\,2}\right)\phi_A - \Delta x_1^{\,2}\phi_B}{\Delta x_1 \Delta x_2\left(\Delta x_1+\Delta x_2\right)} \tag{9}$$

$$\phi_x^{(2)}\Big|_A = \frac{1}{\Delta x_1+\Delta x_2}\left[2\Delta x_1\frac{\phi_S-\phi_B}{\Delta x_1+\Delta x_2} + \left(\Delta x_2-\Delta x_1\right)\phi_x\Big|_S\right] \tag{10}$$

and

$$\phi_x\Big|_A = \beta\phi_x^{(1)}\Big|_A + (1-\beta)\phi_x^{(2)}\Big|_A \tag{11}$$

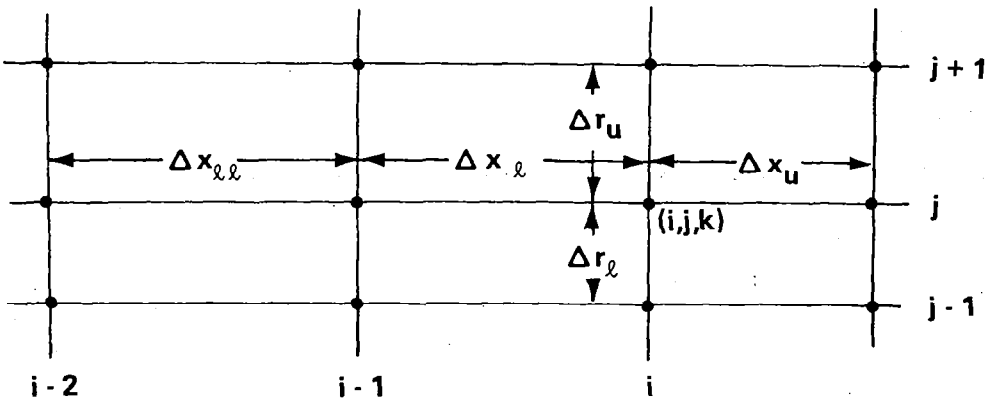

a.) **REGULAR FIELD POINT**

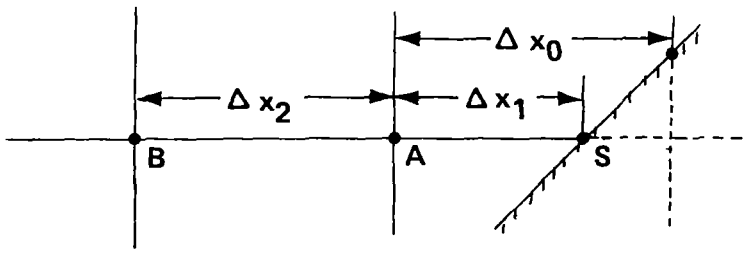

b.) **SURFACE ADJACENT FIELD POINT**

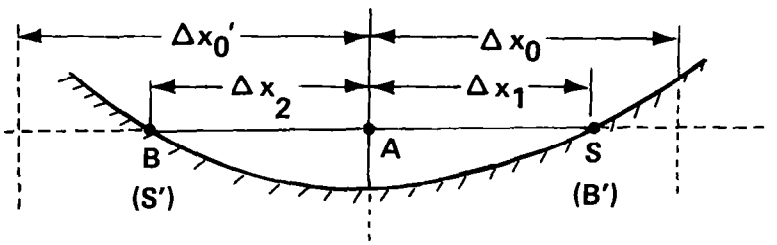

c.) **SURFACE ADJACENT IN OPPOSITE DIRECTIONS FIELD POINT**

Figure 3. Nomenclature for Typical Difference Quotients

where

$$\beta = \begin{cases} \Delta x_1 / \frac{1}{2}\Delta x_0 & \Delta x_1 < \frac{1}{2}\Delta x_0 \\ 1.0 & \Delta x_1 \geq \frac{1}{2}\Delta x_0 \end{cases} .$$

$\phi_x|_S$ is the value of ϕ_x for the surface point S that is calculated from the surface-point ϕ values according to the procedure described in section 2.4.

If the field point is surface-adjacent in x in the opposite direction as well (fig. 3c)

$$\phi_x^{(3)}\Big|_A = \frac{\Delta x_1 \phi_x\Big|_{S'} + \Delta x_2 \phi_x\Big|_S}{\Delta x_1 + \Delta x_2} \tag{12}$$

$$\beta' = \begin{cases} \Delta x_2 / \frac{1}{2}\Delta x_0' & \Delta x_2 < \frac{1}{2}\Delta x_0' \\ 1.0 & \Delta x_2 \geq \frac{1}{2}\Delta x_0' \end{cases}$$

$$\beta'' = \text{minimum}(\beta, \beta')$$

and

$$\phi_x\Big|_A = \beta'' \phi_x^{(1)}\Big|_A + (1-\beta'')\phi_x^{(3)}\Big|_A . \tag{13}$$

2.3.2 DIFFERENCE QUOTIENTS FOR ϕ_{xx}, ϕ_{rr}, AND $\phi_{\theta\theta}$

The difference quotients used for replacing the second derivatives affect the stability of the relaxation scheme. Central differencing is preferred for accuracy, but leads to unstable behavior if the flow becomes supersonic. The technique for avoiding this problem is to switch to upwind difference quotients when the flow becomes supersonic.

It would be desirable if all new ϕ values could be used in the difference quotients, but that leads to a coupled equation set that is impractical to solve. The equations presented here are coupled only along radial lines and are of tridiagonal form. There is a relatively simple, well-known, efficient, algorithm for performing a direct solution of tridiagonal systems. The algorithm is presented in appendix A. For x derivatives, new values are used at i-1 because they are available and an over-relaxation parameter, ω_x, is used to speed convergence for the subsonic central-difference quotient. The central-difference quotient for $\phi_{\theta\theta}$ uses old values at k-1 and k+1 in order that all coefficients for an x equals constant plane can be calculated at one time. This is desirable to exploit the vector speed of the CYBER 203. An under-relaxation parameter, ω_θ, is used to maintain stability.

Central-difference formulas:

$$\phi_{xx} = \left\{\Delta x_\ell \phi_{i+1,j,k} - (\Delta x_\ell + \Delta x_u)\left[\frac{1}{\omega_x}\phi_{i,j,k}^{+} + \left(1-\frac{1}{\omega_x}\right)\phi_{i,j,k}\right] + \Delta x_u \phi_{i-1,j,k}^{+}\right\} \div \left[\frac{1}{2}\Delta x_\ell \Delta x_u (\Delta x_\ell + \Delta x_u)\right] \tag{14}$$

$$\omega_x = 1 + \left(\frac{\Delta x_\ell + \Delta x_u}{\text{maximum}\,(\Delta x_\ell, \Delta x_u)} - 1\right)(\bar{\omega}_x - 1) \tag{15}$$

$$\phi_{rr} = \frac{\Delta r_\ell \phi_{i,j+1,k}^{+} - (\Delta r_\ell + \Delta r_u)\phi_{i,j,k}^{+} + \Delta r_u \phi_{i,j-1,k}^{+}}{\frac{1}{2}\Delta r_\ell \Delta r_u (\Delta r_\ell + \Delta r_u)} \tag{16}$$

$$\phi_{\theta\theta} = \left\{\Delta\theta_\ell \phi_{i,j,k+1} - (\Delta\theta_\ell + \Delta\theta_u)\left[\frac{1}{\omega_\theta}\phi_{i,j,k}^{+} + \left(1-\frac{1}{\omega_\theta}\right)\phi_{i,j,k}\right] + \Delta\theta_u \phi_{i,j,k-1}\right\} \div \left[\frac{1}{2}\Delta\theta_\ell \Delta\theta_u (\Delta\theta_\ell + \Delta\theta_u)\right] \tag{17}$$

$$\omega_\theta = 1 + \left(\frac{\Delta\theta_\ell + \Delta\theta_u}{\text{maximum}\,(\Delta\theta_\ell, \Delta\theta_u)} - 1\right)(\bar{\omega}_\theta - 1) \tag{18}$$

$\bar{\omega}_x$ and $\bar{\omega}_\theta$ are reference over- and under-relaxation parameters. They are the values used for a uniform mesh. The values ω_x and ω_θ have been modified for the local mesh spacing.

The same formulas are used if a surface point, or points, are involved in the differencing, except that the appropriate surface point ϕ value(s) and step size(s) are substituted.

The upwind difference formulas for ϕ_{xx}, ϕ_{rr}, and $\phi_{\theta\theta}$ use a mixture of old and new ϕ values for stability and improved rate of convergence. Where a new value of ϕ is shown in a formula, an old value is used, if the flow direction is such that a new value is not available.

The switch between central and upwind differencing takes place as the coefficient of the second derivative changes sign. This leads to a smooth stable behavior of the solution process. As an example, central differencing is used for ϕ_{xx} if $|\phi_x|<a$ and upwind differencing if $|\phi_x|>a$.

Upwind difference formulas are shown only for ϕ_{xx} for one flow direction. Difference quotients for r and θ and other flow directions are similar. For a point that is regular in x and for $|\phi_x|>a$,

$$\phi_{xx} = \frac{(\Delta x_\ell+\Delta x_{\ell\ell})(\phi_{i,j,k}^{+} - \phi_{i-1,j,k}^{+}) - \Delta x_\ell(\phi_{i,j,k} - \phi_{i-2,j,k})}{\frac{1}{2}\Delta x_\ell \Delta x_{\ell\ell}(\Delta x_\ell+\Delta x_{\ell\ell})} . \quad (19)$$

If the point (i-1, j, k) is surface adjacent in the x coordinate with the surface between (i-2, j, k) and (i-1, j, k), the following formulas are used:

$$\phi_{xx}^{(1)} = \frac{(\Delta x_1+\Delta x_2)(\phi_{i,j,k}^{+} - \phi_{i-1,j,k}^{+}) - \Delta x_2(\phi_{i,j,k} - \phi_S)}{\frac{1}{2}\Delta x_1\Delta x_2(\Delta x_1+\Delta x_2)} \quad (20)$$

$$\phi_{xx}^{(2)} = \frac{\frac{\phi_{i,j,k}^{+} - \phi_S^{+}}{\Delta x_1+\Delta x_2} - \phi_x|_S}{\frac{1}{2}(\Delta x_1+\Delta x_2)} \quad (21)$$

$$\phi_{xx} = \beta\phi_{xx}^{(1)} + (1-\beta)\phi_{xx}^{(2)} \quad (22)$$

where

$$\beta = \begin{cases} \Delta x_2 / \frac{1}{2}\Delta x_1 & \Delta x_2 < \frac{1}{2}\Delta x_1 \\ 1.0 & \Delta x_2 \geq \frac{1}{2}\Delta x_1 \end{cases}$$

and S is the surface point and Δx_2 is the step size between the surface point and (i-1, j, k).

If the point (i, j, k) is surface-adjacent in negative x,

$$\phi_{xx} = \frac{\dfrac{\phi_{i,j,k}^{+} - \phi_S^{+}}{\Delta x_1} - \phi_x\Big|_S}{\frac{1}{2}\Delta x_1} \tag{23}$$

where Δx_1 is the step size between point S and (i, j, k).

2.3.3 DIFFERENCE QUOTIENTS FOR ϕ_{xr}, $\phi_{r\theta}$, AND $\phi_{\theta x}$

For subsonic flow, central-difference formulas are used for accuracy. The formulas are obtained by setting

$$\begin{aligned} \phi_{xr} &= \frac{\partial(\phi_x)}{\partial r} \\ \phi_{r\theta} &= \frac{\partial(\phi_r)}{\partial \theta} \\ \phi_{\theta x} &= \frac{\partial(\phi_x)}{\partial \theta} \end{aligned} \tag{24}$$

and using formulas 8 or 9 with appropriate changes. As an example, for a field point that is adjacent to a surface point S and lies below S,

$$\phi_{xr} = \frac{\Delta r_2^{\,2}\phi_x\Big|_S + \left(\Delta r_1^{\,2} - \Delta r_2^{\,2}\right)\phi_x\Big|_A - \Delta r_1^{\,2}\phi_x\Big|_B}{\Delta r_1 \Delta r_2 \left(\Delta r_1 + \Delta r_2\right)} . \tag{25}$$

Weighting is not necessary in these terms as the resulting difference equations are weighted (see Section 2.5.2).

The difference quotients for the cross-derivatives are also switched between central and upwind formulas depending on flow Mach number. The switching procedure is somewhat more complicated because the coefficients of these derivatives do not necessarily switch signs anywhere.

The upwind-difference quotients for cross-derivatives are relatively simple, but there are many variations depending on flow direction. Representative examples of upwind differencing for a field point that is regular with $\phi_x>0$ and $\phi_r>0$ (fig. 4a) are

$$\phi_{xr} = \frac{\phi_{i,j,k}^{+} - \phi_{i-1,j,k}^{+} - \phi_{i,j-1,k}^{+} + \phi_{i-1,j-1,k}^{+}}{\Delta x \Delta r} . \tag{26}$$

For the configuration of figure 4b,

$$\phi_{xr}\Big|_A = \frac{\dfrac{\phi_A^{+} - \phi_{S_1}^{+}}{\Delta x_1} - \dfrac{\phi_{i,j-1,k} - \phi_{S_2}}{\Delta x_2}}{\Delta r} . \tag{27}$$

For the configuration of figure 4c,

$$\phi_{xr}\Big|_A = \frac{\dfrac{\phi_A^{+} - \phi_{S_1}^{+}}{\Delta r_1} - \dfrac{\phi_{i-1,j,k}^{+} - \phi_{S_2}^{+}}{\Delta r_2}}{\Delta x} . \tag{28}$$

Although, the configuration shown in figure 4d is unlikely since supersonic flow is shown coming out of the surface, it can happen under unusual circumstances, particularly for very coarse meshes. For the configuration of figure 4d,

$$\phi_{xr}\Big|_A = \frac{\dfrac{\phi_A^{+} - \phi_{S_1}^{+}}{\Delta x} - \phi_x\Big|_{S_2}}{\Delta r} . \tag{29}$$

There is a mixture of new and old ϕ values in this formula. The philosophy is to use new values for ϕ where they are available, consistent with the line relaxation, except in the case of equations 27 and 29 which are of the form $(\phi_x^{+} - \phi_x)/\Delta r$.

The code uses central differencing if the local Mach number is less than one and upwind differencing if either velocity component is supersonic. The upwind- and central-difference formulas for cross-derivatives are weighted together between these two conditions. In summary, if $M<1$,

$$\phi_{xr} = \phi_{xr}\Big|_{\text{central differenced}}$$

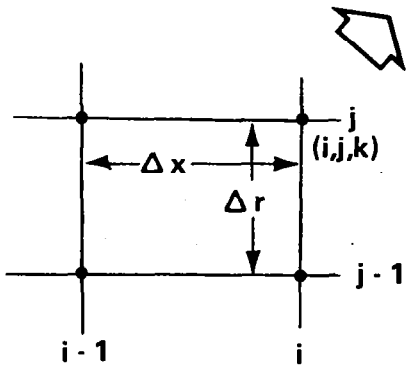

a.) REGULAR DIFFERENCING

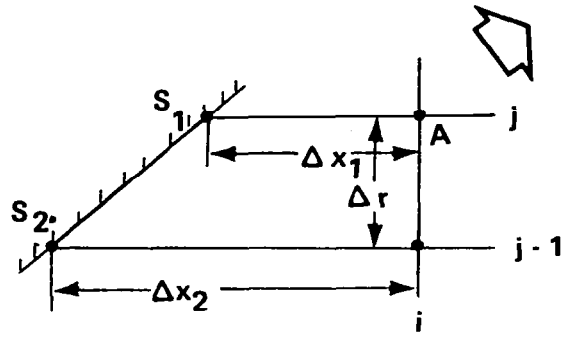

b.) SURFACE AFFECTED

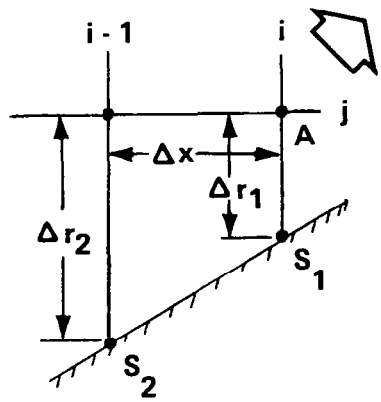

c.) SURFACE AFFECTED

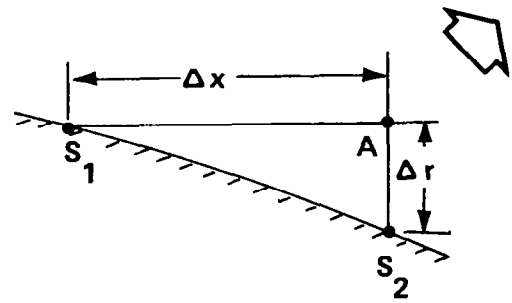

d.) SPECIAL SURFACE AFFECTED

Figure 4. Example Configurations for Upwind Differencing of Cross-Derivatives

and if $|\phi_x|>a$ or $|\phi_r|>a$

$$\phi_{xr} = \phi_{xr}|_{\text{upwind difference,}}$$

otherwise,

$$\phi_{xr} = \beta\phi_{xr}\Big|_{\text{central diff.}} + (1-\beta)\phi_{xr}\Big|_{\text{upwind diff.}} \tag{30}$$

where

$$\beta_{xr} = \frac{(a^2-u^2)(a^2-u_r^2)}{(q^2-u^2)(q^2-u_r^2)} . \tag{31}$$

It can be seen that $\beta_{xr} = 1.0$, when M = 1.0 and $\beta_{xr} = 0$ when $|u|$ or $|u_r| = a$.

2.3.4 SPECIAL θ-DIFFERENCE QUOTIENTS

Special difference quotients for ϕ_θ and $\phi_{\theta\theta}$ are derived in reference 3. These formulas are equivalent to the usual formulas to the order of $\Delta\theta^2$. They are considerably more accurate than the standard formulas if $\Delta\theta$ is large ($\Delta\theta = \pi/4$ or $\pi/2$) and ϕ is of the form

$$\phi(x,r,\theta) = \phi_1(x,r) + \phi_2(x,r)\sin\theta + \phi_3(x,r)\cos\theta \tag{32}$$

ϕ has approximately the above form in the far field for inlet computations, and in the near field if the inlet is nearly axisymmetric and centered on the axis. The advantage of the special formulas is improved accuracy for very coarse meshes. Such very coarse meshes can be desirable if a sequence of computational meshes is used for convergence acceleration. The formulas are

$$\phi_\theta = \left[\left(1-\cos\Delta\theta_\ell\right)\left(\phi_{i,j,k+1} - \phi_{i,j,k}\right) + \left(1-\cos\Delta\theta_u\right)\left(\phi_{i,j,k} - \phi_{i,j,k-1}\right)\right] \div \left[\sin\Delta\theta_\ell\left(1-\cos\Delta\theta_u\right) + \sin\Delta\theta_u\left(1-\cos\Delta\theta_\ell\right)\right] \tag{33}$$

$$\phi_{\theta\theta} = \left\{\sin\Delta\theta_\ell \phi_{i,j,k+1} - \left(\sin\Delta\theta_\ell + \sin\Delta\theta_u\right)\left[\frac{1}{\omega_\theta}\phi_{i,j,k} + \left(1 - \frac{1}{\omega_\theta}\right)\phi_{i,j,k}\right] + \sin\Delta\theta_u \phi_{i,j,k-1}\right\} \tag{34}$$

$$\div \left[\sin\Delta\theta_\ell \left(1 - \cos\Delta\theta_u\right) + \sin\Delta\theta_u \left(1 - \cos\Delta\theta_\ell\right)\right] .$$

The use of the above difference quotients instead of formulas 8, 9,and 17 is available as a program option.

2.4 SURFACE DERIVATIVES

Before the field is swept, the velocity is calculated at all surface points using all old ϕ values. The velocity components ϕ_{s_x}, ϕ_{s_r}, and $\phi_{s\theta}$ are computed first. These are the components of velocity along constant x, r, and θ cuts of surfaces, and, except at end points of the cuts, are computed using central-difference formulas similar to equation 8. One-sided differences are used at end points. Weighting is used to eliminate possible problems due to very closely spaced points. For any given surface point, only two of these velocity components can be computed in this manner. As an example, ϕ_{s_x} cannot be computed directly for an x-intersection surface point, that is, a point created by a mesh line parallel to the axis intersecting the surface.

At any point the remaining surface-derivative can be computed from

$$n_x\sqrt{n_r^2+n_\theta^2}\,\phi_{s_x} + n_r\sqrt{n_\theta^2+n_x^2}\,\phi_{s_r} + n_\theta\sqrt{n_x^2+n_r^2}\,\phi_{s_\theta} = 0 \tag{35}$$

if the magnitude of the direction cosine (n_x with ϕ_{s_x}, etc.) is not very small. If the magnitude of the direction cosine associated with the velocity component to be computed is very small, the above formula can be very badly behaved since it involves the reciprocal of the direction cosine. In such a situation, the missing velocity component is calculated by interpolating along one of the two cuts through the point. The cut selected is the one for which the interpolation will be the most accurate.

After all three surface velocities have been computed for each surface point, the velocity components ϕ_x, ϕ_r,and ϕ_θ for surface points are computed from

$$\phi_x = n_x\phi_n - n_r\sqrt{n_x^2+n_r^2}\,\phi_{s_\theta} + n_\theta\sqrt{n_x^2+n_\theta^2}\,\phi_{s_r}$$

$$\phi_r = n_r\phi_n - n_\theta\sqrt{n_r^2+n_\theta^2}\,\phi_{s_x} + n_x\sqrt{n_r^2+n_x^2}\,\phi_{s_\theta}$$

$$\frac{\phi_\theta}{r} = n_\theta\phi_n - n_x\sqrt{n_\theta^2+n_x^2}\,\phi_{s_r} + n_r\sqrt{n_\theta^2+n_r^2}\,\phi_{s_x} \qquad (36)$$

where $\phi_n = 0$.

These velocity components are used in the calculation of the cross-derivatives, ϕ_{xr}, $\phi_{r\theta}$, and $\phi_{\theta x}$, for subsonic flow, in the surface-point boundary-condition (eq. 47) under certain circumstances, and for the surface properties printed for program output.

2.5 FIELD-POINT DIFFERENCE EQUATIONS

A difference equation is generated for each field point. The difference equation is generated by dividing the partial differential equation (eq. 1) into terms and then splitting each term into a coefficient and an unknown. The unknown is the second derivative in the term, except for the last term of the equation where the unknown is taken as ϕ_r. The coefficients involve only first derivatives and are calculated using all old values of ϕ. The remaining part of the difference equation is linear in ϕ and theoretically could be solved simultaneously for the new potential values, ϕ^+, but as stated earlier, this is not practical. To make the solution process simpler for a single sweep or iteration, the unknowns are generated using difference quotients that have a mixture of old and new ϕ values.

The terms in the difference equation are listed in Table 1, including the coefficient, the unknown term, and an index to the difference quotients used in differencing for the unknown terms.

The difference equations are generated using a nonconservative approach. The terms conservative or nonconservative refer to whether or not the differencing scheme explicitly conserves mass. The principal flow region where this nonconservative scheme fails to conserve mass very well is at shocks. Other than at shocks, mass conservation can be improved by using a denser mesh. The errors caused by a failure to conserve mass exactly, as determined by comparison with experimental results, appear to be relatively small.

2.5.1 AXIS

Points on the axis are a special case because the potential equation expressed in cylindrical coordinates is singular on the axis. This is a problem with the coordinate system and not a physical problem with the flow. This problem is resolved by requiring 0 degrees, 90 degrees, 180 degrees, and 270 degrees to be in the θ mesh, and using the Cartesian form of the potential equation (eq. 3) at nodes on the axis.

For nodes on the axis, the terms in the potential equation are given in Table 2. Coordinates and notation are shown in figure 5. The points A, B, C, and D can be field or surface nodes. The differencing for ϕ_x and ϕ_{xx} is the same as for the equation in cylindrical coordinates. The differencing for ϕ_y and ϕ_z uses equation 8 or 9 with appropriate ϕ values and step sizes. The differencing for ϕ_{yy} and ϕ_{zz} uses difference quotients (eq. 16) with appropriate ϕ values and step sizes.

Table 1. Terms and Difference Quotients for Field-Point Difference Equations

TERM	COEFFICIENT	UNKNOWN	FORMULA(S) FOR SUBSONIC FLOW		FORMULA(S) FOR TRANSONIC FLOW	
			REGULAR	SURFACE ADJACENT	REGULAR	SURFACE ADJACENT
1.	$a^2-\phi_x^2$	ϕ_{xx}	14	14	19	20,21, 22,23
2.	$a^2-\phi_r^2$	ϕ_{rr}	16†	16†	19	20,21, 22,23
3.	$\left(a^2-\frac{\phi_\theta^2}{r^2}\right)\frac{1}{r^2}$	$\phi_{\theta\theta}$	17,34**	17,34**	19	20,21, 22,23
4.	$-2\phi_x\phi_r$	ϕ_{xr}	24*	24*	26	27,28,29
5.	$-2\phi_r\phi_\theta\frac{1}{r^2}$	$\phi_{r\theta}$	24*	24*	26	27,28,29
6.	$-2\phi_\theta\phi_x\frac{1}{r^2}$	$\phi_{\theta x}$	24*	24*	26	27,28,29
7.	$\left(a^2+\frac{\phi_\theta^2}{r^2}\right)\frac{1}{r}$	ϕ_r	8†	9†	8†	9†

* USES ALL OLD VALUES OF ϕ
† USES ALL NEW VALUES OF ϕ ,(ϕ^+)
** OPTIONAL FORMULA

Table 2. Terms for the Difference Equation in Cartesian Coordinates

	TERM	COEFFICIENT	UNKNOWN
1.	$\left(a^2-\phi_x^2\right)\phi_{xx}$	$a^2-\phi_x^2$	ϕ_{xx}
2.	$\left(a^2-\phi_y^2\right)\phi_{yy}$	$a^2-\phi_y^2$	ϕ_{yy}
3.	$\left(a^2-\phi_z^2\right)\phi_{zz}$	$a^2-\phi_z^2$	ϕ_{zz}
4.	$-2\phi_x\phi_y\phi_{xy}$	$-2\phi_x\phi_y$	ϕ_{xy}
5.	$-2\phi_y\phi_z\phi_{yz}$	$-2\phi_y\phi_z$	ϕ_{yz}
6.	$-2\phi_z\phi_x\phi_{zx}$	$-2\phi_z\phi_x$	ϕ_{zx}

The cross-derivatives for subsonic flow are calculated as follows:

$$\begin{aligned}
\phi_{xy} &= \frac{\partial}{\partial y}\left(\phi_x\right), \\
\phi_{yz} &= \frac{1}{2}\frac{\partial}{\partial y}\left(\phi_z\right) + \frac{1}{2}\frac{\partial}{\partial z}\left(\phi_y\right), \\
\phi_{zx} &= \frac{\partial}{\partial z}\left(\phi_x\right).
\end{aligned} \tag{37}$$

As an example,

$$\frac{\partial}{\partial y}\left(\phi_z\right) = \frac{\Delta y_2^{\,2} u_\theta\big|_A + \left(\Delta y_1^{\,2}-\Delta y_2^{\,2}\right)\phi_z\big|_{i,1,1} + \Delta y_1^{\,2} u_\theta\big|_B}{\Delta y_1 \Delta y_2 \left(\Delta y_1+\Delta y_2\right)} \tag{38}$$

where $u_\theta|_A$, $u_\theta|_B$, and $\phi_z|_{i,1,1}$ have been previously calculated.

A typical supersonic-flow difference quotient for $\phi_y > a$ and $\phi_z > a$ is

$$\phi_{yz} = \frac{\dfrac{\phi^{+}_{i,1,1} - \phi_D}{\Delta z_2} + u_\theta|_B}{\Delta y_2} . \tag{39}$$

Changes are made in the differencing at the axis if flow symmetry planes are used. If the flow is symmetrical about the plane defined by $\theta = 0$ degrees or 180 degrees, ϕ_z equals zero on the plane of symmetry, and the potential equation for $\theta = 0$ degrees or 180 degrees becomes

$$\left(a^2 - \phi_x^2\right)\phi_{xx} + \left(a^2 - \phi_y^2\right)\phi_{yy} + a^2\phi_{zz} - 2\phi_x\phi_y\phi_{xy} = 0 . \tag{40}$$

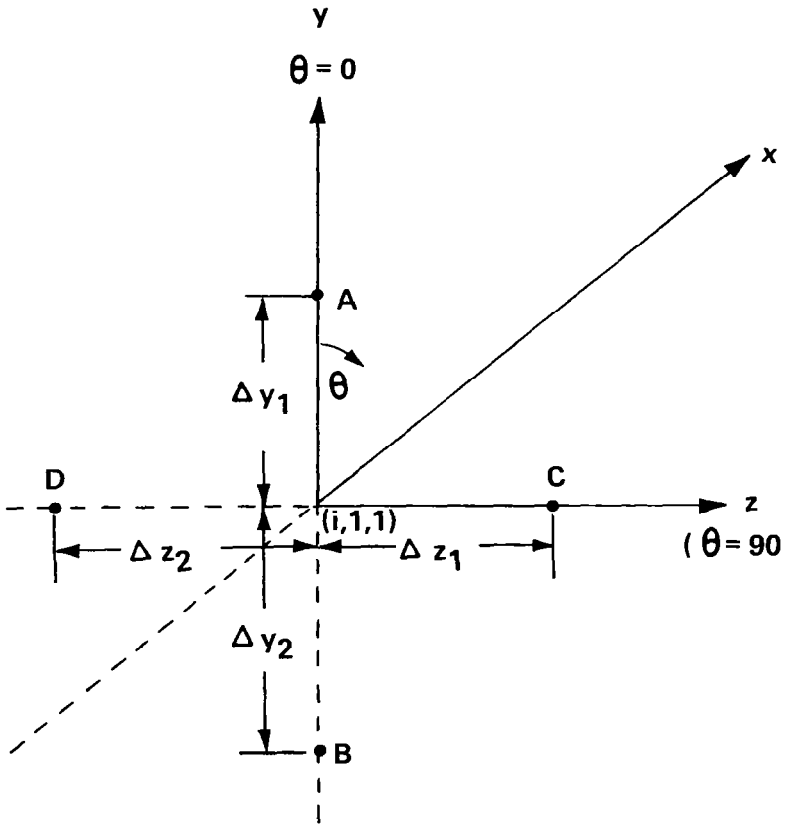

Figure 5. Notation for the Axis

The difference quotient ϕ_{zz} is obtained by setting $\phi_D = \phi_C$ and $\Delta z_2 = \Delta z_1$. If the plane defined by $\theta = \theta_\xi$ is also a plane of symmetry, then ϕ_y and ϕ_z must be equal to 0.0 at the axis, and at the axis the potential equation is

$$\left(a^2-\phi_x^2\right)\phi_{xx} + a^2\phi_{yy} + a^2\phi_{zz} = 0 , \tag{41}$$

and it can be shown that

$$\phi_{zz} = \left(\phi_{\xi\xi} - \cos^2\theta_\xi \phi_{yy}\right) / \sin^2\theta_\xi , \tag{42}$$

where $\xi = r$ for $\theta = \theta_\xi$.

2.5.2 MODIFIED DIFFERENCE EQUATION FOR FIELD POINTS ADJACENT TO SURFACE

The finite-difference equation for a field point next to one or more surface points can cause numerical problems if the spacing to adjacent surface points is small relative to the local mesh spacing. The analysis uses the flow equation at the field point when the field point is not close to surface points. An interpolation equation is used to obtain the field-point ϕ value when the surface and the field point are very close. This is accomplished by the following formulas which weight between the flow equation and interpolation formulas depending on the step size(s) between the field point and the surface point(s).

The weights β_x, β_r, and β_θ for the x, r, and θ interpolation formulas, respectively, are computed by using the following relationships. The equations presented are based on the configuration of figure 3c. Cubic interpolation is used.

$$\beta_{1x} = \begin{cases} 1 - 2\Delta x_1/\Delta x_0 & 2\Delta x_1 < \Delta x_0 \\ 0 & 2\Delta x_1 \geq \Delta x_0 \\ 0 & \text{if the field point is not adjacent in x to a surface point} \end{cases} \tag{43}$$

The formulas for β_{1r} and $\beta_{1\theta}$ are similar.

$$\beta_x = \beta_{1x} - \tfrac{1}{2}\beta_{1x}\left(\beta_{1r}+\beta_{1\theta}\right) + \tfrac{1}{3}\beta_{1x}\beta_{1r}\beta_{1\theta} . \tag{44}$$

The formulas for β_r and β_θ are similar.

The interpolation equation for x interpolation is

$$\phi_A^+ = \eta^2(3-2\eta)\phi_S^+ + (1-\eta)^2(1+2\eta)\phi_B^* - \eta(1-\eta)\left[\eta\phi_\eta\Big|_S - (1-\eta)\phi_\eta\Big|_B\right]$$

where

$$\eta = \Delta x_2 / \left(\Delta x_1 + \Delta x_2\right)$$

and

$$\phi_\eta = \left(\Delta x_1 + \Delta x_2\right)\phi_x \tag{45}$$

and ϕ_B^* is either ϕ_B or ϕ_B^+ if a new value of ϕ is available at B.

The final difference equation for ϕ at the field point A is

$(1 - \beta_x - \beta_r - \beta_\theta)$ (Difference representation of the potential equation)
$+ C\beta_x$ (x-interpolation equation)
$+C\beta_r$ (r-interpolation equation)
$+ C\beta_\theta$ (θ -interpolation equation) = 0 (46)

where C is the coefficient of ϕ_A^+ in the regular-difference flow equation for point A.

2.6 SURFACE-POINT DIFFERENCE EQUATIONS

The boundary condition at solid surfaces is that there is no flow through the surface, which requires that the velocity normal to the surface, ϕ_n, be zero. The velocity, ϕ_n, can be expressed in terms of its components and the direction cosines (n_x, n_r, n_θ) of the unit surface normal, $\bar{n}$,

$$\phi_n = n_x\phi_x + n_r\phi_r + n_\theta\frac{\phi_\theta}{r} \tag{47}$$

Referring to figure 6 for notation, the difference equation for the surface boundary condition for a surface point created by a radial mesh line intersecting the surface (r-intersect surface point) is

$$n_x \left[2\frac{\phi_S^+ - \phi_{P''}}{\Delta x} - \phi_x\Big|_{P''} \right] + n_r \left\{ \beta \left[2\frac{\phi_A^+ - \phi_S^+}{\Delta r_1} - \phi_r\Big|_A \right] \right.$$

$$\left. + (1-\beta) \left[2\frac{\phi_B^+ - \phi_S^+}{\Delta r_1 + \Delta r_2} - \phi_r\Big|_B \right] \right\} + \frac{n_\theta}{r} \left[2\frac{\phi_S^+ - \phi_{P'}}{\Delta\theta} - \phi_\theta\Big|_{P'} \right]$$

$$- \phi_n = 0 ,$$

where

$$\beta = \begin{cases} \left(2\Delta r_1 / \Delta r_0\right)^2 & 2\Delta r_1 < \Delta r_0 \\ 1 & 2\Delta r_1 \geq \Delta r_0 \end{cases} . \qquad (48)$$

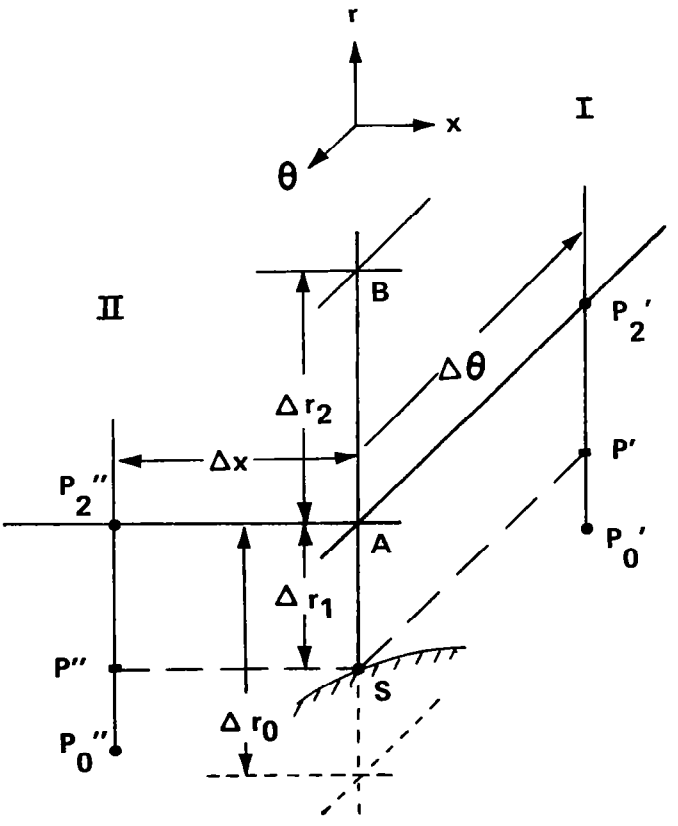

Figure 6. Nomenclature for Typical Surface-Point Boundary-Condition Equation

Currently ϕ_n is taken as zero, however, the difference equation is expressed in terms of ϕ_n anticipating a later version of the code accounting for boundary-layer displacement effects by using appropriate ϕ_n values.

The values of ϕ at the points P′ and P″ are obtained by cubic interpolation using the values of ϕ and ϕ_r at points P_0 and P_2. As an example

$$\phi_{P'} = \eta^2(3-2\eta)\phi_{P_0} + (1-\eta)^2(1+2\eta)\phi_{P_2} - \eta(1-\eta)\left[\eta\phi_\eta\Big|_{P_0} - (1-\eta)\phi_\eta\Big|_{P_2}\right] \tag{49}$$

where

$$\eta = \Delta r_1 / \Delta r_0$$

and

$$\phi_\eta = -\Delta r_0 \phi_r .$$

The values of ϕ_θ at P′ and ϕ_x at P″ are obtained by linear interpolation between points P_0 and P_2. As an example,

$$\phi_\theta\Big|_{P'} = \eta\phi_\theta\Big|_{P_0} + (1-\eta)\phi_\theta\Big|_{P_2} . \tag{50}$$

The point P_0 may be a field or surface node depending on geometry.

If the point P′ or P″ does not lie in the flowfield (i.e., is interior to the surface), equation 48 is modified by using the value for ϕ_θ or ϕ_x (for P′ or P″ respectively) computed by differencing along the surface. (See Section 2.4.)

The formulas for θ or x surface intersections are similar.

If the surface point is also a field-point mesh node, P′ and P″ are field points, point B is not used, and $\beta = 1.0$. If the surface point is on the axis or adjacent to the axis, some modifications to the formulas are made.

2.7 SOLUTION PROCEDURE

For problems such as this one which require significant quantities of computer resources (central-processor time, memory, etc.), it is essential that the code be organized for maximum efficiency. This includes such aspects as organizing the computation to minimize the amount of information transferred and the number of times information is transferred between core and disk memory. This can be done by

careful planning of the sequence of computations as well as reducing memory requirements to a minimum. Computer central-processor time requirements can be greatly affected by the sequence in which order independent quantities are calculated.

2.7.1 CODE ORGANIZATION

One of the major problems with three-dimensional codes is storage in the computer. Storing a three-dimensional field when using a typical mesh requires a large number of words. For example, an inlet mesh with x, r, and θ dimensions of 81 x 41 x 16, respectively, requires 53136 locations for the potential function alone. If a copy of the potential function at a previous step is required for extrapolation or other convergence acceleration procedures, another 53136 locations are required. Any geometric information requires additional storage. Since these numbers are large compared to what is available, even for the vector computers such as the CYBER 203, it is essential that the scheme used for storing and accessing geometrical information be designed to minimize storage requirements. Disk storage may be used to provide more memory, but there are large time penalties for using disk storage; thus it is desirable to minimize its use.

Storing a flag or index for each field point so that the code can determine if the field point is next to the surface, and if so, which surface point, requires at least one storage location for each field point. This type of scheme is conceptually simple, but inefficient. To minimize storage and maximize the percentage of vector code, an inverse scheme is used in this code. Surface-affected field points are processed by sweeping through the surface points. A bit array rather than a full word (64 bits) array is used to signal whether grid points are in the flowfield or not. A bit array is used for each of the three coordinates to mark whether field points are surface-adjacent in either or both directions in that coordinate. Total storage for the four bit arrays is 4/64 of 53136 or 3321 words. The bit arrays are used to inhibit storage of contributions to coefficients from regular field-point formulas when the field point is irregular (surface-affected). The correct contributions to coefficients of the finite-difference equations are then generated and stored by sweeping through the surface points.

The geometric information stored for each surface point includes the index of the adjacent field point.

Code efficiency on a vector machine is improved by ensuring that most computation is done in a vector mode. On the CYBER 203, longer vectors (up to a maximum length of 65536) give higher computation rates. However, most vector computation involves intermediate results which are also vectors and must be stored. Hence there is a trade between the additional memory required for the intermediate vectors and the inceased computation rates obtained using longer vectors. For this problem, computing coefficients for one axial plane at one time appears to be a reasonable tradeoff.

Surface points are grouped by type, adjacent in x, adjacent in r, adjacent in θ, or both a surface point and a field point, for each axial plane (plane perpendicular to axis). Quantities needed for coefficient calculation are gathered for all surface points of the same type, the coefficients are then calculated as a group using vector arithmetic, and the contributions to the coefficients are then scattered to the correct field-point

equations. This maximizes the number of vector calculations and minimizes the storage of geometric information. The primary penalty is the inefficiency of the gathering and scattering operations on the CYBER 203. The gather/scatter operations are more efficient on some other computers, and on the CYBER 205 which is the successor to the CYBER 203.

2.7.2 PROCEDURE FOR SWEEPING

The sequence of computations for taking a single relaxation sweep, or iteration, for a given mesh follows:

I. The three components of velocity are calculated for all surface nodes.

II. The field is swept one axial plane (constant x) at a time in the direction of increasing x.

   A. The three components of velocity at all field nodes are calculated for the axial plane ahead of the one being processed. (The velocities are saved for the plane being swept and the planes adjacent to the plane being swept.)

   B. The coefficients for the surface-node difference equations for all surface nodes on or adjacent to the plane being processed are calculated.

   C. The coefficients for the terms in the partial differential equation are calculated for all field nodes.

   D. The coefficients of the difference equation for all field-point nodes are calculated.

   E. The surface-node equations are used to eliminate the values of ϕ at surface nodes from the field-point difference equations.

   F. The first radial line of difference equations is solved including the value for ϕ on the axis.

   G. The new value of ϕ on the axis is used in the solution of all remaining radial lines.

   H. The new ϕ values at field nodes are substituted into the surface-point difference equations and new values of ϕ are obtained at all surface nodes.

III. The entire field has been updated and a decision is made on whether to continue sweeping, extrapolate, change meshes,or stop.

2.7.3 CONVERGENCE ACCELERATION

The basic method described above is stable and convergent, but the rate of convergence for dense meshes can be very slow and computer times significant. There is substantial benefit from any procedure that will speed convergence and decrease the cost of a solution. Analysis and code development have been structured to facilitate the use of various techniques for convergence acceleration. One technique currently used is extrapolation of solutions as described in reference 6. The theory for

this technique can be obtained by approximating the solution process as a linear one and looking at the eigenvalues of a matrix. The number of eigenvalues is of the order of the number of field points. This approach behaves best when the eigenvalues are discrete, which is more likely when there are few of them. As a consequence, this technique works best for very coarse meshes and much less satisfactorily for fine meshes.

If $\phi^{(n)}$ is ϕ at iteration n, and $\| \quad \|$ is a norm, then

$$\lambda = \frac{\left\|\phi^{(n)}\right\|}{\left\|\phi^{(n-1)}\right\|} \tag{51}$$

and the extrapolation formula is

$$\phi_{\text{extrapolated}} = \frac{1}{1-\lambda}\left(\phi^{(n)} - \phi^{(n-1)}\right) + \phi^{(n-1)} . \tag{52}$$

In practice, two norms are calculated after each sweep

$$\left\|\phi^{(n)}\right\|_1 = \sum_{\substack{\text{all field} \\ \text{nodes}}} \left|\phi_{i,j,k}^{(n)} - \phi_{i,j,k}^{(n-1)}\right| \tag{53}$$

and

$$\left\|\phi^{(n)}\right\|_2 = \text{maximum} \left|\phi_{i,j,k}^{(n)} - \phi_{i,j,k}^{(n-1)}\right| \tag{54}$$

where the maximum is taken over all field nodes.

Extrapolation occurs whenever the eigenvalues λ_1 and λ_2 corresponding to $\| \quad \|_1$ and $\| \quad \|_2$ are steady and approximately the same for several sweeps. If they are reasonably close to being constant for several sweeps, it is assumed that the problem is behaving linearly and an extrapolation of the field will be of benefit.

Another technique for convergence acceleration is initial convergence on a coarse mesh to obtain an approximate solution, continuation of the convergence on a medium-density mesh to obtain a more accurate approximation of the solution, and then final convergence on a fine mesh. The number of mesh for each coordinate is doubled for every successive mesh. There is approximately a factor of 16 change in

convergence rate per sweep, in terms of computer central-processor time, between successive meshes. This arises due to a factor of eight change in number of mesh points, and a factor of two in the rate of ϕ change per sweep. Once the solution nears convergence on one of the coarse meshes, there is no further gain in continuing relaxation on the mesh because of the large truncation errors. For the meshes used in the calculations of this report, there was about one-third decrease in run time using this approach. The reason for such a small improvement is the very slow convergence on the final mesh. It takes half as many sweeps to improve the solution from coarse meshes on the final mesh as it would to do the entire calculation using the finest mesh. Very good convergence on a coarse mesh takes less than 100 sweeps. Good convergence using the fine mesh exclusively takes about 400 sweeps. Use of a still finer mesh starts to become very impractical due to the number of sweeps required and the time per sweep.

Parametric cubic interpolation as described in appendix B is used to interpolate the solution from the current mesh to the next finer mesh.

A further refinement on convergence acceleration is the multilevel technique described by Brandt[8]. This procedure uses coarse meshes to resolve the errors determined on finer meshes. The number of sweeps required on the finest mesh should be small (on the order of ten to thirty) and independent of the fineness of the mesh. The majority of sweeping would be on the coarsest mesh. As can be seen from the discussion of the preceding paragraph this technique becomes better and better, relative to the existing approach, as the meshes become denser. This analysis has been established with the anticipation of implementing a multilevel procedure in the future.

2.8 GEOMETRY SPECIFICATION

The basic analysis procedure described has no inherent limitations on kinds of geometries that can be analyzed, but any implementation on the computer does have limitations. Two sources of limitations are the number of mesh that can be used and the boundary conditions that can be applied. A limitation independent of the flow analysis code is the user's ability to specify the geometry and extract the surface/mesh intersections.

The computer code for this analysis requires that all intersections of the mesh with the geometry, plus components of the surface normals, be input. The flow code then orders the points and makes some checks for completeness and consistency. The actual values could come from any source; no particular order is assumed by the flow code. The three-dimensional geometries used as samples in this report were described by a geometry system[9] which breaks the surface into subsections or patches. The coordinates of the surface on the patch are specified by parametric bicubics. This leads to an explicit specification of the surface. A separate program exists to intersect the surface so described, with a computational mesh and to generate the coordinates and surface normals at the mesh intersections.

2.9 RESULTS

Comparisons between the analysis and experiment have been made for two asymmetric geometries. In addition, a mixer-lobe geometry has been analyzed to verify the program's general three-dimensional capabilities, although no experimental results are available for comparison. The first comparison between

theory and experiment is for an asymmetric tilt-nacelle V/STOL airplane inlet, tested in the NASA-Ames Research Center's 40- by 80-ft wind tunnel. Figure 7 presents a graphic display of the inlet and spinner geometry. The geometry description used in the analysis is smooth and the entire inlet is specified. Only half the inlet is shown in figure 7, and curves are represented using linked straight-line segments due to limitations of the plotting equipment. The test and results of the test are described in reference 10. Tabular data from the test is found in reference 11.

Predictions of the analysis have been compared with experimental measurements for three test cases (figs. 8, 9, and 10). There are two comparisons for an angle of attack of 60 degrees. The second comparison is for a greater airflow and freestream Mach number than the first. The last comparison is for an angle of attack of 90 degrees. The analysis predicts the experimentally measured Mach number distribution very closely. There is a slight, but consistent, under-prediction of the peak Mach number. This is possibly due to grid density and is discussed later. The only poor prediction is for the external lee side for 90 degree angle of attack (fig. 10). This probably is an interference or boundary-layer effect in the experiment.

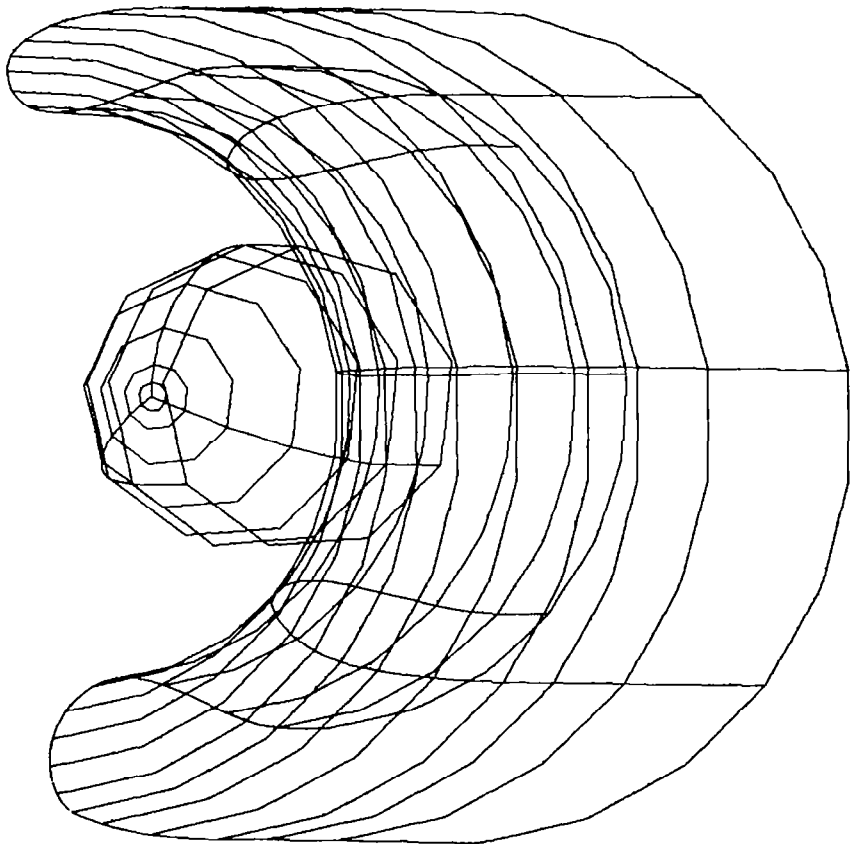

Figure 7. Graphical Display of V/STOL Airplane Inlet Geometry

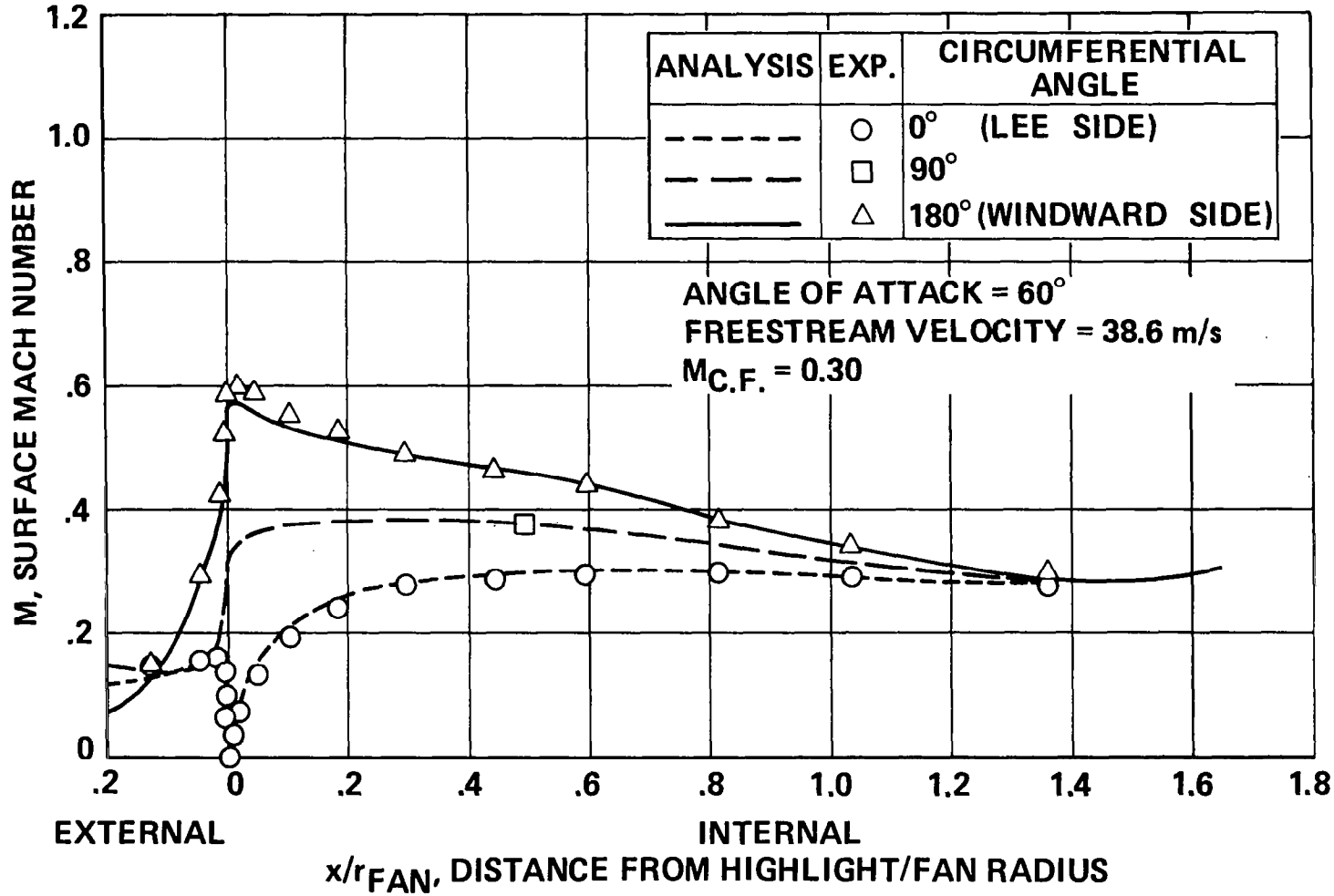

Figure 8. Cowl Surface Mach Number Distribution for an Asymmetric V/STOL Airplane Inlet

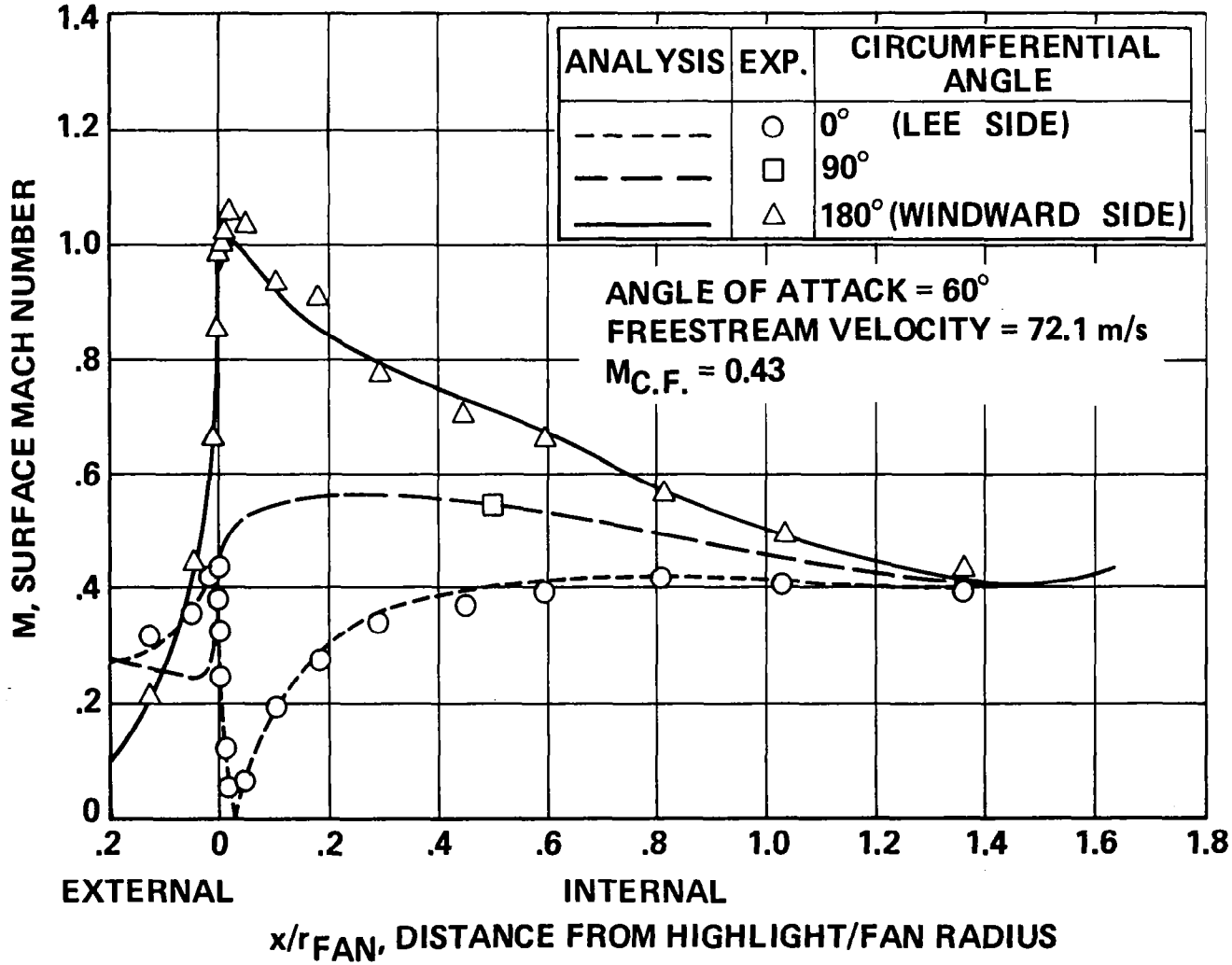

Figure 9. Cowl Surface Mach Number Distribution for an Asymmetric V/STOL Airplane Inlet

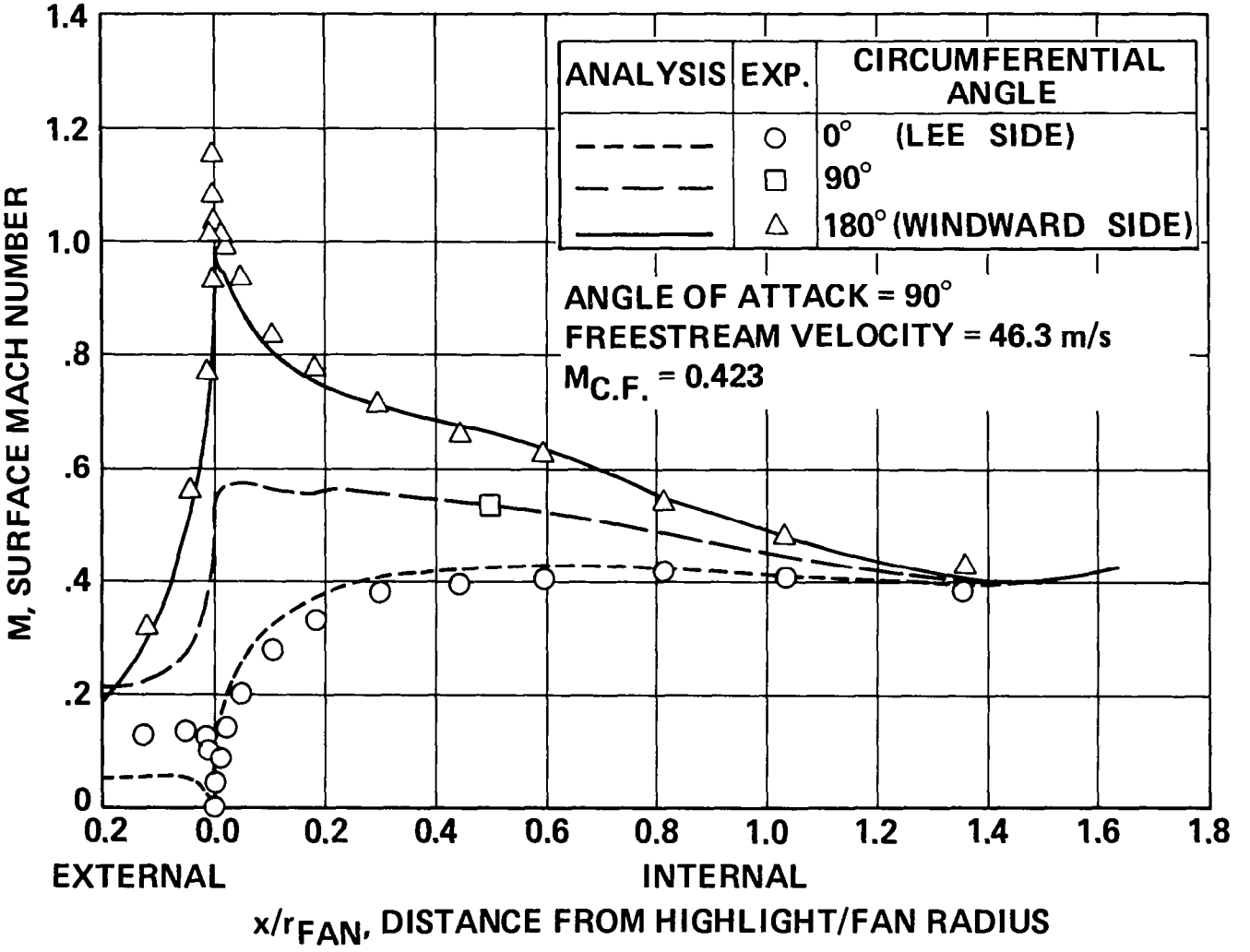

Figure 10. Cowl Surface Mach Number Distribution for an Asymmetric V/STOL Airplane Inlet

A series of comparisons have been made for a typical commercial-transport turbofan-engine inlet design. It has an asymmetric lip section varying both in section shape and contraction ratio. The contraction ratio on the lee side is 1.246 and on the windward side 1.28. The inlet was designed with an axisymmetric diffuser. The inlet centerline is tilted down five degrees with respect to the engine centerline and a short transition region exists between the inlet and the compressor (fan) face. This tilt of the inlet centerline is to reduce cruise drag by aligning the inlet with the local flowfield while still placing the engine and hence its thrust vector in the desired orientation. The inlet flowfield was computed using engine-centerline oriented coordinates, and as a consequence, the inlet appears very asymmetric. A cross-section of the inlet along with a computational mesh is shown in figure 11. Dimensions are in meters for the full-scale inlet.

A 0.16 scale model of the inlet has been tested* in the Boeing 9- by 9-ft low-speed propulsion wind tunnel. The same inlet configuration in a 0.47 scale was tested[12] in the NASA-Ames Research Center's 40- by 80-ft wind tunnel. The NASA-Ames test model was modified slightly in the vicinity of the fan face to attach to a different engine than that for which the inlet was originally designed. The Boeing 9- by 9-ft tunnel test used a suction source instead of an engine at the fan face. The 9- by 9-ft tunnel test gave results at greater airflows than could be obtained in the Ames test.

The comparisons between analysis and experiment for the 0.16 scale model are shown in figures 12 and 13. Figures 14 and 15 show results for the 0.47 scale model. The most significant discrepancy between the results of the analysis and the experimental measurements is for the greatest peak Mach number (fig. 13). Some of the discrepancy is due to blockage effects of a thick boundary layer in the diffuser on the windward side. This condition is near where the inlet boundary layer separates. The analysis curves are drawn to the compressor station. As the inlet is tilted relative to the engine, each curve ends at a different inlet centerline station.

A single lobe of a mixer has been analyzed with this code. The lobe is shown in figure 16. This is a shaded-graphic representation[13] of the upper surface of the mixer. The inner surface was a constant-diameter cylinder. The lobe extended from 0 degrees to 45 degrees and represents one lobe of an eight-lobe jet-engine mixer nozzle. Half a lobe could have been analyzed by taking advantage of the center plane of symmetry. The mixer shape was developed as a computer-program test case and not an actual mixer. It is shown to illustrate possible applications of the code. As there is no experiment with which to compare, the computed results are not shown. Use of the code for configurations other than inlets should include code validation by comparison of predictions with experiments for such configurations.

2.10 ACCURACY

The comparison between analysis and experiment for the V/STOL airplane inlet (figs. 8, 9, and 10) show almost perfect agreement except at the point of peak Mach number on the windward side of the inlet. The progression of peak Mach number values for the case of figure 9 is 0.743, 0.893, and 1.007 for the three mesh levels used, clearly indicating a trend of an increase in peak Mach number for finer meshes. It is believed that the fine mesh used is the coarsest that will yield adequate accuracy for inlet

*Boeing data, unpublished.

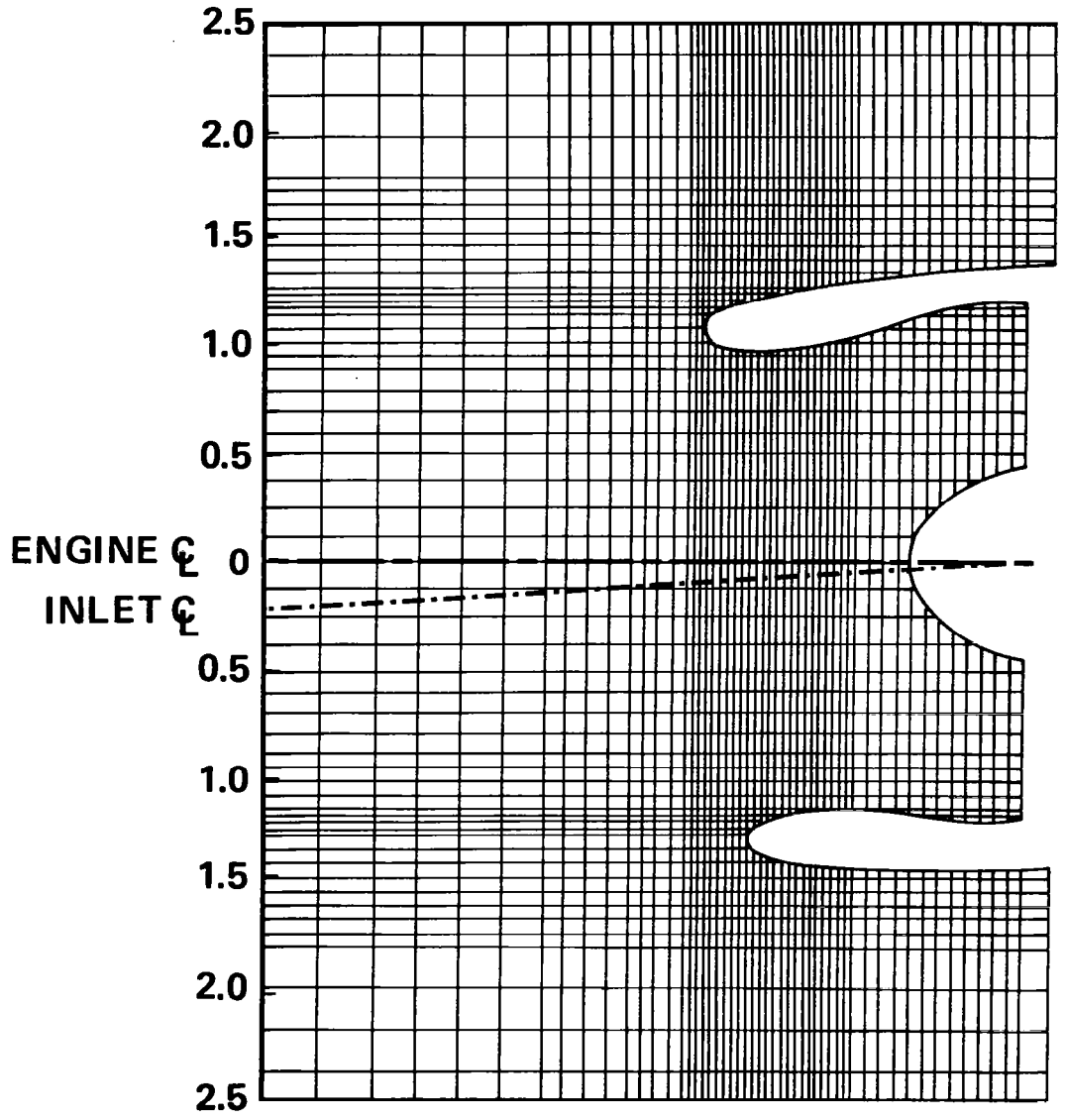

Figure 11. Computational Flowfield and Mesh in the Vicinity of a Commercial-Transport Turbofan-Engine Type Inlet

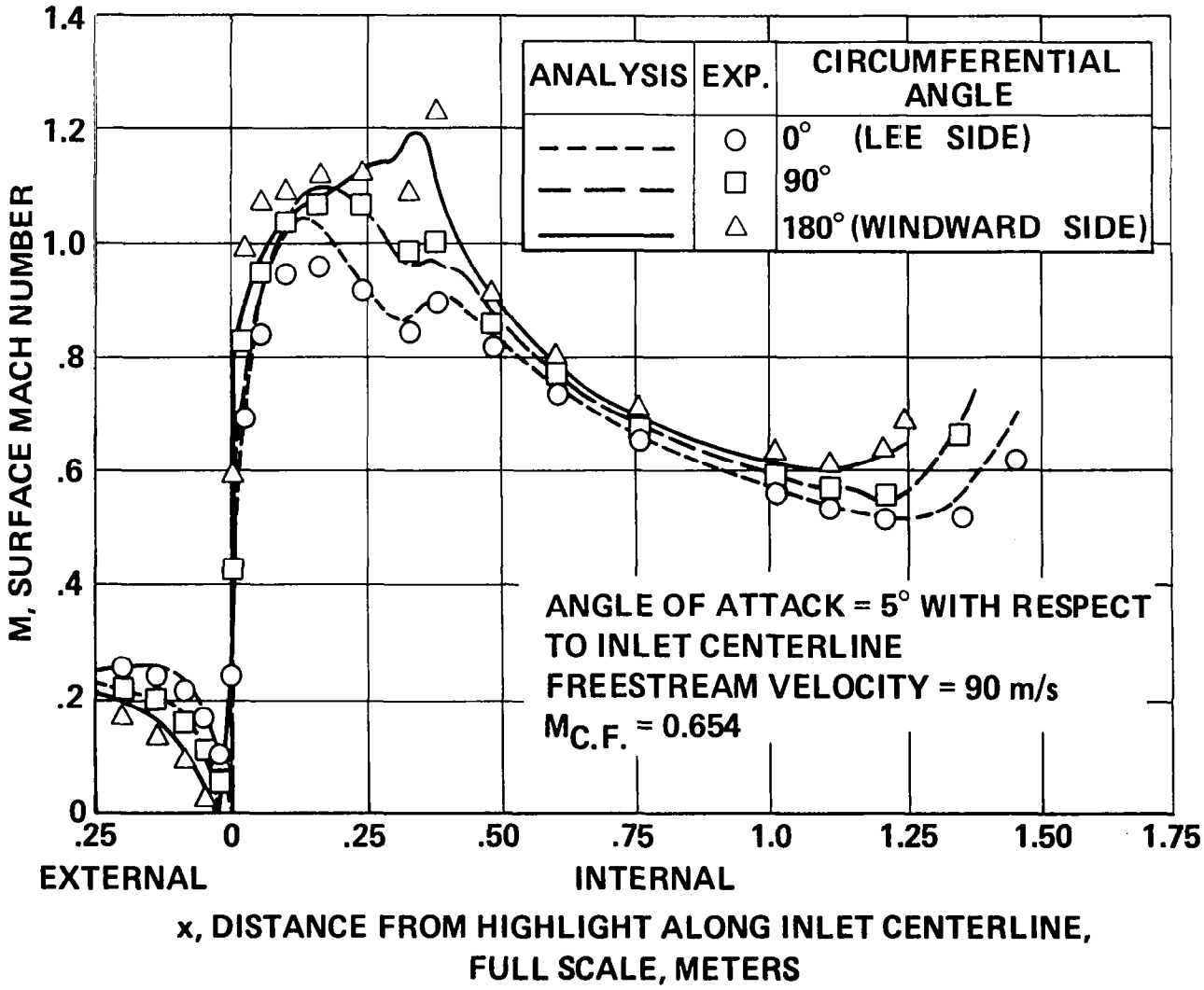

Figure 12. Cowl Surface Mach Number Distribution for an Asymmetric Commercial-Transport Turbofan-Engine Type Inlet

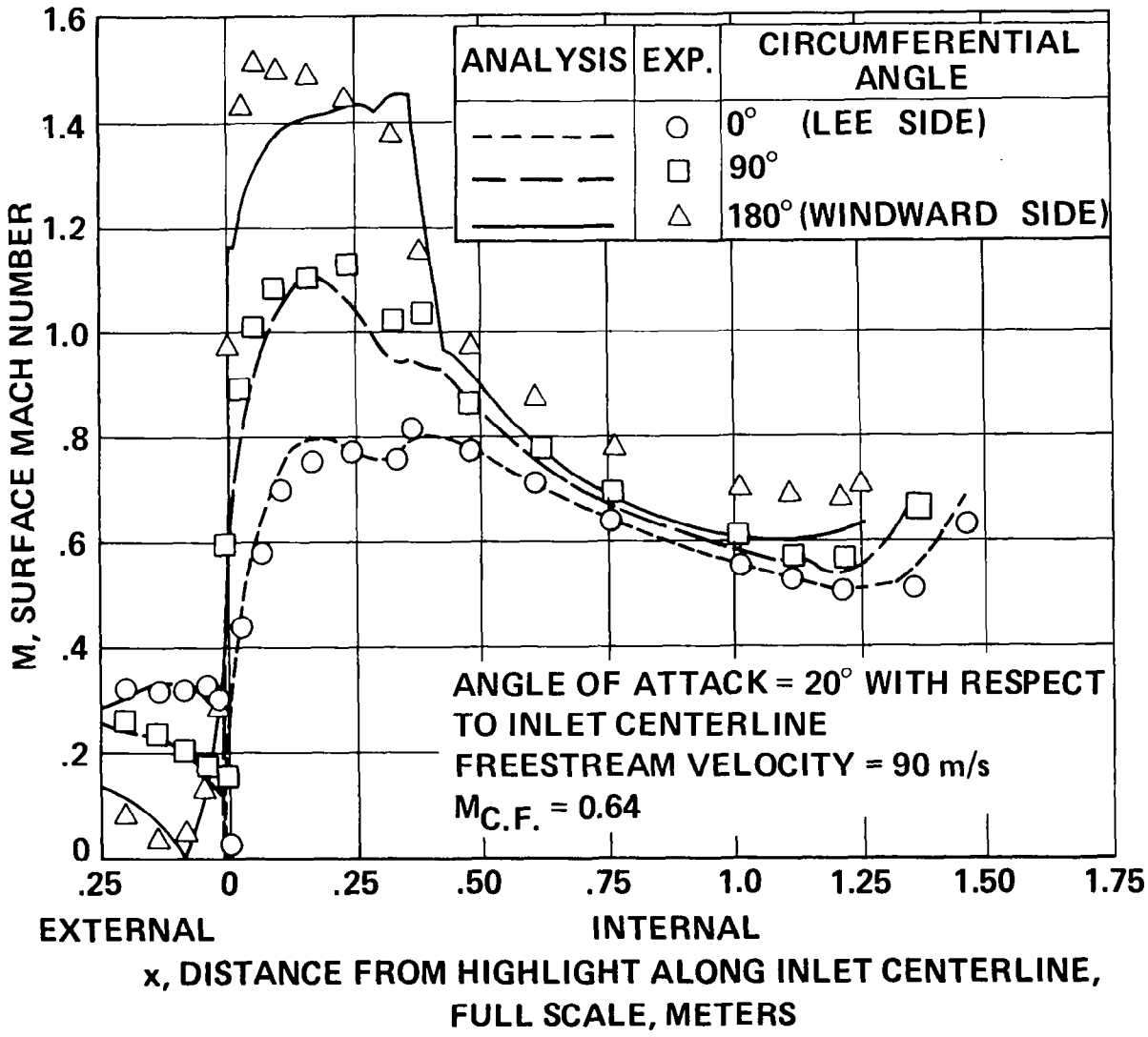

Figure 13. Cowl Surface Mach Number Distribution for an Asymmetric Commercial-Transport Turbofan-Engine Type Inlet

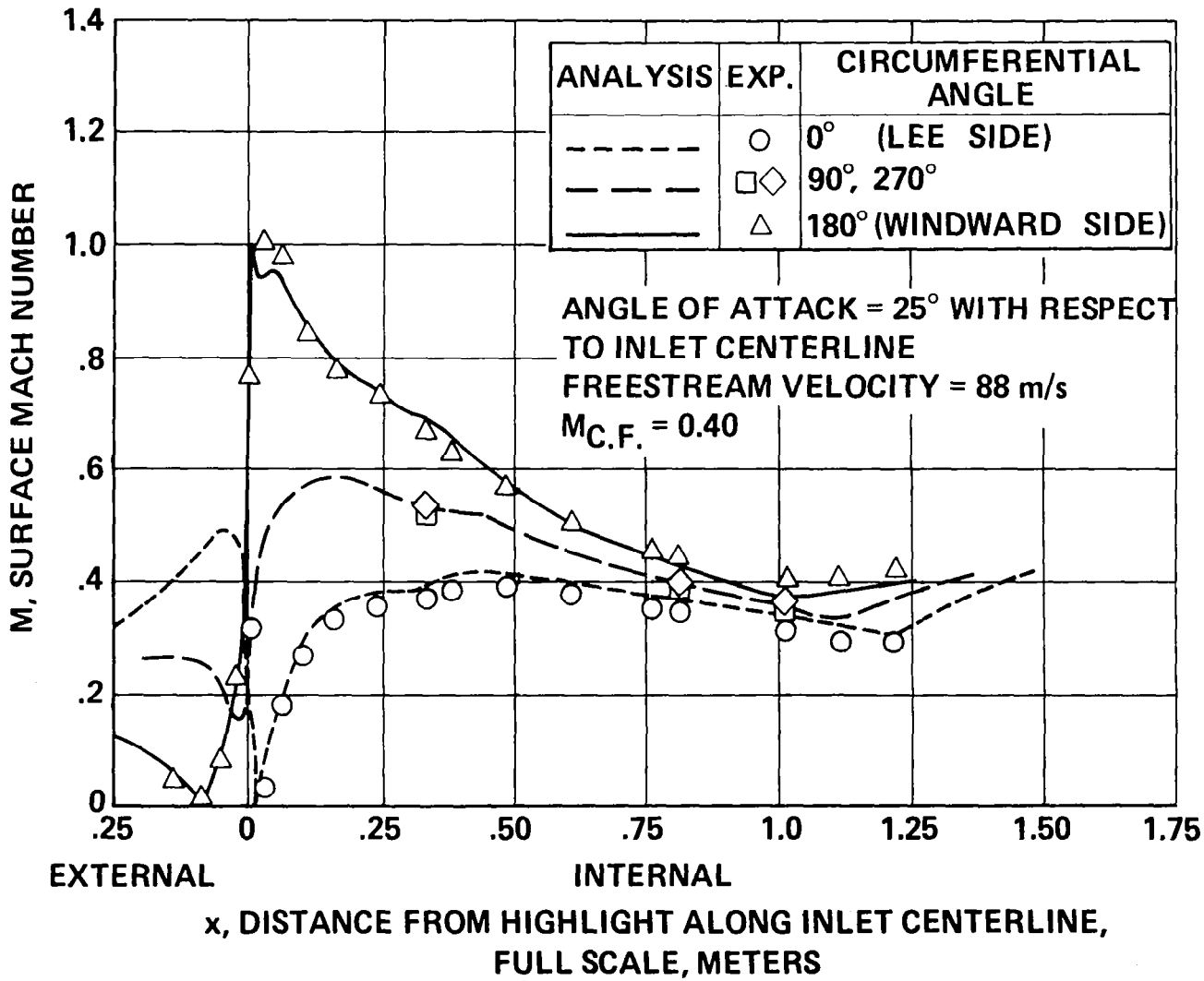

Figure 14. Cowl Surface Mach Number Distribution for an Asymmetric Commercial-Transport Turbofan-Engine Type Inlet

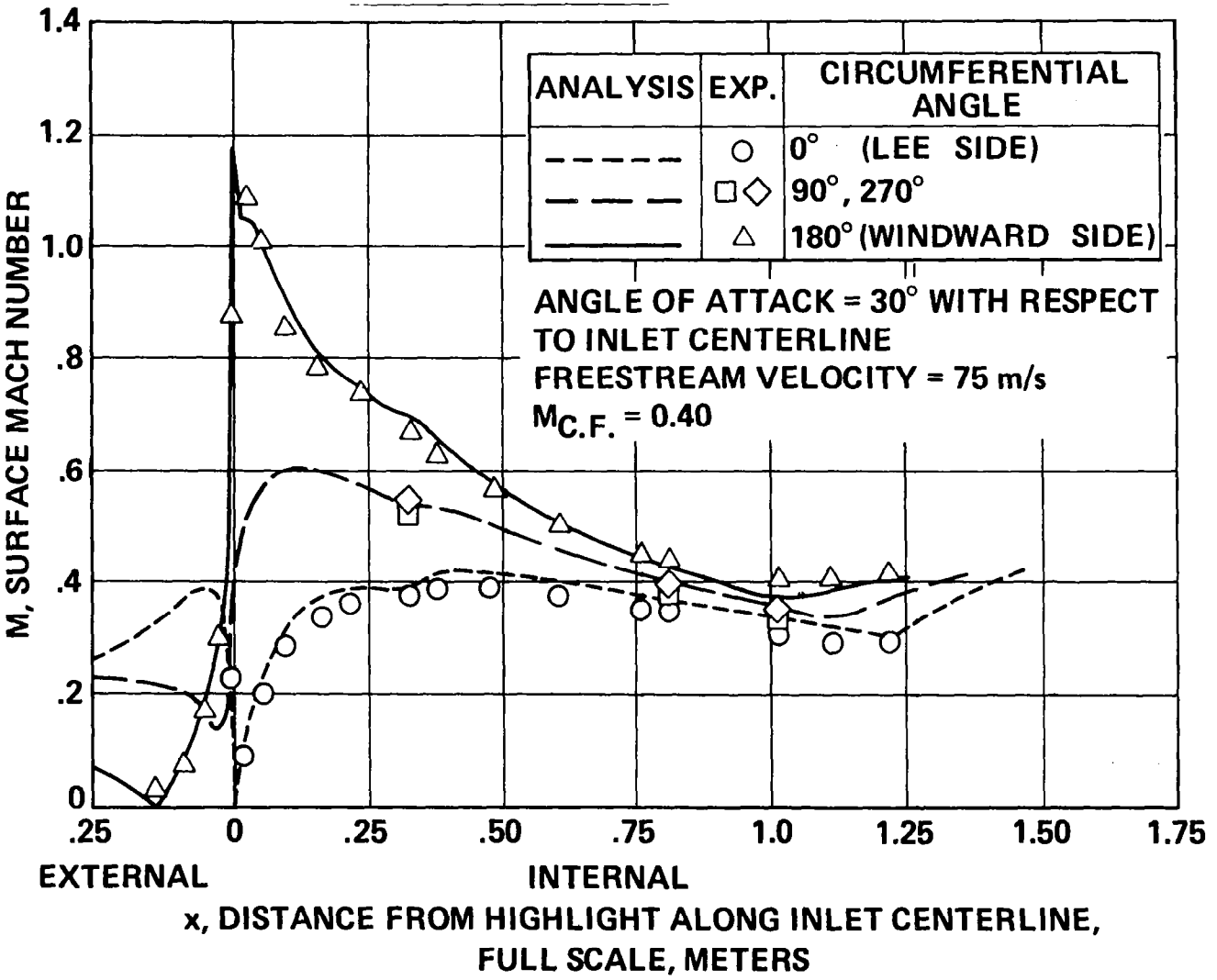

Figure 15. Cowl Surface Mach Number Distribution for an Asymmetric Commercial-Transport Turbofan-Engine Type Inlet

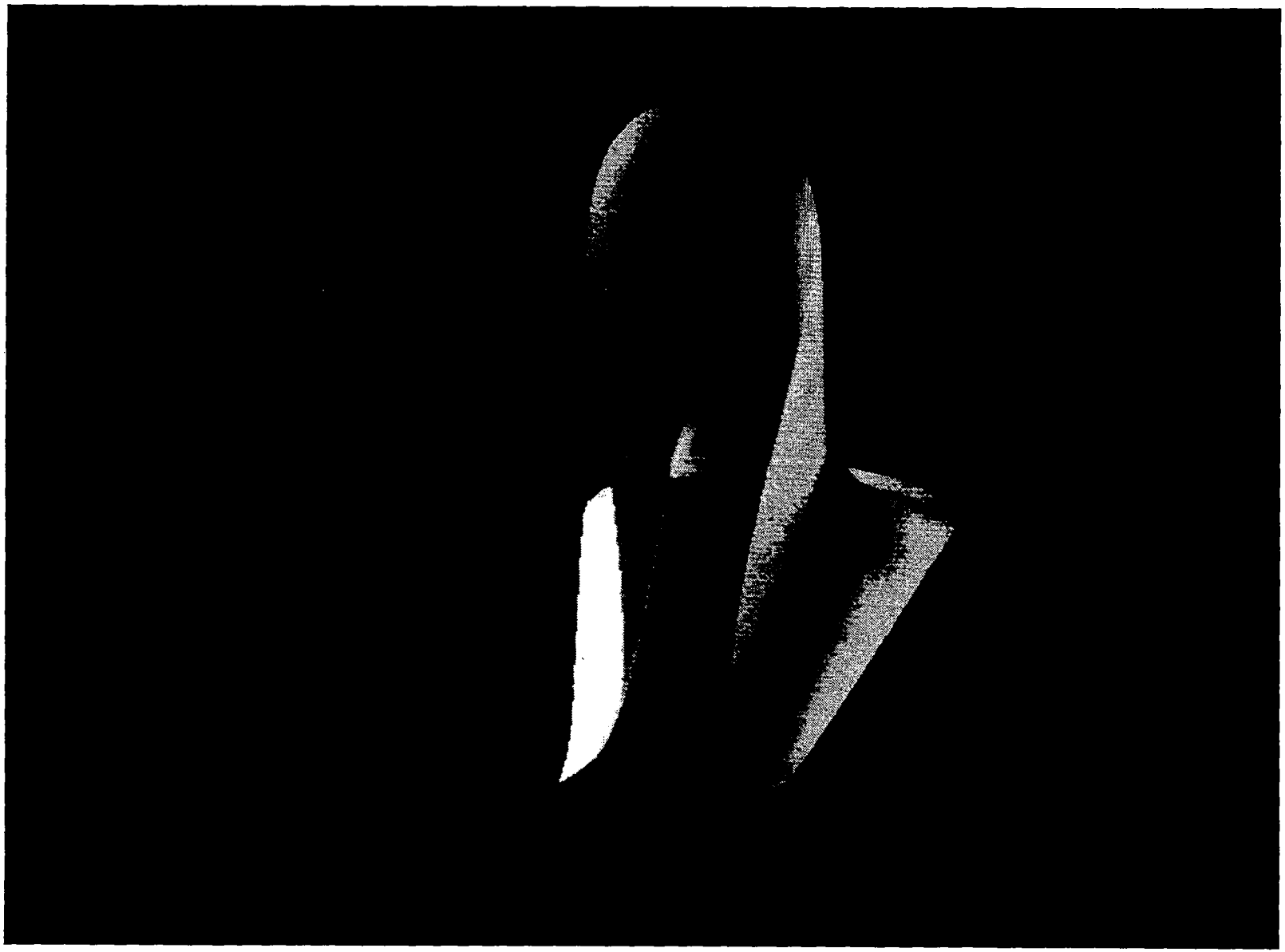

Figure 16. View of Upper Surface of a Mixer Lobe

design and analysis. The mesh used is an excellent tradeoff between cost and accuracy, since the solution for any significantly denser mesh would be extremely expensive to compute. It does appear that use of a finer mesh would result in higher predicted peak Mach numbers and slightly better agreement with experiment. Such calculations will be made when the multilevel technique of Brandt is implemented.

There is an additional check on solution accuracy built into the program. The computed velocity and density profiles in the inlet are integrated at each axial station to compute mass flow, and the error relative to the mass flow enforced as a boundary condition is determined. Typical maximum errors are one-half to one-and-one-half percent. The magnitude of the error is a function of the complexity of the geometry, the mesh used, the degree of convergence, and the strength of any internal shocks.

Overall, the program appears to predict inviscid flowfields to the accuracy that they can be measured experimentally. At flow conditions where Mach number gradients are large and boundary layers are thick, or shock-wave/boundary-layer interactions are present, agreement with experiment is not as good. It is expected that use of denser meshes and more stringent convergence tolerances would slightly improve agreement with experiment at the cost of significantly increased computer-time requirements. Improved accuracy for flows with significant viscous effects would require that viscous (boundary-layer) corrections be made to the inviscid flowfield.

2.11 CONCLUSIONS

The analysis technique described is capable of quite acceptable prediction for aircraft design and analysis purposes of flowfields for single-object geometries with essentially inviscid, irrotational flow.

Reasonable predictions can be made for flows which are primarily irrotational except for thick, but attached, boundary layers. Geometry limitations are primarily due to the number of mesh lines the computer code can use and still have reasonable computation times. The restriction is that any major geometric variations have to have a scale of several mesh spacings. The restriction to inviscid irrotational flow is simply because viscous or boundary-layer effects have not been incorporated into the flow analysis. If these effects are significant, such as occurs with very thick or separated boundary layers, predictions will be poor.

3.0 USE OF THE PROGRAM

This section discusses the use of the program exclusive of the generation of the geometry file. A detailed description of the input formats along with sample input and output files, and a troubleshooting guide, are presented. Also included is a discussion of selection of the computation mesh.

The problem of specifying the geometry is not discussed. The specification of geometry and generation of the geometry part of the input file can be a major task. It has been treated as a separate topic with separate documentation. The code will accept geometry files from any source. The program does not require any special order to the points in the geometry file.

The code, in its present form, can handle inlets with or without centerbodies, three-dimensional bodies, ducts, and bodies or inlets in a duct (e.g., wind tunnel). Specific limitations on geometries relative to mesh placement are discussed.

3.1 COMPUTATIONAL PARAMETERS

The analysis is programmed in CDC CYBER 200 FORTRAN language 1.4[14] for the Control Data Corporation CYBER 203 computer. The code makes extensive use of the vector extensions of this language and is explicitly vectorized. Use is made of most of the million-word memory of the CYBER 203 at the NASA-Langley Research Center.

A typical fine mesh for an inlet calculation is 69 axial-mesh by 37 radial-mesh by 16 circumferential-mesh or 40848 points. The calculation of a solution, using just the fine mesh, to reasonable convergence takes approximately 400 sweeps and seven to eight minutes of central-processor time. Essentially the same solution can be obtained using a sequence of three grids in approximately five- and one-half minutes. A reasonable convergence pattern is 100 sweeps on the coarsest mesh (18 by 10 by 16), 150 sweeps on the intermediate mesh (35 by 19 by 16), and 200 sweeps on the fine mesh. Typical times per sweep are 0.18 seconds per sweep on the coarse mesh, 0.42 seconds per sweep on the intermediate mesh, and 1.1 seconds per sweep on the fine mesh. Some additional time is required for setting up geometry parameters, mesh changing, and printing the solution. Solutions have been calculated using a sequence of 4, 8, and 16 circumferential meshes, but the coarsest mesh had a $\Delta\theta$ of 90 degrees and it is possible for this coarse spacing to cause some problems. Consequently, better convergence is presently obtained by keeping the number of θ mesh constant at 16. Run time is slightly dependent on the number of supersonic field points that have to be calculated.

3.2 INPUT FORMAT

The first two cards of the input deck are title cards and are printed at the start of the output for identification purposes. All input except the title cards is by means of order independent groups headed by keywords. The purposes of this particular input format are to allow certain groups to be optional, make the input file more readable, and to facilitate checking of input data by the program. Certain input groups are mandatory, and others are optional and may be omitted. All input, except for title cards, consists of numbers or words (depending on group) in fields of 10 columns wide, maximum of six fields per input line. All numbers are floating point and require a decimal point. Only the first four characters of keywords are checked.

There are certain interrelations among various input groups that have to be taken into account. If convergence is to be obtained on a sequence of meshes, the number of x, r, and θ mesh can have only certain values. This is because coarser meshes are formed by deleting every other mesh line. Also, a compressor face, if there is one, must lie on an x mesh belonging to the coarsest mesh. There are restrictions on number of mesh and number of surface points relating to declared array lengths in the computer code.

The program has the capability to use up to three mesh-density levels to provide more efficient convergence. The number of levels is controlled by the SWEEPS option. The mesh and geometry for the finest mesh level must be input. Coarser meshes for x and r are formed by deleting exactly every other mesh from the previous mesh. This places restrictions on the number of mesh allowed in the finest mesh, as the first and last mesh line have to remain when every other mesh is deleted. The θ mesh is a special case. There is an option to control the manner in which the θ mesh is varied between levels. The number of θ mesh can be held constant for two successive levels, or every other θ mesh value can be deleted for the coarser mesh.

The program allows the use of planes of symmetry to cut the number of mesh needed to make a calculation. If the largest θ mesh value input is 180.00 degrees, the plane 0 degrees to 180 degrees is taken to be a plane of symmetry. If the largest θ mesh input is less than 180 degrees the flow is assumed symmetrical about 0 degrees and the largest θ value input. Zero degrees must always be input as a θ mesh.

3.2.1 INPUT-GROUP SUMMARY

REQUIRED

Keyword	Description
FREEstream	Speed of sound, freestream velocity, angle of attack, and angle of yaw
XMESh	Axial mesh values
RMESh	Radial mesh values
TMESh	Circumferential mesh values
GEOMetry	Surface/mesh intersections: coordinates and surface normals values

OPTIONAL

Keyword	Description
COMPressor	Indicates an inlet geometry and specifies inlet mass flow
SWEEps	Convergence control parameters
THETa	Control of number of θ planes for each mesh-density level

SCDIff	Indicate special θ differencing to be used
PRINt op	Requests printout of various categories of geometrical information
SFLOw	Requests surface flow variable printout at end of run
SURF pr	Requests printout of flow variables along θ constant cuts of surface
FIELd pr	Requests printout of flow variables at constant θ cuts of flowfield
IPRI	Request for printout at other than level 3 for multilevel calculation

OPTIONAL (Diagnostic)

Keyword	Description
DEBUg	Requests print of coefficients, velocities and potential function for a specified axial cut and sweep number

3.2.2 INPUT-GROUP DESCRIPTIONS

FREESTREAM

This group specifies the velocity and orientation for the freestream relative to the geometry.

The scaling of the velocities is essentially arbitrary except that they should be of order one to avoid difficulties with print formats. Note that $q_\infty/a_\infty = M_\infty$.

Required input group, no default values.

Card 1	Cols.	1-4	'FREE'	Keyword
Card 2	Cols.	1-10	AINF	a_∞, freestream speed of sound
		11-20	QINF	q_∞, freestream velocity
		21-30	ALPHA	α, angle of attack, degrees, arctan (v_∞/u_∞)
		31-40	BETA	β, angle of yaw, degrees, arctan (w_∞/u_∞)

Note: Input of "FREE STREAM" which is 11 characters instead of "FREE" or "FREESTREAM" will draw an error message.

XMESH
RMESH
TMESH

These groups handle the input of the computational mesh, x, r, and theta, theta in degrees. The values do not have to be in any order. Theta mesh must include 0, 90, 180, and 270 degrees unless there is a plane of symmetry. Zero degrees must always be included.

Required input groups, no default values.

Card 1	Cols.	1-4	'XMES' or 'RMES' or 'TMES'	Keyword
		11-20	NX or NR or NT	Number of mesh values to be read, six per card. $5 \leq NX \leq 101$, $5 \leq NR \leq 81$, $3 \leq NT \leq 41$
Card 2	Cols.	1-10	MESH(1)	Axial, radial or circumferential
		11-20	MESH(2)	location of mesh,
		21-30		six values per card, as many cards
		.	.	as required. Theta must
		.	.	be in degrees.
		.	.	
		.	.	
.		.	.	
.		.	.	

Note:

1) $NX*NR*NT \leq 56000$

2) $NR*NT < 800$

3) $NX*NR \leq 2800$

4) If three mesh levels are to be used in the analysis:
   NX-1=4,8,12,16,....., or 100.
   NR-1=4,8,12,16,....., or 80

5) The compressor face, if there is one, must lie on a x mesh in the coarsest mesh (i.e., $x_{CF}=x_i$, i=1, or 5, or 9, or 13 etc. for a 3-level mesh).

GEOMETRY

This group consists of the coordinates of the intersections of the mesh with the geometry and the direction cosines of the surface normal at each intersect.

Required input group, no default values.

Card 1	Cols.	1-4	'GEOM'	Keyword
		11-20	NSURTOT	number of intersects
Card 2	Cols.	1-10	SURFX(1)	x
		11-20	SURFR(1)	r
		21-30	SURFT(1)	θ (degrees)
		31-40	COSX(1)	n_x
		41-50	COSR(1)	n_r
		51-60	COST(1)	n_θ
Card 3	Cols.	1-10	SURFX(2)	
		.	.	
		.	.	
.		.	.	
.		.	.	

} one intersect per card

Card
NSURTOT+1

COMPRESSOR (Optional

Signals that there is an inlet geometry and specifies the Mach number at the compressor face.

Card 1	Cols.	1-4	'COMP'	Keyword
		11-20	AMACHCF	Mach number to be enforced at compressor face.

SWEEPS (Optional)

This group controls the sweeping process by allowing control of the number of mesh-density levels, the maximum number of sweeps on each mesh-density level and a convergence criteria for each mesh-density level.

Default is a three-level mesh with default values listed .

Card 1	Cols.	1-4	'SWEE'	Keyword
Card 2	Cols.	1-10	NSWPM(1)	Maximum number of sweeps on coarsest mesh (or total if one-level calculation)
		11-20	NSWPM(2)	Maximum number of sweeps on level 2, level 3 for a two-level calculation (zero implies a single-level calculation)
		21-30	NSWPM(3)	Maximum number of sweeps on level 3 (zero for a one- or two-level calculation)

Card 3	Cols.	1-10	CONVT(1)	Convergence parameter, change in ϕ
		11-10	CONVT(2)	times 10^6. Sweeping on a
		21-30	CONVT(3)	level will stop when
				$\lvert\Delta\phi\rvert/(\phi_{max}-\phi_{min}) \times 10^6 \leq$ CONVT(i)

CONVT(i) corresponds to the same level as NSWPM(i)

Default values: 3 levels
NSWPM(1) = 200.
NSWPM(2) = 200.
NSWPM(3) = 200.

CONVT(1) = 1.0
CONVT(2) = 1.0
CONVT(3) = 1.0

THETA (Optional)

This group controls the number of θ grid used for each mesh-density level. The number of levels is controlled by either the SWEEPS option or the default value (three levels). The number of θ intervals can be held constant or doubled for any mesh change. The values for the number of θ grid must be consistent with the symmetry flag.

Default for this option is no change in θ grid for different levels.

Card 1	Cols.	1-4	'THET'	Keyword
Card 2	Cols.	1-10	NT_1	Number of θ grid for coarsest mesh-density level
		11-20	NT_2	Number of θ grid for level 2 (level 3 for a two-level calculation)
		21-30	NT_3	Number of θ grid for level 3 (for a three-level calculation)

Note that if there is a plane of symmetry (less than 0 degrees to 360 degrees geometry input)

$$NT_i = NT_{i+1} \text{ or } NT_i = (NT_{i+1}+1)/2.0,$$

otherwise,

$$NT_i = NT_{i+1} \text{ or } NT_i = NT_{i+1}/2.0$$

SCDIff (Optional)

This group allows use of special θ differencing for improved accuracy with very coarse θ meshes.

Default is regular differencing.

Card 1	Cols.	1-4	'SCDI'	Keyword
		11-20	ANUM	0.0 Regular differencing. 1.0 Special θ differencing (any other value than 0.0 or 1.0 will be treated as 0.0).

PRINT OP (Optional)

Inputs any or all of a group of keywords to obtain printed output for certain geometrical quantities.

Card 1	Cols.	1-4	'PRIN'	Keyword
Card 2	Cols.	1-10 11-20 . . .		Up to six keywords as described below. Can be in any order.

SPINPUT	List of the surface points in the order read.
SPORDER	List of surface points in the internal ordering used in the analysis.
SPECPNTS	List of special points.
TYPE2	List of Type 2 points.
MAP	Lists of x, r, and θ constant cuts of the surface. Lists include surface-point indexes, surface-point coordinates, arc length along the cuts, and components of the surface normals.
CUTS	Lists of x, r, and θ constant cuts of the surface. Lists include surface-point indexes, surface-point coordinates and surface velocities.

SFLOW (Optional)

This group controls printing of flow properties along the surface. Default is printing of every fourth cut for all surfaces. This default corresponds to coarse-mesh cuts for a three-level calculation.

Card 1	Cols.	1-4	'SFLO'	Keyword
Card 2	Cols.	1-10	SKIPX	See below.
		11-20	SKIPR	
		21-30	SKIPT	

For the fine mesh, every constant x cut will be printed if SKIPX = 1. If SKIPX = 0 no cuts will be printed. Otherwise, cuts will be printed for x = X(I), I = 1, 1 + SKIPX, 1 + 2*SKIPX, etc. SKIPR and SKIPT work the same for r and θ constant cuts of the surfaces respectively.

SURFACE PR (Optional)

Surface properties along θ constant cuts are printed for θ equal to 0 degrees, 90 degrees, 180 degrees, and 270 degrees for all runs except those with planes of symmetry. This option allows the printing of surface properties at other θ mesh values.

Card 1	Cols.	1-4	'SURF'	Keyword
		11-20	NSURPR	Number of extra θ printout planes.
Card 2	Cols.	1-10	THET(1)	θ values for extra surface-property output. Six values per card (in degrees).
		11-20	THET(2)	
		.	.	
		.	.	
.		.	.	
.		.	.	
.		.	.	

FIELD PR (Optional)

This option determines for which θ mesh values the field properties are to be printed.

Card 1	Cols.	1-4	'FIEL'	Keyword
		11-20	NFFPR	Number of θ values for which field properties are to be printed.
Card 2	Cols.	1-10	THET(1)	Values of θ mesh for printing field properties. Six values per card (in degrees).
		11-20	.	
		.	.	
		.	.	
.		.	.	
.		.	.	

IPRI (Optional)

This option allows printing of solution properties for the coarse meshes including mass-flow conservation computation. Default is no printout for coarse meshes.

Card 1	Cols.	1-4	'IPRI'	Keyword

DEBUG (Optional)

Diagnostic print option. Prints internal parameters for a given x mesh index and sweep number.

Card 1	Cols.	1-4	'DEBU'	Keyword
Card 2	Cols.	1-10	NPROPPR	Sweep number
		11-20	IPROPPR	x-plane index

3.2.3 GEOMETRY SPECIFICATION

Given a mesh, the user is required to provide all intersections between the mesh and the geometry to be analyzed. The information to be provided is the x, r, and θ coordinates of the intersection, and the components of the unit normal to the surface at that intersection point, n_x, n_r, and n_θ. The surface normals must be oriented such that the normals point from the surface into the flow. No particular order has to be followed in providing the intersections, but the set has to be complete. The program checks that the input points are complete and self-consistent, and generates internal maps connecting the points in x, r, and θ constant cuts.

The geometry points can come from any source. A package of procedures using parameteric bicubic patches has been developed to specify the geometry, and generate the geometry input file. It is documented separately (ref. 9).

The program has been used to calculate the flow about three-dimensional ducts, inlets and bodies. Most of the program is extremely general and the flow about other geometries could possibly be calculated with minor program modifications.

3.2.4 MESH SPECIFICATION

The selection of the computational mesh can have a very significant effect on the cost and accuracy of a calculation. This is because the mesh affects the accuracy of the final converged solution through the truncation errors, and the rate of convergence of the solution. The influence of these effects is understood only in qualitative terms. In general, squarer meshes ($\Delta x \approx \Delta r \approx r\Delta\theta$) converge better. The critical mesh aspect ratio is $\Delta x/r\Delta\theta$ since the use of line relaxation in the radial direction eliminates some of the effects of Δr. As the ratio of $\Delta x/r\Delta\theta$ departs significantly from unity, problems with convergence can occur. It is not possible, for inlet computations, to keep the far-field boundaries where they belong, keep a reasonable mesh near the inlet, and keep the mesh aspect ratio near unity everywhere. The best solution to this dilemma is to insure that any extreme aspect ratios occur in the far field where the solution changes little from the initial field.

For accuracy, very fine meshes must be used in regions of the flow where large velocity gradients are expected. Inside ducts (including inlet ducts) it is desirable to have a reasonably dense mesh with mesh aspect ratios near unity in order to have good conservation of mass by the analysis.

Table 3 gives a sample coarse mesh for a typical inlet configuration shown in figure 17. The fine meshes for x and r are generated by inserting three equally-spaced mesh lines between each of the coarse mesh lines. This will give a reasonable mesh for the inlet configuration shown. For vastly different geometries, the user may have to experiment with several possible meshes. It is very strongly suggested that the user make a sketch to scale, such as figure 17, showing the geometry and coarse mesh for any critical cuts, and take a good look at the sketch.

Mesh Selection General Rules

- Finer mesh in critical flow areas, that is areas where flow gradients are expected to be large.

Table 3. Standard Coarse Mesh for an Inlet

	x MESH	r MESH	θ MESH
1.	-4.0 L	0.0	0.0
2.	-2.0 L	0.3 R	22.5
3.	-1.0 L	0.6 R	45.0
4.	-0.5 L	0.8 R	67.0
5.	-0.2 L	0.9 R	90.0
6.	-0.1 L	1.0 R	112.5
7.	0.0	1.2 R	135.0
8.	0.1 L	1.6 R	157.5
9.	0.2 L	2.4 R	180.0
10.	0.4 L	4.0 R	202.5
11.	0.6 L	7.0 R	225.0
12.	0.8 L	10.0 R	247.5
13.	1.0 L		270.0
14.	1.2 L		292.5
15.	1.5 L		315.0
16.	2.0 L		337.5

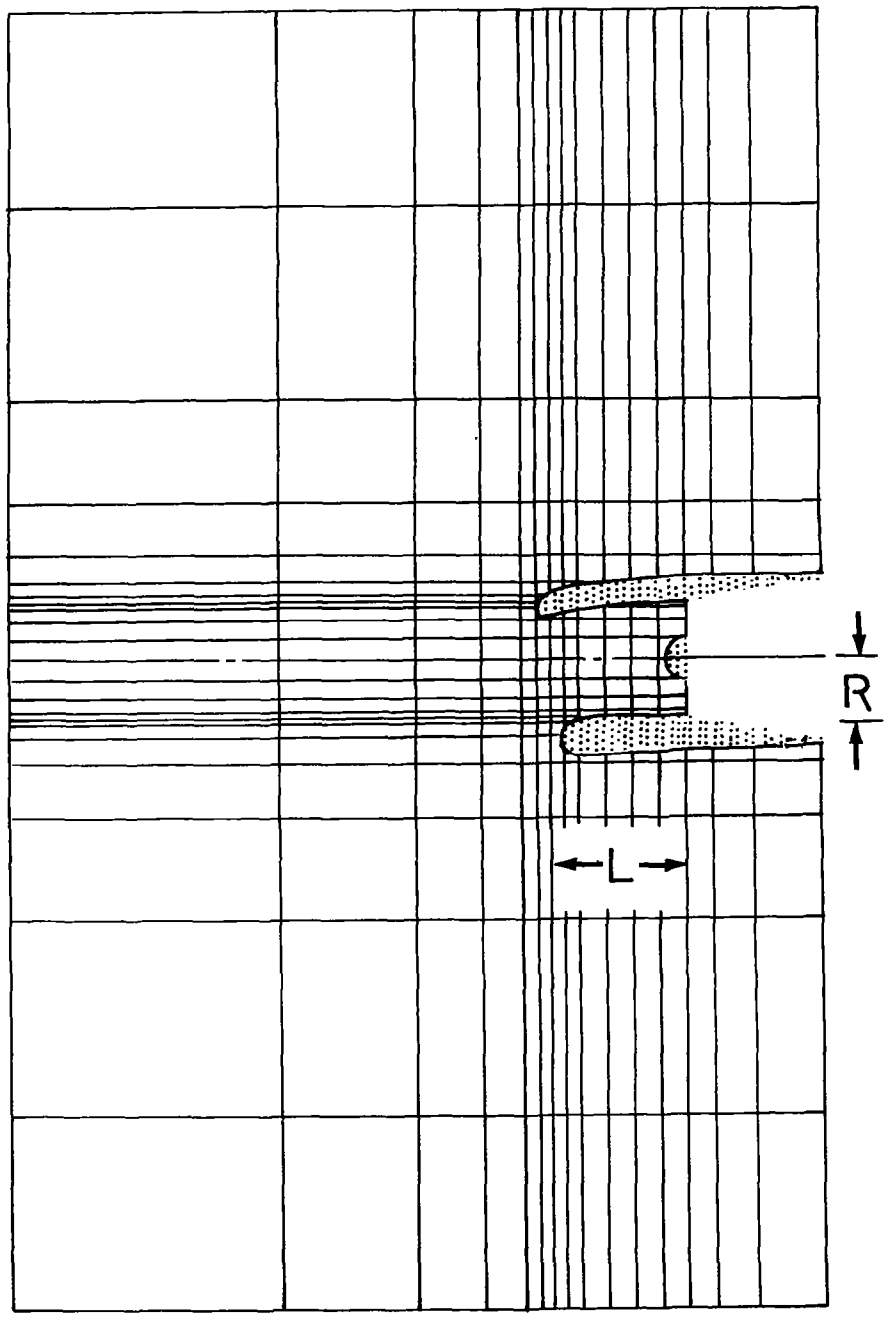

Figure 17. Standard Coarse Mesh for an Inlet Flowfield Calculation

- Uniform or near-uniform meshes in ducts (including inlet ducts).

- Mesh spacing should never be more than half or double between adjacent mesh (in the same coordinate).

3.2.5 GEOMETRY LIMITATIONS

This section is an attempt to give the user some understanding of what flowfields the code can successfully analyze, and those which it cannot. Also, it is intended to give the user some basic understanding of what the problems are when the program cannot successfully calculate the flowfield about a geometry as it may be possible to make a simple modification to the code to allow it to calculate a flowfield for which it previously was unsuccessful.

The analysis is very general with respect to bodies lying internal to the computational volume. The primary limitations internal to the computational volume are mesh density and placement. Two difficulties may occur: the code may fail completely or it may give the wrong answer. Figure 18 illustrates limitations on mesh density in a passage between surfaces. If any one of a sequence of meshes is as shown in figure 18a the code will fail. A mesh such as that shown in figure 18b will not cause the code to fail, but accuracy probably would be poor. This may not be a problem if, for example, the mesh shown is the coarsest of a sequence of three meshes as the accuracy of the final solution is primarily dependent on the density of the finest mesh. Figure 19 illustrates that the mesh must be dense enough to resolve important features of the geometry. A solution calculated using the mesh shown in figure 19a would not predict any effects due to the wavy wall. A solution calculated using the mesh of figure 19b will predict at least some of the effects due to the wavy wall.

The user has some control over placement of mesh, but certain mesh placement patterns could cause severe difficulties with convergence. Uniformly spaced mesh lines result in the best convergence behavior. A very irregular spacing of mesh lines, in an attempt to place the mesh where they are required for accuracy, may be self-defeating in that it might take a totally unreasonable number of sweeps to obtain convergence. This is a dilemma that would require numerical experiments to resolve for any given geometry.

There are limitations on the total number of mesh that can be used which are built into the computer code. These could be changed by changing the code, but if the total number of mesh is increased, the run-time of the computer code also increases, and by a significantly greater factor. This run-time problem will be substantially alleviated when a version of the code with the multilevel procedure incorporated is available.

Another limitation on the current version of the code is that there is no provision for application of a Kutta condition. While there is not believed to be any fundamental reason why a Kutta boundary-condition option could not be added to the code, it is thought to require a signficant engineering effort to incorporate.

The external (edge of computational volume) boundary conditions allowed are those for an inlet, duct, body, or a body or inlet in a duct. Other geometries are possible with program modifications. The nature and degree of difficulty of such modifications would vary from problem to problem.

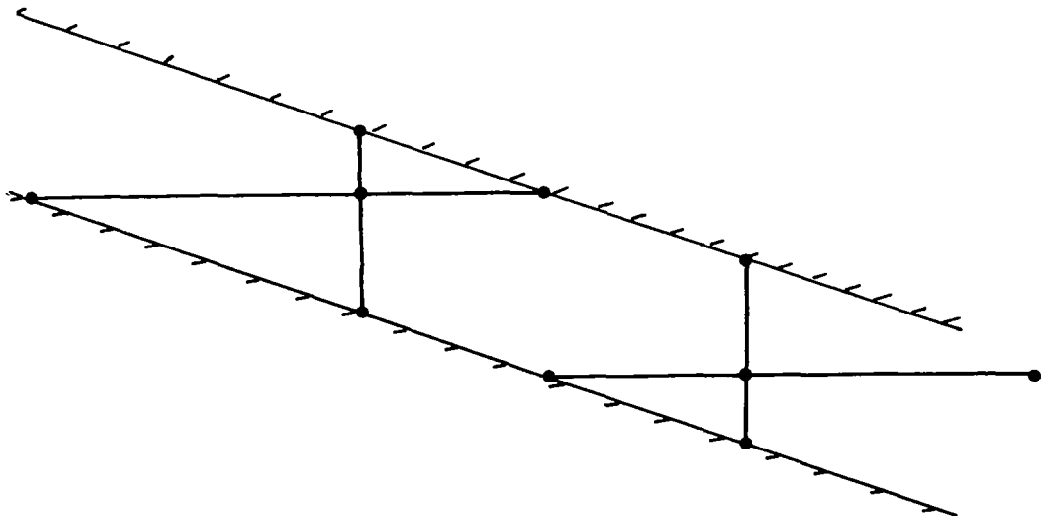

a.) MESH TOO COARSE, CODE WILL FAIL

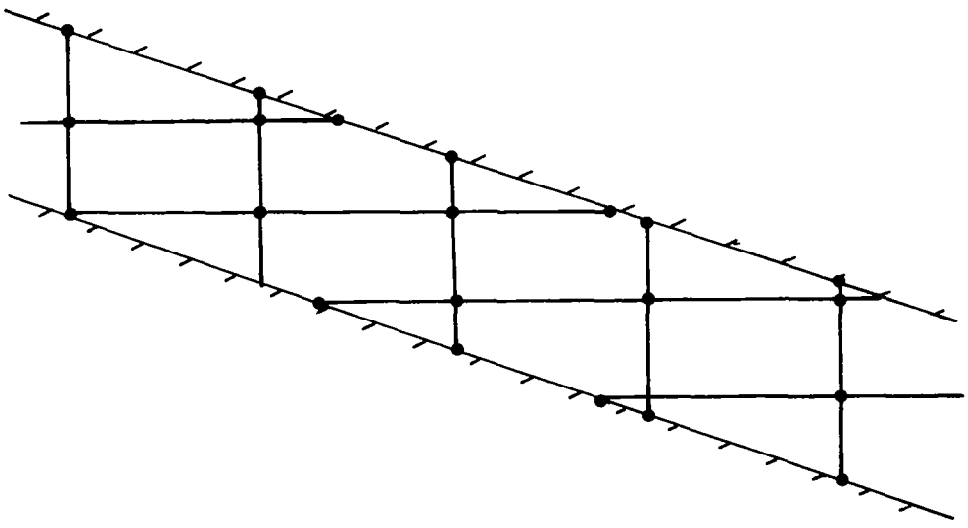

b.) MESH MINIMAL, BUT CODE WILL WORK

Figure 18. Mesh-Density Limitations Between Surfaces

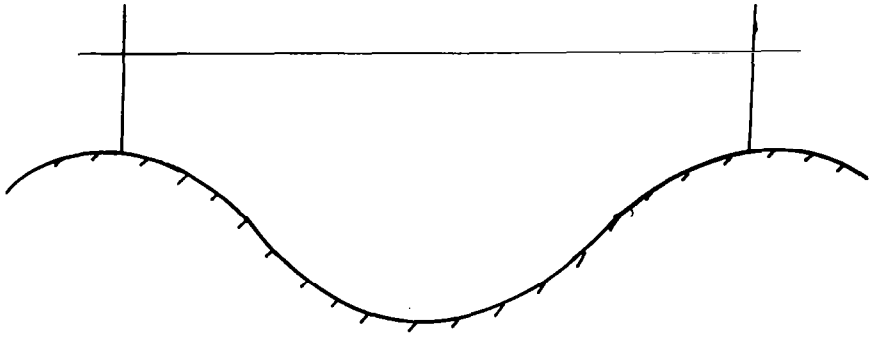

a.) INADEQUATE MESH FOR GEOMETRY RESOLUTION

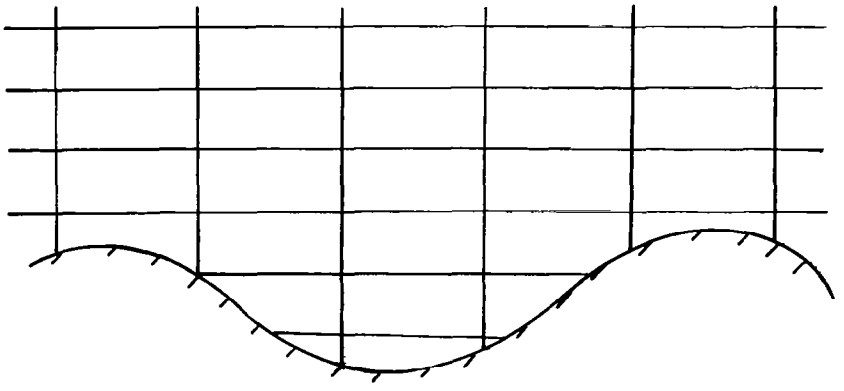

b.) ADEQUATE MESH FOR GEOMETRY RESOLUTION

Figure 19. Mesh-Density Limitations Relative to Surface Geometry

The program uses cylindrical coordinates which are reasonably efficient for shapes that are nearly bodies of revolution. It is planned to incorporate a Cartesian-coordinate option in a later version of the code. Cartesian coordinates are much more efficient than cylindrical coordinates for analyzing some flowfields.

3.2.6 SAMPLE INPUT FILES

Several examples of input files (figs. 20a and 20b) are shown in an abbreviated form in order to help clarify the input file descriptions of Section 3.2.2. The files have been shortened by deleting most of the list of intersections and normals from the input files. The input groups on the files have been arranged for convenience of display by placing the "GEOMETRY" group as the last group on each file.

The input file of figure 20a is the file used to generate the sample output of Section 3.3.

3.3 PROGRAM OUTPUT

The program output is arranged so that there is an introductory section, convergence history, and the flowfield solution. The introductory section (fig. 21a) presents program title, abstract, informative messages, and a list of consultants followed by specific information about the current run. The specific run information consists of run title, a repeat of program inputs such as free-stream conditions, convergence parameters, program options selected, etc. These are followed by the mesh. Input surface points and other geometry information can be printed at the user's option. The headings used on surface point and geometry printouts are explained in Table 4.

The convergence history (fig. 21b) includes sweep number, maximum and average residues for field points and surface points, location of maximum residue, number of supersonic points, the extrapolation parameters $1/(1-\lambda_1)$ and $1/(1-\lambda_2)$, and flags to indicate convergence/divergence and extrapolation. Headings for the convergence history are listed in Table 5.

Following the convergence history for each level, timing information for that level is printed (fig. 21c).

After the timing information for the last level (and optionally for other levels), surface properties for $\theta = 0$ degrees, 90 degrees, 180 degrees and 270 degrees cuts (optionally for other θ cuts), are printed (fig. 21d). The headings for surface-property printouts are listed in Table 6. Field properties may be printed at the user's option (fig. 21e). Headings for field-property printouts are listed in Table 7.

A mass-flow computation (fig. 21f) is printed as a check on program convergence and/or accuracy. The mass flow for a duct is computed at each x station by integrating the computed solution profiles. The calculated mass flow is compared to the mass flow specified at the exit station.

The last printout (fig. 21g) is optional (controlled by the SFLO input group) and allows printing of surface properties for x, r or θ constant cuts. Headings are explained in Table 6.

```
XXX INLET   APRIL 22,1980   16 THETA PLANES
175 KNOTS   MCF=0.64   ALPHA=25.0 DEGREES   R 19   C 3
FREESTREAM
1.0       0.265      25.0       0.0
SWEEPS
100.0     150.0      200.0
1.        1.         1.
THETA LEV
16.0      16.0       16.0
COMPRESSOR0.64
SFLOW
4.0       4.0        4.0
SCDIF     1.0
SURFACE PR2.0
135.0     225.0
FIELD PR  1.0
180.0
XMESH     69.0
-250.00000-218.75000-187.50000-156.25000-125.00000-108.75000
 -92.50000 -76.25000 -60.00000 -50.00000 -40.00000 -30.00000
 -20.00000 -12.50000  -5.00000   2.50000  10.00000  13.75000
  17.50000  21.25000  25.00000  27.50000  30.00000  32.50000
  35.00000  36.25000  37.50000  38.75000  40.00000  41.25000
  42.50000  43.75000  45.00000  46.25000  47.50000  48.75000
  50.00000  51.25000  52.50000  53.75000  55.00000  56.25000
  57.50000  58.75000  60.00000  61.25000  62.50000  63.75000
  65.00000  67.50000  70.00000  72.50000  75.00000  77.50000
  80.00000  82.50000  85.00000  87.50000  90.00000  92.50000
  95.44000 100.00000 105.00000 110.00000 115.00000 119.75000
 124.50000 129.25000 134.00000
RMESH     37.0
   0.00000   5.00000  10.00000  15.00000  20.00000  23.75000
  27.50000  31.25000  35.00000  37.50000  40.00000  42.50000
  45.00000  46.25000  47.50000  48.75000  50.00000  52.50000
  55.00000  57.50000  60.00000  62.50000  65.00000  67.50000
  70.00000  77.50000  85.00000  92.50000 100.00000 112.50000
 125.00000 137.50000 150.00000 175.00000 200.00000 225.00000
 250.00000
TMESH     16.0
   0.00000  22.50000  45.00000  67.50000  90.00000 112.50000
 135.00000 157.50000 180.00000 202.50000 225.00000 247.50000
 270.00000 292.50000 315.00000 337.50000
GEOMETRY  1808.
   37.9789   42.5000    0.0000  -.998896  -.046984   .000001
   38.7500   44.6861   22.5000  -.825046   .565030   .006288
   38.7500   44.6861  337.5000  -.825036   .565045  -.006288
   38.7500   44.7495    0.0000  -.752486   .658608   .000000
   38.9909   45.0000    0.0000  -.696756   .717308  -.000000
   38.9948   45.0000   22.5000  -.745554   .666445   .000735
   38.9948   45.0000  337.5000  -.745547   .666453  -.000735
   39.1819   45.0000   45.0000  -.931933   .361689   .026095
   39.1819   45.0000  315.0000  -.931928   .361704  -.026096
   40.0000   45.0000   64.4733  -.996627  -.026199   .077768
   40.0000   45.0000  295.5275  -.996627  -.026183  -.077769
   40.0000   45.7338    0.0000  -.495294   .868725  -.000000
   40.0000   45.8325   22.5000  -.530264   .847771  -.010236
   40.0000   45.8325  337.5000  -.530260   .847773   .010235
   40.0000   46.1618   45.0000  -.673944   .738626  -.015237
   40.0000   46.1618  315.0000  -.673939   .738630   .015236
   40.1000   46.2500   45.0000  -.656499   .754125  -.017445
   40.1000   46.2500  315.0000  -.656483   .754139   .017446
   40.3403   46.2500   67.5000  -.924221   .379650   .041008
   40.3404   46.2500  292.5000  -.924222   .379648  -.041009
   40.7701   46.2500   22.5000  -.459877   .887885  -.013136
   40.7701   46.2500  337.5000  -.459869   .887889   .013135
   41.0892   46.2500    0.0000  -.375960   .926636  -.000000
```

Figure 20a. Truncated Input File For An Inlet

```
FORCED MIXER GEOMETRY   MAY 23, 1980
M EXIT SET TO 0.45
FREESTREAM
1.0         0.45        0.0         0.0
SWEEPS
200.0       200.0
1.0         1.0
IPRI
COMPRESSOR0.45
FIELD PR  3.0
0.0         7.5         15.0
THETA LEV
17.0        17.0        17.0
XMESH       61.0
0.0         0.1         0.2         0.3         0.4         0.5
0.6         0.7         0.8         0.9         1.0         1.1
1.2         1.3         1.4         1.5         1.6         1.7
1.8         1.9         2.0         2.1         2.2         2.3
2.4         2.5         2.6         2.7         2.8         2.9
3.0         3.1         3.2         3.3         3.4         3.5
3.6         3.7         3.8         3.9         4.0         4.1
4.2         4.3         4.4         4.5         4.6         4.7
4.8         4.9         5.0         5.1         5.2         5.3
5.4         5.5         5.6         5.7         5.8         5.9
6.0
RMESH       37.0
0.4         0.5         0.6         0.7         0.8         0.9
1.0         1.1         1.2         1.3         1.4         1.5
1.6         1.7         1.8         1.9         2.0         2.1
2.2         2.3         2.4         2.5         2.6         2.7
2.8         2.9         3.0         3.1         3.2         3.3
3.4         3.5         3.6         3.7         3.8         3.9
4.0
TMESH       17.0
0.0         0.9375      1.875       2.8125      3.75        4.6875
5.625       6.5625      7.50        8.4375      9.375       10.3125
11.25       12.1875     13.125      14.0625     15.0
GEOMETRY  3186.
    0.0000    2.9400     0.0000   0.000000 -1.000000   0.000000
    0.0000    2.9400      .9375    .000025 -1.000000   0.000000
    0.0000    2.9400    1.8750     .000031 -1.000000   0.000000
    0.0000    2.9400    2.8125    -.000048 -1.000000   0.000000
    0.0000    2.9400    3.7500    -.000018 -1.000000   0.000000
    0.0000    2.9400    4.6875    -.000315 -1.000000   0.000000
    0.0000    2.9400    5.6250     .000212 -1.000000   0.000000
    0.0000    2.9400    6.5625    -.000398 -1.000000   0.000000
    0.0000    2.9400    7.5000     .000271 -1.000000   0.000000
    0.0000    2.9400    8.4375     .000197 -1.000000   0.000000
    0.0000    2.9400    9.3750    -.000129 -1.000000   0.000000
    0.0000    2.9400   10.3125     .000095 -1.000000   0.000000
    0.0000    2.9400   11.2500     .000244 -1.000000   0.000000
    0.0000    2.9400   12.1875    -.000085 -1.000000   0.000000
    0.0000    2.9400   13.1250    -.000300 -1.000000   0.000000
    0.0000    2.9400   14.0625    -.000238 -1.000000   0.000000
    0.0000    2.9400   15.0000    0.000000 -1.000000   0.000000
     .1000    2.9396   12.1875    -.007258  -.999973    .000800
     .1000    2.9396   13.1250    -.007751  -.999969   -.000977
     .1000    2.9396   14.0625    -.008033  -.999968    .000234
     .1000    2.9396   15.0000    -.008031  -.999968   0.000000
     .1000    2.9397    1.8750    -.005385  -.999985   -.000173
     .1000    2.9397    2.8125    -.005571  -.999984   -.000447
     .1000    2.9397    3.7500    -.005800  -.999983    .000246
     .1000    2.9397    6.5625    -.005002  -.999987   -.000605
     .1000    2.9397    9.3750    -.006119  -.999981   -.000975
     .1000    2.9397   10.3125    -.006129  -.999979   -.002120
```

Figure 20b. Truncated Input File For A Mixer Lobe

```
**********      P 4 6 5 A  -  THREE-DIMENSIONAL TRANSONIC POTENTIAL FLOW PROGRAM      **********

                                VERSION OF MARCH 17, 1981

                                RUN DATE -  03/23/81
```

ABSTRACT -

P465 COMPUTES SOLUTIONS FOR THE COMPLETE EQUATION FOR COMPRESSIBLE POTENTIAL FLOW. IT CAN PREDICT SUBSONIC OR TRANSONIC FLOW FIELDS ABOUT FULLY THREE-DIMENSIONAL INLETS, DUCTS AND BODIES. THE ANALYSIS USES CYLINDRICAL COORDINATES, FINITE DIFFERENCES AND SUCCESSIVE LINE OVER RELAXATION (SLOR). EXTRAPOLATION AND A SEQUENCE OF INCREASINGLY DENSER MESHES CAN BE USED TO ACCELERATE CONVERGENCE. THE ANALYSIS IS PROGRAMMED IN EXTENDED FORTRAN IV FOR THE CONTROL DATA CORPORATION CYBER 203 COMPUTER.

INITIAL RELEASE OF P465 - VERSION A - NOVEMBER 1, 1980.

REFERENCE - REYHNER, T. A., "TRANSONIC POTENTIAL FLOW COMPUTATION ABOUT THREE-DIMENSIONAL INLETS, DUCTS AND BODIES," AIAA PAPER 80-1364, SNOWMASS, COLORADO, JULY 1980.

CONSULTATION -

T. A. REYHNER	BOEING COMMERCIAL AIRPLANE CO.	(206) 237-2519
R. G. JORSTAD	BOEING COMPUTER SERVICES, INC.	(206) 656-5745
D. E. REUBUSH	NASA LANGLEY RESEARCH CENTER	(804) 827-2675

RUN TITLE -

```
XXX INLET   APRIL 22,1980   16 THETA PLANES
175 KNOTS   MCF=0.64   ALPHA=25.0 DEGREES   R 19   C 3
```

THE FLOW FIELD PARAMETERS ARE -

AINF	=	1.000000	
QINF	=	.265000	
ALPHA (ANGLE OF ATTACK)	=	25.000	DEGREES
BETA (ANGLE OF YAW)	=	.000	DEGREES

GEOMETRY -

INLET GEOMETRY - COMPRESSOR FACE MACH NO. = .640

MESH AND CONVERGENCE PARAMETERS -

LEVEL NUMBER	1	2	3

Figure 21a. Sample Output – Introductory Section

```
          NX                                    18          35          69

          NR                                    10          19          37

          NT                                    16          16          16

          MAXIMUM NUMBER OF SWEEPS              100         150         200

          CONVERGENCE TEST VALUES *(10**6)      1.0000      1.0000      1.0000

SPECIAL SIN/COS DIFFERENCE QUOTIENTS USED FOR THETA COORDINATE

SURFACE FLOW PROPERTIES PRINT REQUESTED -

          X CONSTANT CUTS       X=X(I)          (I-1) DIVISIBLE BY   4

          R CONSTANT CUTS       R=R(J)          (J-1) DIVISIBLE BY   4

          THETA CONSTANT CUTS   THETA=THETA(K)  (K-1) DIVISIBLE BY   4

IN ADDITION TO THE 0, 90, 180, AND 270 DEGREE PLANES
 SURFACE POINT PRINTOUT HAS BEEN REQUESTED AT -

               135.0 DEG.
               225.0 DEG.

PRINTOUT OF THE FLOWFIELD HAS BEEN REQUESTED AT -

               180.0 DEG.

MESH -

          NX*NR*NT =  40848       THIS DATA CASE USES  40848 OF THE AVAILABLE 56000 FIELD POINTS

          NR*NT =       592       THE LIMIT IS 800


                         **********
                 ******** X MESH ********
                         **********

  1) -250.0000     24)   32.5000     47)   62.5000
  2) -218.7500     25)   35.0000     48)   63.7500
  3) -187.5000     26)   36.2500     49)   65.0000
  4) -156.2500     27)   37.5000     50)   67.5000
  5) -125.0000     28)   38.7500     51)   70.0000
  6) -108.7500     29)   40.0000     52)   72.5000
  7)  -92.5000     30)   41.2500     53)   75.0000
  8)  -76.2500     31)   42.5000     54)   77.5000
  9)  -60.0000     32)   43.7500     55)   80.0000
 10)  -50.0000     33)   45.0000     56)   82.5000
 11)  -40.0000     34)   46.2500     57)   85.0000
 12)  -30.0000     35)   47.5000     58)   87.5000
 13)  -20.0000     36)   48.7500     59)   90.0000
 14)  -12.5000     37)   50.0000     60)   92.5000
 15)   -5.0000     38)   51.2500     61)   95.4400
 16)    2.5000     39)   52.5000     62)  100.0000
 17)   10.0000     40)   53.7500     63)  105.0000
 18)   13.7500     41)   55.0000     64)  110.0000
 19)   17.5000     42)   56.2500     65)  115.0000
 20)   21.2500     43)   57.5000     66)  119.7500
```


Figure 21a. Continued

```
 21)   25.0000     44)   58.7500     67)  124.5000
 22)   27.5000     45)   60.0000     68)  129.2500
 23)   30.0000     46)   61.2500     69)  134.0000

                    **********
                ******** R MESH ********
                    **********

  1)     .0000     13)   45.0000     25)   70.0000
  2)    5.0000     14)   46.2500     26)   77.5000
  3)   10.0000     15)   47.5000     27)   85.0000
  4)   15.0000     16)   48.7500     28)   92.5000
  5)   20.0000     17)   50.0000     29)  100.0000
  6)   23.7500     18)   52.5000     30)  112.5000
  7)   27.5000     19)   55.0000     31)  125.0000
  8)   31.2500     20)   57.5000     32)  137.5000
  9)   35.0000     21)   60.0000     33)  150.0000
 10)   37.5000     22)   62.5000     34)  175.0000
 11)   40.0000     23)   65.0000     35)  200.0000
 12)   42.5000     24)   67.5000     36)  225.0000
                                     37)  250.0000

                    **********
                ******** T MESH ********
                    **********

  1)     .0000      6)  112.5000     11)  225.0000
  2)   22.5000      7)  135.0000     12)  247.5000
  3)   45.0000      8)  157.5000     13)  270.0000
  4)   67.5000      9)  180.0000     14)  292.5000
  5)   90.0000     10)  202.5000     15)  315.0000
                                     16)  337.5000

INPUT PROCESSING COMPLETED

GEOMETRY PROCESSING COMPLETED - LEVEL 3

MESH FOR LEVEL 2 -

                    **********
                ******** X MESH ********
                    **********

  1) -250.0000     12)   30.0000     23)   60.0000
  2) -187.5000     13)   35.0000     24)   62.5000
  3) -125.0000     14)   37.5000     25)   65.0000
  4)  -92.5000     15)   40.0000     26)   70.0000
  5)  -60.0000     16)   42.5000     27)   75.0000
  6)  -40.0000     17)   45.0000     28)   80.0000
  7)  -20.0000     18)   47.5000     29)   85.0000
  8)   -5.0000     19)   50.0000     30)   90.0000
  9)   10.0000     20)   52.5000     31)   95.4400
 10)   17.5000     21)   55.0000     32)  105.0000
 11)   25.0000     22)   57.5000     33)  115.0000
                                     34)  124.5000
                                     35)  134.0000

                    **********
                ******** R MESH ********
                    **********
```

Figure 21a. Continued

```
 1)      .0000      7)    45.0000     13)    70.0000
 2)    10.0000      8)    47.5000     14)    85.0000
 3)    20.0000      9)    50.0000     15)   100.0000
 4)    27.5000     10)    55.0000     16)   125.0000
 5)    35.0000     11)    60.0000     17)   150.0000
 6)    40.0000     12)    65.0000     18)   200.0000
                                      19)   250.0000

                    **********
                ******** T MESH ********
                    **********

 1)      .0000      6)   112.5000     11)   225.0000
 2)    22.5000      7)   135.0000     12)   247.5000
 3)    45.0000      8)   157.5000     13)   270.0000
 4)    67.5000      9)   180.0000     14)   292.5000
 5)    90.0000     10)   202.5000     15)   315.0000
                                      16)   337.5000

GEOMETRY PROCESSING COMPLETED - LEVEL 2

MESH FOR LEVEL 1 -

                    **********
                ******** X MESH ********
                    **********

 1) -250.0000      7)    35.0000     13)    65.0000
 2) -125.0000      8)    40.0000     14)    75.0000
 3)  -60.0000      9)    45.0000     15)    85.0000
 4)  -20.0000     10)    50.0000     16)    95.4400
 5)   10.0000     11)    55.0000     17)   115.0000
 6)   25.0000     12)    60.0000     18)   134.0000

                    **********
                ******** R MESH ********
                    **********

 1)      .0000      4)    45.0000      7)    70.0000
 2)    20.0000      5)    50.0000      8)   100.0000
 3)    35.0000      6)    60.0000      9)   150.0000
                                      10)   250.0000

                    **********
                ******** T MESH ********
                    **********

 1)      .0000      6)   112.5000     11)   225.0000
 2)    22.5000      7)   135.0000     12)   247.5000
 3)    45.0000      8)   157.5000     13)   270.0000
 4)    67.5000      9)   180.0000     14)   292.5000
 5)    90.0000     10)   202.5000     15)   315.0000
                                      16)   337.5000

GEOMETRY PROCESSING COMPLETED - LEVEL 1
```

Figure 21a. Concluded

CONVERGENCE HISTORY - LEVEL NUMBER 1

SWEEP	FIELD POINTS AVE RESIDUE	I	J	K	MAX RESIDUE		SURFACE POINTS AVE RESIDUE	I	J	K	INDEX	MAX RESIDUE	M>1	EIGEN1	EIGEN2
1	.77038E-03	16	4	9	.31551E-01	***	.51178E-02	16	4	9	368	.32044E-01	0	-.16587E-02	-.27199E+00
2	.64244E-03	15	4	9	.16105E-01	**	.29924E-02	15	4	9	320	.16402E-01	0	.33528E+01	.20424E+01
3	.59142E-03	15	4	9	.11401E-01	**	.24174E-02	15	4	9	320	.11687E-01	0	.77278E+01	.34219E+01
4	.53283E-03	15	4	9	.89023E-02	**	.19864E-02	15	4	9	320	.90558E-02	0	.75869E+01	.45580E+01
5	.47503E-03	16	4	9	.71500E-02	**	.16780E-02	15	4	9	320	.72300E-02	0	.78805E+01	.50734E+01
6	.43254E-03	16	4	9	.60413E-02	**	.15232E-02	15	4	9	320	.60882E-02	0	.11014E+02	.64377E+01
7	.39265E-03	15	4	9	.50224E-02	**	.13803E-02	15	4	7	314	.50710E-02	0	.10744E+02	.59207E+01
8	.36764E-03	15	4	7	.44443E-02	**	.12890E-02	15	4	7	314	.44841E-02	0	.15417E+02	.86698E+01
9	.33497E-03	15	4	7	.37364E-02	**	.11630E-02	15	4	7	314	.37691E-02	0	.10823E+02	.62705E+01
10	.31995E-03	15	4	7	.33978E-02	**	.10924E-02	15	4	7	314	.34211E-02	0	.19646E+02	.11016E+02
11	.29861E-03	15	4	7	.29661E-02	**	.10023E-02	15	4	7	314	.29858E-02	0	.13768E+02	.78618E+01
12	.28685E-03	15	4	7	.27457E-02	**	.94837E-03	15	4	7	314	.27605E-02	0	.22353E+02	.13441E+02
13	.27118E-03	15	4	7	.24782E-02	**	.88278E-03	15	4	7	314	.24908E-02	0	.16681E+02	.10252E+02
14	.26131E-03	15	4	7	.23226E-02	**	.84060E-03	15	4	7	314	.23326E-02	0	.24687E+02	.15914E+02
15	.24714E-03	15	4	7	.21069E-02	**	.78332E-03	15	4	7	314	.21158E-02	0	.16890E+02	.10760E+02
16	.23905E-03	15	4	7	.19938E-02	**	.75024E-03	15	4	7	314	.20009E-02	0	.27705E+02	.18609E+02
17	.23160E-03	15	4	7	.18930E-02	**	.72134E-03	15	4	7	314	.18990E-02	0	.29618E+02	.19773E+02
18	.22488E-03	15	4	7	.18027E-02	**	.69533E-03	15	4	7	314	.18079E-02	0	.31784E+02	.20959E+02
19	.21867E-03	15	4	7	.17210E-02	**	.67171E-03	15	4	7	314	.17256E-02	0	.33536E+02	.22057E+02
20	.21298E-03	15	4	7	.16469E-02	**	.65007E-03	15	4	7	314	.16510E-02	0	.35531E+02	.23233E+02
21	.20764E-03	15	4	7	.15792E-02	**	.63041E-03	15	4	7	314	.15829E-02	0	.37247E+02	.24334E+02
22	.20258E-03	15	4	7	.15173E-02	**	.61230E-03	15	4	7	314	.15206E-02	0	.38694E+02	.25494E+02
23	.19782E-03	15	4	7	.14602E-02	**	.59542E-03	15	4	7	314	.14632E-02	0	.40231E+02	.26613E+02
24	.19336E-03	15	4	7	.14076E-02	**	.57960E-03	15	4	7	314	.14104E-02	0	.41859E+02	.27756E+02
25	.18921E-03	15	4	7	.13589E-02	**	.56468E-03	15	4	7	314	.13614E-02	0	.43648E+02	.28883E+02

Figure 21b. Convergence History

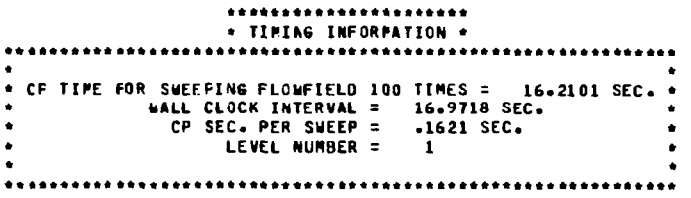

Figure 21c. Timing Information

****
***** SURFACE PROPERTIES ***** THETA= .000 DEGREES
****

INDEX	X	R	S	MACH	PHI	CP	Q	U	U-RADIAL	U-THETA
1619	95.4400	46.8514	159.2577	.6794	113.7437	-4.6610	.6546	.6482	-.0915	.0000
1565	92.5000	47.1843	156.2979	.5740	111.9464	-3.2584	.5599	.5591	-.0291	.0000
1519	90.0000	47.1951	153.7970	.5206	110.6462	-2.5858	.5106	.5102	.0203	.0000
1469	87.5000	47.0023	151.2890	.5092	109.3890	-2.4467	.5000	.4969	.0552	.0000
1419	85.0000	46.6547	148.7647	.5103	108.1302	-2.4601	.5010	.4943	.0817	.0000
1394	82.8263	46.2500	146.5535	.5180	107.0178	-2.5537	.5082	.4977	.1024	.0000
1342	82.5000	46.1820	146.2202	.5197	106.8484	-2.5742	.5097	.4987	.1053	.0000
1284	80.0000	45.6090	143.6552	.5350	105.5254	-2.7637	.5240	.5089	.1249	.0000
1279	77.6294	45.0000	141.2076	.5529	104.2239	-2.9885	.5405	.5222	.1393	.0000
1228	77.5000	44.9654	141.0737	.5539	104.1515	-3.0018	.5415	.5230	.1400	.0000
1150	75.0000	44.2771	138.4806	.5747	102.7233	-3.2667	.5605	.5395	.1521	.0000
1092	72.5000	43.5615	135.8802	.5965	101.2406	-3.5498	.5803	.5575	.1613	-.0000
1034	70.0000	42.8358	133.2770	.6184	99.7033	-3.8383	.6002	.5764	.1671	-.0000
1025	68.8433	42.5000	132.0725	.6286	98.9752	-3.9753	.6094	.5852	.1701	-.0000
985	67.5000	42.1099	130.6738	.6422	98.1149	-4.1563	.6215	.5970	.1730	.0000
944	65.0000	41.3930	128.0730	.6703	96.4670	-4.5372	.6466	.6222	.1757	.0000
906	63.7500	41.0439	126.7752	.6855	95.6195	-4.7452	.6600	.6363	.1755	.0000
864	62.5000	40.7041	125.4798	.7017	94.7555	-4.9674	.6742	.6513	.1742	.0000
826	61.2500	40.3759	124.1874	.7189	93.8748	-5.2036	.6892	.6674	.1717	.0000
786	60.0000	40.0618	122.8985	.7373	92.9767	-5.4586	.7051	.6849	.1676	.0000
783	59.7457	40.0000	122.6368	.7412	92.7915	-5.5120	.7085	.6886	.1664	.0000
741	58.7500	39.7658	121.6140	.7559	92.0605	-5.7169	.7211	.7030	.1606	.0000
696	57.5000	39.4922	120.3344	.7738	91.1274	-5.9660	.7364	.7209	.1505	.0000
647	56.2500	39.2454	119.0602	.7889	90.1799	-6.1750	.7491	.7366	.1367	.0000
599	55.0000	39.0295	117.7917	.7988	89.2226	-6.3131	.7575	.7481	.1191	.0000
553	53.7500	38.8486	116.5286	.8013	88.2623	-6.3481	.7596	.7533	.0977	.0000
507	52.5000	38.7067	115.2705	.7831	87.3075	-6.0943	.7442	.7408	.0718	.0000
459	51.2500	38.5956	114.0156	.7577	86.3919	-5.7413	.7226	.7199	.0630	.0000
408	50.0000	38.4872	112.7609	.7542	85.4940	-5.6923	.7196	.7171	.0606	.0000
354	48.7500	38.3898	111.5071	.7668	84.5868	-5.8680	.7304	.7287	.0503	-.0000
301	47.5000	38.3202	110.2551	.7823	83.6638	-6.0842	.7436	.7430	.0298	.0000
246	46.2500	38.2949	109.0048	.7935	82.7260	-6.2390	.7530	.7530	-.0014	.0000
186	45.0000	38.3301	107.7541	.7962	81.7805	-6.2774	.7553	.7541	-.0426	.0000
137	43.7500	38.4430	106.4987	.7853	80.8331	-6.1248	.7461	.7401	-.0946	.0000
95	42.5000	38.6604	105.2295	.7540	79.8971	-5.6896	.7194	.7019	-.1578	-.0000
57	41.2500	39.0198	103.9280	.6907	78.9848	-4.8156	.6645	.6254	-.2246	-.0000
33	40.0000	39.5966	102.5494	.5784	78.1219	-3.3143	.5639	.4860	-.2859	-.0000
4	39.4027	40.0000	101.8281	.5016	77.7386	-2.3547	.4929	.3894	-.3021	-.0000
12	38.7500	40.6162	100.9290	.3949	77.3386	-1.1593	.3916	.2545	-.2976	-.0000
1	37.9789	42.5000	98.8575	.0643	76.7779	.9559	.0647	.0030	-.0647	-.0000
13	38.7500	44.7495	96.4237	.2587	77.2093	.0464	.2588	.1704	.1947	-.0000
5	38.9909	45.0000	96.0761	.2829	77.3094	-.1367	.2826	.2027	.1969	-.0000
34	40.0000	45.7338	94.8251	.3305	77.7050	-.5382	.3292	.2860	.1631	-.0000
20	41.0892	46.2500	93.6189	.3445	78.1172	-.6659	.3429	.3177	.1289	-.0000
58	41.2500	46.3125	93.4463	.3445	78.1777	-.6660	.3429	.3205	.1218	-.0000
96	42.5000	46.7208	92.1309	.3373	78.6274	-.5998	.3359	.3232	.0913	-.0000
138	43.7500	47.0355	90.8418	.3245	79.0528	-.4854	.3234	.3155	.0712	-.0000
187	45.0000	47.2949	89.5651	.3114	79.4575	-.3713	.3106	.3050	.0587	-.0000
179	46.1158	47.5000	88.4306	.2998	79.8034	-.2737	.2992	.2949	.0510	-.0000
247	46.2500	47.5237	88.2943	.2985	79.8437	-.2628	.2979	.2934	.0517	-.0000

Figure 21d. Surface Properties – θ-Constant Cuts

X= 47.5000 THETA=180.000 DEGREES

R	MACH	PHI	CP	U	U-RADIAL	U-THETA	V	W
.0000	.5598	81.3583	-3.0756	.5372	-.1019	-.0000	.1019	.0000
5.0000	.5703	80.8256	-3.2107	.5451	-.1121	-.0000	.1121	.0000
10.0000	.5868	80.2368	-3.4235	.5578	-.1247	-.0000	.1247	.0000
15.0000	.6095	79.5786	-3.7209	.5751	-.1410	-.0000	.1410	.0000
20.0000	.6390	78.8273	-4.1142	.5969	-.1629	.0000	.1629	-.0000
23.7500	.6662	78.1807	-4.4809	.6159	-.1845	.0000	.1845	-.0000
27.5000	.6982	77.4438	-4.9182	.6368	-.2118	.0000	.2118	-.0000
31.2500	.7356	76.5920	-5.4352	.6591	-.2465	-.0000	.2465	.0000
35.0000	.7800	75.5947	-6.0511	.6822	-.2908	-.0000	.2908	.0000
37.5000	.8151	74.8262	-6.5404	.6982	-.3275	-.0000	.3275	.0000
40.0000	.8577	73.9574	-7.1304	.7151	-.3726	-.0000	.3726	.0000
42.5000	.9127	72.9629	-7.8864	.7336	-.4311	-.0000	.4311	.0000
45.0000	.9917	71.8017	-8.9493	.7546	-.5138	-.0000	.5138	.0000
46.2500	1.0447	71.1285	-9.6405	.7662	-.5670	-.0000	.5670	.0000
47.5000	1.1125	70.3843	-10.4929	.7798	-.6308	-.0000	.6308	.0000
48.7500	1.2246	69.5514	-11.8134	.7992	-.7287	-.0000	.7287	.0000
49.1134	1.2676	69.2790	-12.2883	.8106	-.7589	-.0000		
*****								
53.3622	.2584	65.0955	.0484	-.2291	-.1198	-.0000		
55.0000	.1122	64.9361	.8304	-.0426	-.1045	-.0000	.1045	.0000
57.5000	.1261	64.6474	.7816	.0529	-.1152	-.0000	.1152	.0000
60.0000	.1516	64.3601	.6774	.1011	-.1139	-.0000	.1139	.0000
62.5000	.1714	64.0776	.5841	.1305	-.1122	-.0000	.1122	.0000
65.0000	.1863	63.7992	.5069	.1505	-.1108	-.0000	.1108	.0000
67.5000	.1977	63.5235	.4433	.1651	-.1098	-.0000	.1098	.0000
70.0000	.2068	63.2499	.3901	.1763	-.1092	-.0000	.1092	.0000
77.5000	.2240	62.4373	.2840	.1967	-.1081	-.0000	.1081	.0000
85.0000	.2346	61.6284	.2150	.2087	-.1079	-.0000	.1079	.0000
92.5000	.2416	60.8195	.1674	.2164	-.1080	-.0000	.1080	.0000
100.0000	.2466	60.0090	.1329	.2218	-.1082	-.0000	.1082	.0000
112.5000	.2520	58.6531	.0944	.2276	-.1087	-.0000	.1087	.0000
125.0000	.2556	57.2906	.0689	.2312	-.1092	-.0000	.1092	.0000
137.5000	.2580	55.9221	.0511	.2337	-.1097	-.0000	.1097	.0000
150.0000	.2598	54.5484	.0383	.2354	-.1101	-.0000	.1101	.0000
175.0000	.2620	51.7878	.0223	.2375	-.1107	-.0000	.1107	.0000
200.0000	.2633	49.0156	.0127	.2388	-.1110	-.0000	.1110	.0000
225.0000	.2641	46.2362	.0065	.2396	-.1113	-.0000	.1113	.0000
250.0000	.2648	43.4526	.0018	.2402	-.1114	.0000	.1114	-.0000

SEGMENT MASS FLOW: 909.0689

Figure 21e. Field Properties

****
* MASS FLOW IN INLET DUCT *
****

X	MASS FLOW	PER CENT ERROR
46.2500	11600.8888	-.86
47.5000	11607.1487	-.81
48.7500	11616.1892	-.73
50.0000	11624.2408	-.66
51.2500	11629.3255	-.62
52.5000	11630.1154	-.61
53.7500	11631.1908	-.60
55.0000	11633.9820	-.58
56.2500	11637.5500	-.55
57.5000	11640.8308	-.52
58.7500	11652.6285	-.42
60.0000	11676.3242	-.22
61.2500	11694.2369	-.06
62.5000	11692.6510	-.08
63.7500	11693.5985	-.07
65.0000	11695.2010	-.06
67.5000	11694.8409	-.06
70.0000	11695.4334	-.05
72.5000	11698.3236	-.03
75.0000	11705.7081	.03
77.5000	11721.2622	.17
80.0000	11736.0964	.29
82.5000	11750.0016	.41
85.0000	11777.5320	.65
87.5000	11788.1267	.74
90.0000	11798.5358	.83
92.5000	11835.7361	1.15
95.4400	11655.7537	-.39

Figure 21f. Mass-Flow Conservation

SURFACE FLOW PROPERTIES - X = CONSTANT CUTS

INDEX	X	R	THETA	S	MACH	CP	PHI	Q	PHI*S	U	U-RADIAL	U-THETA
33	40.0000	39.5966	.0000	.0000	.5784	-3.3143	78.1219	.5639	.0000	.4860	-.2859	-.0000
48	40.0000	40.0000	339.3594	14.3206	.5607	-3.0875	77.7366	.5477	-.0481	.4567	-.3008	.0302
41	40.0000	40.0761	337.5000	15.6222	.5591	-3.0677	77.7051	.5462	-.0522	.4524	-.3043	.0337
39	40.0000	41.5946	315.0000	31.6956	.4955	-2.2819	76.4225	.4872	-.1130	.3354	-.3468	.0678
46	40.0000	42.5000	306.9022	37.7043	.4832	-2.1353	75.7290	.4756	-.1457	.2728	-.3820	.0766
47	40.0000	45.0000	295.5275	47.0879	.1003	.8680	73.9176	.1009	-.0896	-.0038	-.0702	.0724
40	40.0000	46.1618	315.0000	65.0059	.2330	.2252	75.8506	.2334	.0919	.1585	.1427	.0948
42	40.0000	45.8325	337.5000	83.0669	.3028	-.2983	77.2180	.3021	.0513	.2524	.1572	.0532
34	40.0000	45.7338	.0000	101.0392	.3305	-.5382	77.7050	.3292	-.0000	.2860	.1631	-.0000
36	40.0000	45.8325	22.5000	119.0114	.3028	-.2984	77.2179	.3021	-.0513	.2524	.1573	-.0532
38	40.0000	46.1618	45.0000	137.0725	.2330	.2251	75.8506	.2334	-.0919	.1585	.1427	-.0949
45	40.0000	45.0000	64.4733	154.9703	.1002	.8683	73.9179	.1008	.0895	-.0038	-.0700	-.0724
44	40.0000	42.5000	53.1037	164.3524	.4833	-2.1369	75.7284	.4757	.1458	.2725	-.3824	-.0765
37	40.0000	41.5938	45.0000	170.3654	.4957	-2.2838	76.4231	.4873	.1130	.3358	-.3466	-.0679
35	40.0000	40.0762	22.5000	186.4384	.5592	-3.0682	77.7050	.5463	.0522	.4524	-.3043	-.0337
43	40.0000	40.0000	20.6395	187.7408	.5607	-3.0880	77.7365	.5477	.0481	.4567	-.3008	-.0302

INDEX	X	R	THETA	S	MACH	CP	PHI	Q	PHI*S	U	U-RADIAL	U-THETA
186	45.0000	38.3301	.0000	.0000	.7962	-6.2774	81.7805	.7553	-.0000	.7541	-.0426	.0000
210	45.0000	38.6406	337.5000	15.0975	.8120	-6.4974	81.4317	.7686	-.0464	.7651	-.0583	.0440
208	45.0000	39.5468	315.0000	30.4581	.8819	-7.4648	80.3563	.8261	-.0874	.8144	-.1145	.0787
228	45.0000	40.0000	307.3213	35.8070	.9070	-7.8094	79.8994	.8464	-.1013	.8290	-.1459	.0888
206	45.0000	41.0944	292.5000	46.3474	.9602	-8.5301	78.5025	.8885	-.1434	.8508	-.2272	.1179
227	45.0000	42.5000	277.3734	57.4665	.9600	-8.5274	76.7801	.8883	-.1587	.8214	-.3164	.1198
204	45.0000	43.2796	270.0000	63.0403	.9609	-8.5388	75.8852	.8890	-.1653	.8030	-.3639	.1142
226	45.0000	45.0000	255.3176	74.4786	.9757	-8.7362	73.8866	.9005	-.1800	.7511	-.4846	.1096
202	45.0000	45.9916	247.5000	80.7646	.9817	-8.8170	72.7365	.9052	-.1676	.7108	-.5547	.0800
223	45.0000	46.2500	245.5258	82.3746	.9763	-8.7443	72.5451	.9010	-.1708	.6933	-.5706	.0744
224	45.0000	47.5000	236.3133	90.0138	.9638	-8.5772	71.1041	.8912	-.2026	.5922	-.6602	.0885
225	45.0000	48.7500	227.9854	97.1177	.9196	-7.9805	69.5720	.8564	-.2023	.4226	-.7428	.0559
200	45.0000	49.2845	225.0000	99.7268	.9084	-7.8284	69.0798	.8475	-.2055	.3202	-.7841	.0304
222	45.0000	50.0000	222.1347	102.3120	.7740	-5.9686	68.5055	.7366	-.2144	.1219	-.7256	.0353
201	45.0000	51.0875	225.0000	105.5098	.4868	-2.1781	67.8509	.4790	-.1495	-.2006	-.4170	-.1236
203	45.0000	51.0493	247.5000	125.6313	.1088	.8416	69.4193	.1094	.1084	-.0135	-.0096	.1082
205	45.0000	50.1472	270.0000	145.5458	.2024	.4165	72.1787	.2029	.1365	.1442	.0331	.1389
229	45.0000	50.0000	272.7158	147.9238	.2103	.3695	72.2929	.2108	.1385	.1563	.0358	.1369
207	45.0000	49.0561	292.5000	165.0471	.2876	-.1744	74.9868	.2873	.1268	.2512	.0513	.1296
230	45.0000	48.7500	299.5966	171.1119	.2930	-.2178	75.5597	.2925	.1138	.2631	.0506	.1175
209	45.0000	48.1241	315.0000	184.1477	.3164	-.4143	77.4083	.3155	.1170	.2873	.0521	.1195
231	45.0000	47.5000	337.1313	202.6124	.3094	-.3541	78.9180	.3086	.0554	.2977	.0581	.0570
211	45.0000	47.4933	337.5000	202.9181	.3093	-.3534	78.9195	.3085	.0545	.2978	.0581	.0558
187	45.0000	47.2949	.0000	221.5179	.3114	-.3713	79.4575	.3106	-.0000	.3050	.0587	-.0000
189	45.0000	47.4933	22.5000	240.1178	.3093	-.3534	78.9194	.3085	-.0545	.2978	.0581	-.0558
212	45.0000	47.5000	22.8678	240.4228	.3094	-.3541	78.9180	.3086	-.0554	.2977	.0581	-.0570
191	45.0000	48.1241	45.0000	258.8882	.3164	-.4144	77.4081	.3155	-.1169	.2873	.0522	-.1195
213	45.0000	48.7500	60.3888	271.9117	.2930	-.2178	75.5623	.2925	-.1137	.2632	.0502	-.1174
193	45.0000	49.0579	67.5000	277.9891	.2876	-.1748	74.9874	.2873	-.1268	.2513	.0509	-.1296
215	45.0000	50.0000	87.2757	295.1054	.2103	.3695	72.2936	.2108	-.1385	.1562	.0361	-.1369
195	45.0000	50.1473	90.0000	297.4909	.2023	.4167	72.1789	.2029	-.1365	.1442	.0331	-.1389
197	45.0000	51.0494	112.5000	317.4054	.1088	.8416	69.4195	.1094	-.1084	-.0135	-.0096	-.1082
199	45.0000	51.0875	135.0000	337.5269	.4870	-2.1804	67.8514	.4792	.1497	-.2006	-.4171	.1238
221	45.0000	50.0000	137.8708	340.7159	.7742	-5.9711	68.5062	.7367	.2144	.1223	-.7256	-.0353
198	45.0000	49.2845	135.0000	343.3058	.9080	-7.8225	69.0806	.8472	.2052	.3205	-.7836	-.0305
220	45.0000	48.7500	132.0128	345.9165	.9195	-7.9801	69.5728	.8564	.2022	.4226	-.7427	-.0560
219	45.0000	47.5000	123.6931	353.0135	.9641	-8.5823	71.1041	.8915	.2027	.5920	-.6607	-.0884
218	45.0000	46.2500	114.4758	360.6566	.9762	-8.7437	72.5461	.9009	.1708	.6936	-.5701	-.0745
196	45.0000	45.9917	112.5000	362.2679	.9817	-8.8166	72.7373	.9052	.1675	.7111	-.5544	-.0800

Figure 21g. Surface Properties – All Cuts

217	45.0000	45.0000	104.6813	368.5547	.9756	-8.7347	73.8871	.9004	.1800	.7510	-.4844	-.1096
194	45.0000	43.2758	90.0000	379.9922	.9606	-8.5353	75.8851	.8888	.1652	.8028	-.3639	-.1141
216	45.0000	42.5060	82.6258	385.5666	.9601	-8.5284	76.7796	.8884	.1586	.8213	-.3169	-.1197
192	45.0000	41.0934	67.5000	396.6851	.9610	-8.5407	78.5018	.8891	.1435	.8513	-.2277	-.1179
214	45.0000	40.0000	52.6976	407.2120	.9080	-7.8221	79.8980	.8471	.1015	.8297	-.1459	-.0890
190	45.0000	39.5458	45.0000	412.5739	.8828	-7.4768	80.3569	.8269	.0874	.8151	-.1142	-.0788
188	45.0000	38.6402	22.5000	427.9341	.8122	-6.4995	81.4321	.7687	.0463	.7653	-.0582	-.0440

INDEX	X	R	THETA	S	MACH	CP	PHI	Q	PHI,S	U	U-RADIAL	U-THETA
408	50.0000	38.4872	.0000	.0000	.7542	-5.6923	85.4940	.7196	-.0000	.7171	.0606	.0000
438	50.0000	38.7339	337.5000	15.1494	.7683	-5.8891	85.2065	.7317	-.0370	.7287	.0544	.0387
436	50.0000	39.4278	315.0000	30.4989	.8149	-6.5370	84.3593	.7710	-.0802	.7659	.0329	.0822
451	50.0000	40.0000	302.4700	39.2005	.8607	-7.1717	83.5383	.8088	-.0919	.8034	.0107	.0929
434	50.0000	40.5501	292.5000	46.2293	.9188	-7.9696	82.9068	.8558	-.1026	.8496	-.0157	.1017
432	50.0000	42.0722	270.0000	62.5136	1.0764	-10.0440	80.8646	.9767	-.1279	.9627	-.1163	.1166
449	50.0000	42.5000	264.4262	66.6493	1.1054	-10.4058	80.4755	.9979	-.1337	.9797	-.1478	.1190
430	50.0000	43.8741	247.5000	79.4804	1.2002	-11.5360	78.3203	1.0649	-.1597	1.0251	-.2558	.1329
448	50.0000	45.0000	233.8120	90.1573	1.2006	-11.5411	76.6889	1.0652	-.1542	1.0052	-.3293	.1251
428	50.0000	45.6784	225.0000	97.1643	1.2003	-11.5379	75.6018	1.0650	-.1308	.9944	-.3685	.0976
447	50.0000	46.2500	216.5905	103.9361	1.2382	-11.9663	74.8750	1.0908	-.1140	1.0074	-.4098	.0839
426	50.0000	46.9826	202.5000	115.4304	1.3069	-12.7060	73.4354	1.1362	-.0915	1.0312	-.4722	.0681
424	50.0000	47.4511	180.0000	134.0104	1.3719	-13.3609	72.7500	1.1775	.0000	1.0560	-.5211	-.0000
422	50.0000	46.9827	157.5000	152.5906	1.3064	-12.7008	73.4359	1.1359	.0914	1.0309	-.4722	-.0680
446	50.0000	46.2500	143.4075	164.0863	1.2375	-11.9586	74.8750	1.0903	.1139	1.0069	-.4098	-.0838
420	50.0000	45.6784	135.0000	170.8567	1.1995	-11.5285	75.6014	1.0644	.1308	.9939	-.3685	-.0976
445	50.0000	45.0000	126.1876	177.8640	1.2001	-11.5353	76.6883	1.0648	.1542	1.0049	-.3292	-.1251
418	50.0000	43.8743	112.5000	188.5407	1.2001	-11.5349	78.3199	1.0648	.1597	1.0250	-.2558	-.1329
443	50.0000	42.5000	95.5737	201.3719	1.1054	-10.4058	80.4759	.9979	.1338	.9797	-.1478	-.1191
416	50.0000	42.0722	90.0000	205.5075	1.0765	-10.0445	80.8651	.9767	.1279	.9627	-.1163	-.1167
414	50.0000	40.5502	67.5000	221.7918	.9184	-7.9650	82.9072	.8555	.1026	.8493	-.0156	-.1016
441	50.0000	40.0000	57.5285	228.8216	.8605	-7.1690	83.5386	.8087	.0918	.8033	.0107	-.0929
412	50.0000	39.4277	45.0000	237.5222	.8150	-6.5386	84.3593	.7711	.0802	.7660	.0328	-.0822
410	50.0000	38.7337	22.5000	252.8716	.7684	-5.8901	85.2066	.7318	.0370	.7287	.0544	-.0387

INDEX	X	R	THETA	S	MACH	CP	PHI	Q	PHI,S	U	U-RADIAL	U-THETA
409	50.0000	48.2364	.0000	.0000	.2793	-.1088	80.9253	.2791	-.0000	.2714	.0648	-.0000
411	50.0000	48.4486	22.5000	18.9721	.2817	-.1273	80.3473	.2814	-.0672	.2657	.0622	-.0685
440	50.0000	48.7500	35.4171	29.9305	.2677	-.0200	79.3790	.2676	-.0798	.2485	.0563	-.0820
413	50.0000	49.0518	45.0000	38.1140	.2597	.0393	78.7790	.2597	-.0944	.2357	.0511	-.0965
415	50.0000	49.9882	67.5000	57.5745	.2460	.1369	76.2665	.2462	-.1439	.1954	.0340	-.1460
442	50.0000	50.0000	67.7488	57.7920	.2449	.1448	76.2637	.2451	-.1442	.1949	.0340	-.1447
417	50.0000	51.1274	90.0000	77.4582	.2505	.1054	73.1018	.2507	-.1553	.1929	.0293	-.1573
419	50.0000	52.2923	112.5000	97.8010	.2099	.3718	70.0564	.2104	-.1341	.1588	.0258	-.1357
444	50.0000	52.5000	116.7418	101.6856	.1969	.4477	69.7183	.1976	-.1313	.1448	.0239	-.1323
421	50.0000	53.2988	135.0000	118.5670	.1445	.7086	67.3369	.1452	-.1163	.0847	.0149	-.1170
423	50.0000	53.9611	157.5000	139.6517	.0645	.9556	65.5386	.0649	-.0582	.0279	.0058	-.0583
425	50.0000	54.1916	180.0000	160.9040	.0020	1.0176	64.8827	.0020	-.0000	.0019	.0005	-.0000
427	50.0000	53.9611	202.5000	182.1563	.0645	.9556	65.5384	.0649	.0582	.0279	.0058	.0583
429	50.0000	53.2987	225.0000	203.2410	.1445	.7085	67.3367	.1452	.1163	.0847	.0149	.1170
450	50.0000	52.5000	243.2561	220.1205	.1969	.4478	69.7178	.1975	.1313	.1448	.0239	.1323
431	50.0000	52.2922	247.5000	224.0071	.2099	.3718	70.0562	.2104	.1341	.1588	.0258	.1357
433	50.0000	51.1273	270.0000	244.3498	.2505	.1054	73.1016	.2507	.1553	.1929	.0293	.1573
452	50.0000	50.0000	292.2502	264.0151	.2449	.1447	76.2635	.2451	.1442	.1950	.0340	.1447
435	50.0000	49.9882	292.5000	264.2334	.2460	.1368	76.2663	.2463	.1439	.1954	.0341	.1460
437	50.0000	49.0518	315.0000	283.6939	.2597	.0393	78.7789	.2597	.0944	.2357	.0511	.0965
453	50.0000	48.7500	324.5831	291.8776	.2677	-.0200	79.3790	.2676	.0798	.2485	.0563	.0820
439	50.0000	48.4486	337.5000	302.8359	.2817	-.1273	80.3473	.2814	.0672	.2657	.0622	.0685

INDEX	X	R	THETA	S	MACH	CP	PHI	Q	PHI,S	U	U-RADIAL	U-THETA

Figure 21g. Concluded

Table 4. Headings for Surface Point and Surface Geometry Printout

INDEX	Surface point index
X	x
R	r
THETA	θ
NX	n_x, component of unit surface normal
NR	n_r, component of unit surface normal
NT	n_θ, component of unit surface normal
S	s, arc length along cut
PHI,S-XC	ϕ_{s_x}, velocity along x constant cut
PHI,S-RC	ϕ_{s_r}, velocity along r constant cut
PHI,S-TC	ϕ_{s_θ}, velocity along θ constant cut
I, J, K	i, j, k of field point adjacent to surface point
SURFARM	Δx, Δr or $\Delta\theta$ between surface point and adjacent field point
TYPE	-1 = x intersect 0 = theta intersect 1 = r interset 2 = both mesh and surface node

Table 5. Convergence History Headings

SWEEP	Relaxation sweep number, (n)
FIELD POINTS	
AVE RESIDUE	Sum of $\lvert\phi_{i,j,k}^{(n)}-\phi_{i,j,k}^{(n-1)}\rvert$ over all points i,j,k in the flowfield divided by $\phi_{max}^{(n)}-\phi_{min}^{(n)}$ and the number of such field points
I J K MAX RESIDUE	The indices i,j,k of the field point having the maximum change in ϕ and the maximum value of $\lvert\phi_{i,j,k}^{(n)}-\phi_{i,j,k}^{(n-1)}\rvert$ divided by $\phi_{max}^{(n)}-\phi_{min}^{(n)}$
"CONVERGING/ DIVERGING"	**, MAX RESIDUE decreasing, or ***, MAX RESIDUE increasing
SURFACE POINTS	
AVE RESIDUE	Sum of $\lvert\phi_S^{(n)}-\phi_S^{(n-1)}\rvert$ over all surface points S divided by $\phi_{max}^{(n)}-\phi_{min}^{(n)}$ and the number of surface points
I J K INDEX MAX RESIDUE	The indices i,j,k of the field point next to the surface point with the maximum change in ϕ, the index of that surface point, and the maximum value of $\lvert\phi_S^{(n)}-\phi_S^{(n-1)}\rvert$ divided by $\phi_{max}^{(n)}-\phi_{min}^{(n)}$.
M > 1.0	number of field points for which Mach number > 1.0
EIGEN1	$1/(1-\lambda_1)$, equations 51,53
EIGEN2	$1/(1-\lambda_2)$, equations 51,54
"EXTRAPOLATION FLAG"	* indicates flowfield extrapolation using equation (52) was made after this sweep

Table 6. Surface-Point Printout Headings

INDEX	Surface point number
X	x
R	r
THETA	θ
S	s, arc length along the cut of the surface
MACH	Mach Number
CP	C_p, coefficient of pressure, $(p/p_\infty - 1)/\frac{1}{2}\gamma M^2$ (if $M_\infty = 0.0$, then $C_p = (p/p^* - 1)/\frac{1}{2}\gamma$, where the * indicates sonic conditions)
PHI	ϕ
Q	$q = (u^2 + u_r^2 + u_\theta^2)^{1/2}$
PHI,S	u_s, component of velocity along the cut
U	u
U-RADIAL	u_r
U-THETA	u_θ

Table 7. Field-Point Printout Headings

R	r
MACH	M
PHI	ϕ
CP	C_p, coefficient of pressure, $(p/p_\infty-1)/\frac{1}{2}\gamma M^2$ (if $M_\infty = 0.0$, then $C_p = (p/p_*-1)/\frac{1}{2}\gamma$, where the * indicates sonic conditions)
U	u
U-RADIAL	u_r
U-THETA	u_θ
V	v
W	w

3.4 RUN QUALITY

A major concern of the user is the degree to which the computed solution matches a real flowfield. This can be a relatively difficult question to answer. The primary effects are the nature of the flow analyzed, the accuracy of the analysis if a fully-converged solution is obtained, and the degree of convergence. The program predicts potential flow, which is inviscid irrotational flow. A necessary, but not sufficient, condition for acceptable flow prediction is that the flow to be analyzed not be greatly effected by viscous and rotational effects.

If the flow is one for which potential flow is a good approximation, the next question is the acceptability of the mesh placement. If the flow is a duct, the mass-flow integration will give a check on accuracy. Otherwise, the best way to estimate accuracy (assuming a converged solution) is by comparison with experiments for the same or similar configurations.

The question of convergence can be answered, to a large extent, by looking at the AVE RESIDUE in the convergence history. Values of 10^{-6} are usually satisfactory. For any given class of problems a few extra long runs can be made to obtain 10^{-6} or better convergence, and the results compared with lesser levels to see if there are any significant changes in the answers.

3.5 DIAGNOSTICS AND TROUBLESHOOTING

Failure of the program to successfully provide a flow analysis for a data case could be due to a number of causes. Among these are input errors, errors in the program, and geometries the program was not written to handle. As obtaining help to determine if the program is in error can be very time consuming, it is preferable for a user to first check for input errors. The program does a considerable amount of input checking and many of the diagnostics are self-explanatory. The first step in searching for the cause of any run failure should be to check the printout for any diagnostic messages.

One task of the program is checking the input geometry for completeness and self-consistency. Many of the error messages in this section are self-explanatory. One area that may be confusing is the messages from the subroutine which generates internal maps. There is a subroutine in the program that generates the maps that essentially list the surface points in sequence along x, r, and θ constant cuts. If there are points missing, or points that are not consistent with each other, this subroutine will print diagnostic messages. The code works by starting at a surface point on a cut and then trying to follow the cut by finding the surface points in sequence on the cut. If the subroutine cannot find the next point on a cut, and the previous point was not a boundary point of the computational flowfield, an error message is printed and the points on the cut that have already been found will be printed. The problem area is at the end of the printed cut. Some more information may be obtained by looking at similar error printouts next to the one of interest as, usually, the parts of a cut on either side of a bad or missing surface point will be printed separately. The procedure for correcting the input error is to examine the area of difficulty, usually by sketches or plots, to determine the nature of the problem. If all surface points near the problem area are plotted versus the mesh, the problem is usually obvious.

In interpreting the points printed out, the user should be aware that the mapping subroutine starts at a point and tracks the curve until it ends on a boundary or closes on itself. If the cut ends on a boundary, it then is followed in the opposite direction from the start point to the other end of the cut. If the subroutine is successful, the two segments of the curve are connected together in sequence. If the mapping routine fails while following the second segment, the points printed will be in sequence from the start point to the boundary point, followed by a sequence in the opposite sense from the point next to the start point to the problem area.

The most common geometry problems are illustrated in figure 22. The problem of figure 22a is simply a point missing from the geometry file. The problem shown in figure 22b is inconsistent geometry points. Moving A to A′ or B to B′ would make the points consistent. This condition is usually caused by a tolerance problem in the geometry/mesh intersection program. Points A and B are very close to the mesh intersection and have been found by separate passes of the geometry processing code. A small error in position is enough to put the point on the wrong side of the mesh intersect. Often this problem can be fixed by replacing points A and B with a single point at the mesh intersect. Remember there is usually a point C in the third coordinate which should also be consolidated with A and B at the mesh intersect.

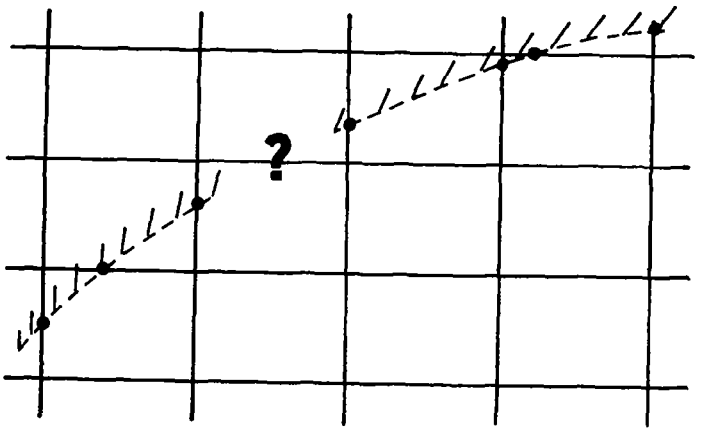

a.) MISSING SURFACE POINT

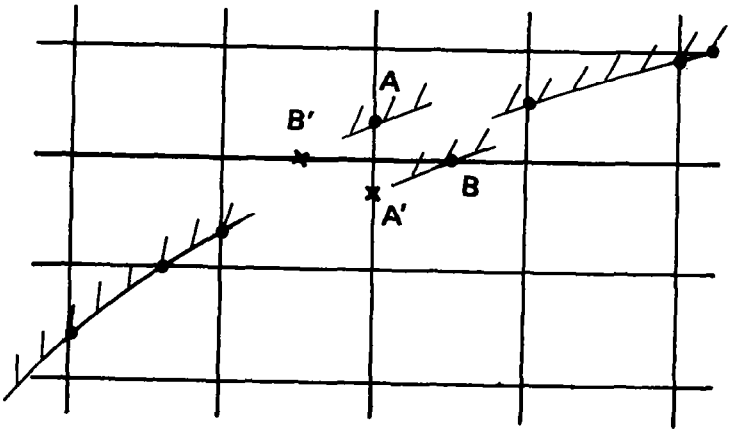

b.) INCONSISTENT SURFACE POINTS

Figure 22. Typical Geometry Problems

REFERENCES

1. Murman, E. M. and Cole, J. D, "Calculation of Plane Steady Transonic Flows," *AIAA Journal,* Vol. 9, January 1971, pp. 114-121.

2. Jameson, A., "Iterative Solution of Transonic Flows Over Airfoils and Wings, Including Flows at Mach 1," *Comm. Pure Appl. Math.,* Vol. 27, May 1974, pp. 283-309.

3. Reyhner, T.A., "Transonic Potential Flow Around Axisymmetric Inlets and Bodies at Angle of Attack," *AIAA Journal,* Vol. 15, September 1977, pp. 1299-1306.

4. Caughey, D. A. and Jameson, A., "Numerical Calculation of Transonic Potential Flow About Wing-Body Combinations," *AIAA Journal,* Vol. 17, February 1979, pp. 175-181.

5. Chen, L-t. and Caughey, D. A. , "Higher-Order, Finite-Difference Scheme for Three-Dimensional Transonic Flowfields about Axisymmetric Bodies," *Journal of Aircraft,* Vol. 17, September 1980, pp. 668-676.

6. Reyhner, T.A., "Cartesian Mesh Solution for Axisymmetric Transonic Potential Flow Around Inlets," *AIAA Journal,* Vol. 15, May 1977. pp. 624-631.

7. Lomax, H. and Steger, J. L., "Relaxation Methods in Fluid Mechanics," *Annual Review of Fluid Mechanics,* Vol. 7, Annual Reviews Inc., Palo Alto, CA 1975, pp. 63-88.

8. Brandt, A., "Multilevel Adaptive Computations in Fluid Dynamics," *AIAA Journal,* Vol. 18, October 1980, pp. 1165-1172.

9. Gibson, S. G., "User's Manual for the Propulsion Bicubic Geometry System (IGS and DRAW6)," D6-48968, Boeing Commercial Airplane Co., Seattle WA, 1980.

10. Syberg, J. and Koncsek, J. L., "Low Speed Tests of a Fixed Geometry Inlet for a Tilt-Nacelle V/STOL Airplane," NASA CR-151922, 1977.

11. Shain, W. M., "Test Data Report, Low-Speed Wind Tunnel Tests of a Full-Scale Lift/Cruise-Fan Inlet, With Engine, At High Angles of Attack," NASA CR-152055, January 1978.

12. Hodder, B. K., "An Investigation of Engine Influence on Inlet Performance Conducted in the Ames 40- by 80-Foot Wind Tunnel," NASA CR-166136, 1981.

13. Lane, J. M., Carpenter, L. C., Whitted, T., and Blinn, J. F., "Scan Line Methods for Displaying Parameterically Defined Surfaces," Comm. ACM, Vol. 23, January 1980, pp. 23-34.

14. CDC CYBER 200 FORTRAN Language 1.4, Reference Manual, Control Data Corporation, Sunnyvale CA, No. 60456040, 1979.

APPENDIX A

TRIDIAGONAL EQUATION SOLVER

The following is the logic for direct solution of a system of N simultaneous linear equations which are of tridiagonal form. If the unknown is ϕ_j, j=1,2...N, the equations are tridiagonal if they can be ordered such that the jth equations involves only ϕ_{j-1}, ϕ_j and ϕ_{j+1}.

The difference equations are:

$$Y_1\phi_1 + Z_1\phi_2 = G_1 \tag{A-1}$$

$$X_j\phi_{j-1} + Y_j\phi_j + Z_j\phi_{j+1} = G_j \qquad 2 \leq j \leq N-1 \tag{A-2}$$

$$X_N\phi_{N-1} + Y_N\phi_N = G_N. \tag{A-3}$$

For the above notation ϕ_j represents $\phi_{i,j,k}$ as the lines for SLOR in this program are radial lines for which j is the radial index.

The equations can be written in matrix notation as

$$PW = R \tag{A-4}$$

where

$$P = \begin{bmatrix} Y_1 & Z_1 & & & & & & \\ X_2 & Y_2 & Z_2 & & & & & \\ & X_3 & Y_3 & Z_3 & & & & \\ & & \cdot & \cdot & \cdot & & & \\ & & & & \cdot\ \cdot & \cdot & & \\ & & & & X_{N-2} & Y_{N-2} & Z_{N-2} & \\ & & & & & X_{N-1} & Y_{N-1} & Z_{N-1} \\ & & & & & & X_N & Y_N \end{bmatrix} \tag{A-5}$$

$$W = \begin{bmatrix} \phi_1 \\ \phi_2 \\ \phi_3 \\ \cdot \\ \cdot \\ \cdot \\ \cdot \\ \cdot \\ \cdot \\ \phi_N \end{bmatrix} \tag{A-6}$$

$$R = \begin{bmatrix} G_1 \\ G_2 \\ G_3 \\ \cdot \\ \cdot \\ \cdot \\ \cdot \\ \cdot \\ \cdot \\ G_N \end{bmatrix} \tag{A-7}$$

P can be decomposed into two triangular matrices, M and N, such that

$$P = MN \tag{A-8}$$

where

$$M = \begin{bmatrix} M_1 & & & & & & \\ X_2 & M_2 & & & & & \\ & X_3 & M_3 & & & & \\ & & \cdot & \cdot & & & \\ & & & X_{N-2} & M_{N-2} & & \\ & & & & X_{N-1} & M_{N-1} & \\ & & & & & X_N & M_N \end{bmatrix} \tag{A-9}$$

and

$$N = \begin{bmatrix} I & N_1 & & & & & \\ & I & N_2 & & & & \\ & & I & N_3 & & & \\ & & & \cdot & \cdot & & \\ & & & & I & N_{N-2} & \\ & & & & & I & N_{N-1} \\ & & & & & & I \end{bmatrix} \tag{A-10}$$

The following relations are then obtained:

$$\begin{aligned} M_1 &= Y_1 \\ M_j &= Y_j - X_j N_{j-1} \qquad 2 \leq j \leq N \\ N_j &= Z_j / M_j \qquad 1 \leq j \leq N-1 \end{aligned} \tag{A-11}$$

The matrix U is defined by

$$MU = R \tag{A-12}$$

where

$$U = \begin{bmatrix} U_1 \\ U_2 \\ U_3 \\ \cdot \\ \cdot \\ \cdot \\ \cdot \\ \cdot \\ U_N \end{bmatrix} \tag{A-13}$$

which gives the relations

$$\begin{aligned} U_1 &= G_1/M_1 \\ U_j &= (G_j - X_j U_{j-1})/M_j \,. \qquad 2 \leq j \leq N \end{aligned} \tag{A-14}$$

When equations (A-8) and (A-12) are substituted into equation (A-4) and the resulting equation is multiplied by M^{-1}, the following matrix equation is obtained:

$$NW = U \tag{A-15}$$

which leads to the following equations for the ϕ_j:

$$\begin{aligned} \phi_N &= U_N \\ \phi_j &= U_j - N_j \phi_{j+1} \,. \qquad 1 \leq j \leq N-1 \end{aligned} \tag{A-16}$$

The solution procedure to obtain the ϕ_j is to use (A-11) to obtain M_j and N_j and (A-14) to obtain the U_j for all j. Then (A-16) is used to calculate the ϕ_j.

APPENDIX B

PARAMETRIC CUBIC INTERPOLATION

Parametric cubic interpolation is used for interpolating to finer meshes as well as in several other areas of the program. It was chosen because odd-order interpolation leads to symmetric formulas, which are preferrable, and first-order or linear interpolation was thought to be too inaccurate. Also, cubic interpolation, as used with function and first derivatives, requires information at only two points. Given points A and B and a parameter u which is zero at A and 1 at B, then a function f(u) can be expressed as

$$f(u) = C_0 + C_1u + C_2u^2 + C_3u^3 \tag{B-1}$$

however, the form

$$f(u) = F_0(u)f(0) + F_1(u)f(1) + D_0(u)f_u(0) + D_1(u)f_u(1) \tag{B-2}$$

where the F_i and D_i are cubics in u, is preferrable for use in the code as it is easier to evaluate.

It can be shown with a little algebra that

$$F_0(u) = (1-u)^2\,(1+2u)$$

$$F_1(u) = u^2(3-2u)$$

$$D_0(u) = u(1-u)^2$$

$$D_1(u) = -u^2(1-u). \tag{B-3}$$

The formulas are expressed in parametric form for simplicity. If x is the coordinate of interest and the known points are x_0 and x_1:

$$u = (x-x_0)/(x_1-x_0) \tag{B-4}$$

$$f_u = (x_1-x_0)f_x. \tag{B-5}$$

The general interpolation formula for a unit cubic box with parametric coordinates u, v, and w is

$$
\begin{aligned}
f(u,v,w) = \sum_{i=0}^{1}\sum_{j=0}^{1}\sum_{k=0}^{1} \Big[& F_i(u)F_j(v)F_k(w)f_{i,j,k} \\
& + D_i(u)F_j(v)F_k(w)f_{u_{i,j,k}} \\
& + F_i(u)D_j(v)F_k(w)f_{v_{i,j,k}} \\
& + F_i(u)F_j(v)D_k(w)f_{w_{i,j,k}} \\
& + D_i(u)D_j(v)F_k(w)f_{uv_{i,j,k}} \\
& + F_i(u)D_j(v)D_k(w)f_{vw_{i,j,k}} \\
& + D_i(u)F_j(v)D_k(w)f_{wu_{i,j,k}} \\
& + D_i(u)D_j(v)D_k(w)f_{uvw_{i,j,k}} \Big]
\end{aligned}
\qquad \text{(B-6)}
$$

where

$$f_{i,j,k} = f(u_i, v_j, w_k)$$

and

$$u_0 = 0,\ u_1 = 1.0,\ v_0 = 0,\ v_1 = 1.0,\ w_0 = 0,\ w_1 = 1.0.$$

The above formula is used in the code for interpolation, except that the last four lines of equation B-6 are neglected. While this is incorrect, and introduces errors of unknown magnitude, it greatly simplifies the coding. Errors in the interpolation due to neglect of terms do not cause errors in the final flow solution, but instead increase the cost of a solution by requiring additional relaxation sweeps to eliminate the errors due to the interpolation process.

Referring to figure B-1 for notation, the value of a function f at (u,v,w) can either be calculated from equation B-6 or by the following procedure:

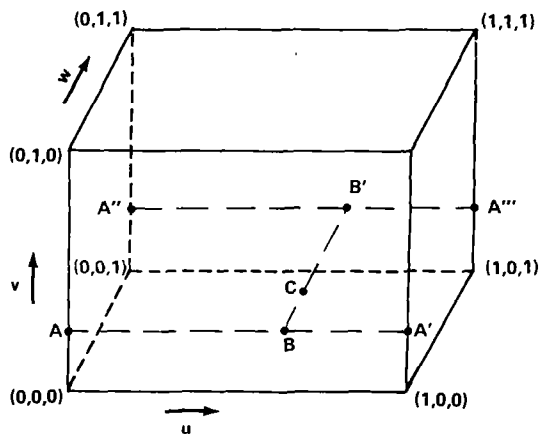

Figure B-1 Rectangular Box for Interpolation

First calculate,

$$
\begin{aligned}
f_A = f(0,v,0) &= \sum_{j=0}^{1} \left[F_j(v)f_{0,j,0} + D_j(v)f_{v_{0,j,0}}\right] \\
f_{u_A} = f_u(0,v,0) &= \sum_{j=0}^{1} \left[F_j(v)f_{u_{0,j,0}} + D_j(v)f_{uv_{0,j,0}}\right] \\
f_{w_A} = f_w(0,v,0) &= \sum_{j=0}^{1} \left[F_j(v)f_{w_{0,j,0}} + D_j(v)f_{vw_{0,j,0}}\right] \\
f_{wu_A} = f_{wu}(0,v,0) &= \sum_{j=0}^{1} \left[F_j(v)f_{wu_{0,j,0}} + D_j(v)f_{uvw_{0,j,0}}\right]
\end{aligned}
\tag{B-7}
$$

The same quantities are calculated at A′, A″, and A′″ by similar formulas. Then calculate

$$
\begin{aligned}
f_B &= f(u,v,0) = F_0(u)f_A + F_1(u)f_{A'} + D_0(u)f_{u_A} + D_1(u)f_{u_{A'}} \\
f_{w_B} &= f_w(u,v,0) = F_0(u)f_{w_A} + F_1(u)f_{w_{A'}} + D_0(u)f_{wu_A} + D_1(u)f_{wu_{A'}}.
\end{aligned}
\tag{B-8}
$$

$f_{B'}$ and $f_{w_{B'}}$ are calculated similarly

Then

$$
f_C = f(u,v,w) = F_0(w)f_B + F_1(w)f_{B'} + D_0(w)f_{w_B} + D_1(w)f_{w_{B'}}. \tag{B-9}
$$

The above procedure is exactly equivalent to using equation B-6. The advantage of the above procedure is that it can easily be used with minor modifications if one or more corners of the box are missing, which can occur in the vicinity of surfaces. This gives a workable interpolation procedure near surfaces, however, the results, when a corner of the box is missing, are not unique. That is, interpolating first in v, then in u, and finally in w as described, is not equivalent to another sequence. It is equivalent only if the rectangular box is complete.

1. Report No.	2. Government Accession No.	3. Recipient's Catalog No.
NASA CR-3514		

4. Title and Subtitle	5. Report Date
COMPUTATION OF TRANSONIC POTENTIAL FLOW ABOUT THREE-DIMENSIONAL INLETS, DUCTS, AND BODIES	March 1982
	6. Performing Organization Code
7. Author(s)	8. Performing Organization Report No.
Theodore A. Reyhner	D6-49848
	10. Work Unit No.
9. Performing Organization Name and Address	
Boeing Commercial Airplane Company P.O. Box 3707 Seattle, WA 98124	11. Contract or Grant No.
	13. Type of Report and Period Covered
12. Sponsoring Agency Name and Address	Contractor Report
National Aeronautics and Space Administration Washington, DC 20546	14. Sponsoring Agency Code

15. Supplementary Notes

Langley Technical Monitor: David E. Reubush
Cooperative Agreement

16. Abstract

An analysis has been developed and a computer code, P465 Version A, written for the prediction of transonic potential flow about three-dimensional objects including inlet, duct, and body geometries. Finite differences and line relaxation are used to solve the complete potential flow equation. The coordinate system used for the calculations is independent of body geometry. Cylindrical coordinates have been used for the computer code. The analysis has been programmed in extended FORTRAN IV for the Control Data Corporation CYBER 203 vector computer. The programming of the analysis has been oriented toward taking advantage of the vector processing capabilities of this computer. Comparisons of computed results with experimental measurements are presented to verify the analysis. Descriptions of program input and output formats are provided.

17. Key Words (Suggested by Author(s))		18. Distribution Statement
Transonic flow	Inlets	Unclassified - Unlimited
Inviscid flow	Nacelles	
Potential flow	Finite differences	
Three-dimensional flow		Subject Category 02

19. Security Classif. (of this report)	20. Security Classif. (of this page)	21. No. of Pages	22. Price*
Unclassified	Unclassified	92	A05

* For sale by the National Technical Information Service, Springfield, Virginia 22161

NASA-Langley, 1982